Optimisation of 3D Profiled Woven Composite Structures

George Spackman

Thesis submitted to The University of Nottingham for the degree of Doctor of Philosophy

October 2023

Abstract

Composite 3D woven components have been used in aerospace components because of their improved through-thickness properties and ability to be woven integrally in near-net shape. The complex stress conditions and long time required to manufacture and test physical specimens means that the relationship between the reinforcement's weaving pattern and the mechanical behaviour of 3D woven composite T-joints is not well understood. With approximately 3.6 million possible combinations of weft yarn configurations alone for a textile with 10 weft layers, an exhaustive search of the design space is not possible. To resolve this, the aim of this project was to apply optimisation algorithms to 3D woven profiled structures such as T-Joints. Previous geometry modelling work in the literature had provided a framework to produce these models but were done by-hand using a manual process.

Initially, flat 3D woven structures were optimised to find the best through-thickness properties using algorithms from MATLAB's optimisation toolbox. Several algorithms were evaluated before determining that the genetic algorithm was the most appropriate based on the time to find an optimum solution and the accuracy. Methods were developed to rule out the large number of spurious weave designs generated by the optimisation algorithm. This resulted in a 94% reduction in run time for function evaluations using periodic boundary conditions when compared to literature values. The reduction in optimisation run time facilitated a novel optimisation of the peak through-thickness load using cohesive zone modelling.

A key outcome was the development of a tool to automatically model T-joint reinforcements using TexGen, the University of Nottingham's 3D woven textile geometry modelling software. Focus was placed on replicating the order in which wefts wrap around each other. This was achieved by determining the ordering of the weft yarn interlacement at the bifurcation region of the 3D weaves. This was then used to facilitate an optimisation of the weft yarn configuration to find the reinforcement weaving pattern that was best able to resist failure under tensile pull-off loading. This resulted with a 3D woven composite T-joint with an 8.8% increase

in the load at initial failure when compared to a T-joint made using an orthogonal weave with no weft yarn crossover or entanglement. An analysis of the results of this optimisation was able to provide information about how weaving features improve the failure behaviour of the joints under tensile loading.

Acknowledgements

After several years there are some people I would like to thank. First, I need to thank my supervisors, Tom Turner, Arthur Jones and, most importantly, Louise Brown. Your patience and guidance over many years are the reasons I have managed to get to this point. I would also like to thank Paul Johns and Liam Woods for their assistance and expertise in the lab. I would also like to take this opportunity to thank the wider Composite Research Group community, in particular Mikhail Matveev, Preetum Mistry, Matt Thompson, Usman Shafique, Ming Xu and Fei Yu along with Albert, Guy, Joe, Grace and Angela for their friendship, wisdom and constructive conversations along the way.

To Harry, you are not just my twin brother but my best friend. Thank you for your patience while I have been working on this, your support has been invaluable, I could not have done this without you. To Phyllida and Evelyn, thanks for believing in me and having my back. To my parents for their love and encouraging me to work hard while supporting me in my education.

More thank-yous go to my closest friends: Eleanor for all the kind encouragement, introducing me to touch rugby and being an all-round great supporter. My life is much better for having you in it. Ellie for all those evening chats, slowly persuading me to aspire to better culinary choices than tuna and ketchup and laughing at my terrible jokes. You are truly a friend for life. Zaki for always being there when needed, I will always be a Fanan and a friend.

To all the TAFKAP alumni: Poppy, Tom, Zaki, Stefan, Tiago, Ellie and Eleanor, thank you for putting up with my weird food habits and awful puns. I hope I repaid the favour by treating you all to my shower singing. You all helped to make the house a home. Furthermore, to all those at Nottingham Touch Club, it has helped enormously to have something outside my research work to occupy me and get out of the house. Maybe one day I will also learn how to pass a ball.

Thanks go to the EPSRC for funding me through this work, Sigmatex for providing the T-joint preforms and to the University of Nottingham HPC service for advice and providing the compute resources needed.

Table of Contents

Chapter 1 - Introduction

1.1 Composite Materials

Composite materials have been widely used in aerospace and automotive applications. One of the key drivers to their use is high stiffness to weight ratios, meaning that structural components can be made lighter while maintaining similar stiffnesses to more traditional materials such as titanium, aluminium and steels [1]. This has both environmental and financial significance to airline operators as lighter airplanes require less fuel burn, resulting in decreased emissions and fuel costs. Further advantages over metals include an improved ease of maintenance [2], with a wide range of non-destructive test methods [3] able to detect damage and with repairs able to be made by patching, this leads to a reduction in costly down time for planes.

The current flagship airplanes from the largest airframers, the Boeing 787 Dreamliner and Airbus A350, are 80% by volume and 50% by weight composite materials [4]. The vast majority of material is made up of laminated carbon fibre composite in the fuselage and wings alongside some additional specialised structures.

Laminated composites consist of multiple plies of laminated carbon fibre bonded together into lamina at angles that can be varied from one ply to the next. Each ply will consist of carbon fibres in set directions which leads to material anisotropy. The anisotropy, where the composite has different mechanical properties along the three cartesian axes, allows the properties of laminated composites to be tailored by varying the angles of the constituent plies.

As a result of the inherent weakness transverse to the fibre direction as well as in the bonding between lamina, which can be exacerbated by mismatches in mechanical properties between differently angled plies, laminated composites are at a high risk of delamination from through-thickness stresses [5]. This can

be a significant issue for load bearing structures as it can lead to failure of the component. As a result, improving the through-thickness properties of composites is important to reducing the barrier to entry for composites into aerospace structural components.

For load bearing profiled structures such as T-Joints, one alternative is to replace laminated pre-preg with 3D woven carbon fibre textile preforms to provide the reinforcement. These are woven on modified Jacquard looms, configured to weave multi-layer fabrics by the use of heddles which are used to form the shed and keep the multiple warp yarn layers apart for weft insertion [6]. After which, the preform is infused with resin using a mould in a process called resin transfer moulding or RTM. The advantages of this approach include superior through-thickness properties and the ability to manufacture preforms in near net shape.

1.2 Industrial Applications of 3D woven composites

The increasing use of 3D woven composites in industry is well reviewed, for instance in [7], and extends back 50 years to the early 1970s when the Avco corporation produced a preform on a loom to replace high temperature alloys in aircraft brakes [8]. Due to the costs of producing 3D woven components and manufacturing times, the uses reported below are primarily focussed on specialised components where in-service through-thickness loads can cause delamination.

One example of 3D woven composites in industrial use is in the fan blade and engine casing for the LEAP engine (see Figure 1-1), developed for use by CFM International and in service on the Airbus A320neo and Boeing 737 Max aircraft [9]. This uses 3D weaving to weave the entire preform to near net shape which means that it gets close to the desired shape of the finished part. The preform is precisely cut where necessary and then infused using RTM. Another application of 3D woven composites in the LEAP engine is in the engine casing. The through-thickness yarns improve the impact resistance which is

important in the event of a fan blade-off event, allowing the casing to contain any flying debris so that the fuselage is not struck.

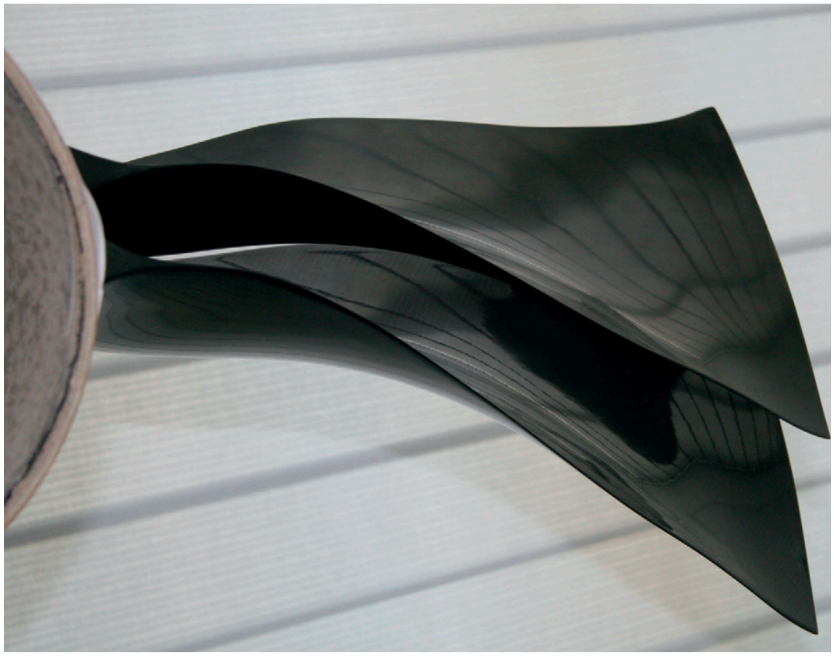

Figure 1-1 LEAP engine 3D woven fan blade.

Aside from applications in aeroengines, the ability to weave preforms to near net shape by making use of bifurcations allows a wide array of 3D profiled structural components to be produced such as T, Pi, H and I shapes (see Figure 1-2). Bifurcations are caused by variations in the binder yarn pattern so that there are local planes in the 3D textile not traversed by binder yarns, leaving two distinct, fully bound fabrics above and below the plane. Such 3D profiled shapes are woven flat and opened out using the bifurcation into the moulding shape. One example is Pi shaped preforms for wind turbine blades [10].

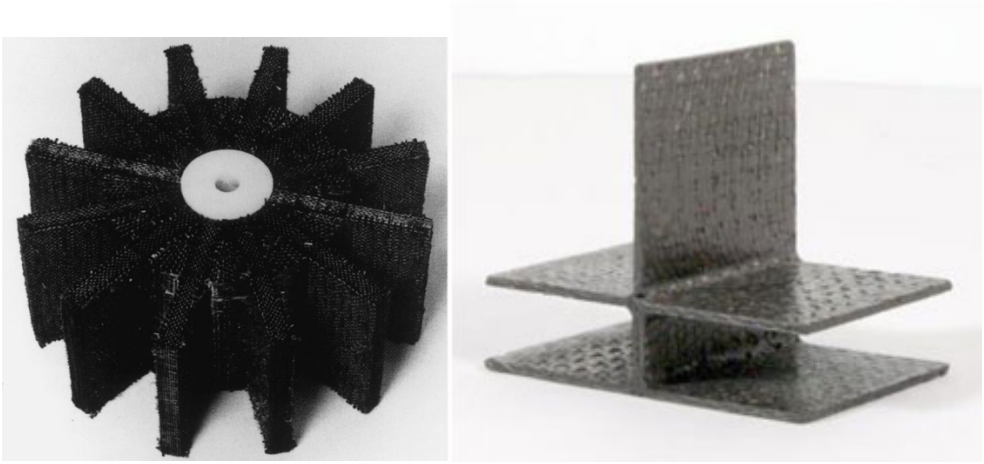

Figure 1-2 Turbine rotors produced by Techniweave, Inc. and Double T-Joint produced by Bally Ribbon Mills.

Composite T-Joints are a light-weight alternative to metallic structural elements. They consist of a web, forming the upright leg of the T profile shape, and the two flanges which together form the cap. The transition zone between the web and the flange is often referred to as the junction region. There is a resin-rich zone in the junction region, which is often filled with a filler material. This gap is also called the noodle region (see Figure 1-3). Due to its location and local lack of fibre reinforcement, the junction region is potentially a site of weakness.

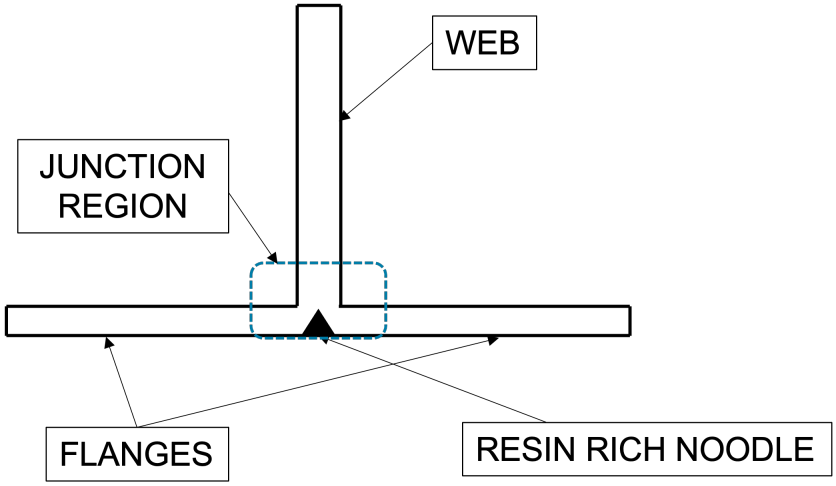

Figure 1-3 Diagram of a typical T-joint.

In aerospace applications, T-Joint structures are used in the wings and as bonding joints between composite panels in the fuselage. They are also often used as stiffeners for composite panels [11] and as such are required to withstand through-thickness tensile and shearing loads. They are traditionally manufactured using laminates, but this leads to problems with cracking in-service (see Chapter 2). As a result, the improvements of 3D woven composites in resistance to failure is of particular interest. When manufactured using 3D woven preforms, these structures have bifurcations which require complex weaving geometries at the junction region of the T-Joint where the weft yarns wrap around each other as they transition from the web to the flange of the component (see Figure 1-4).

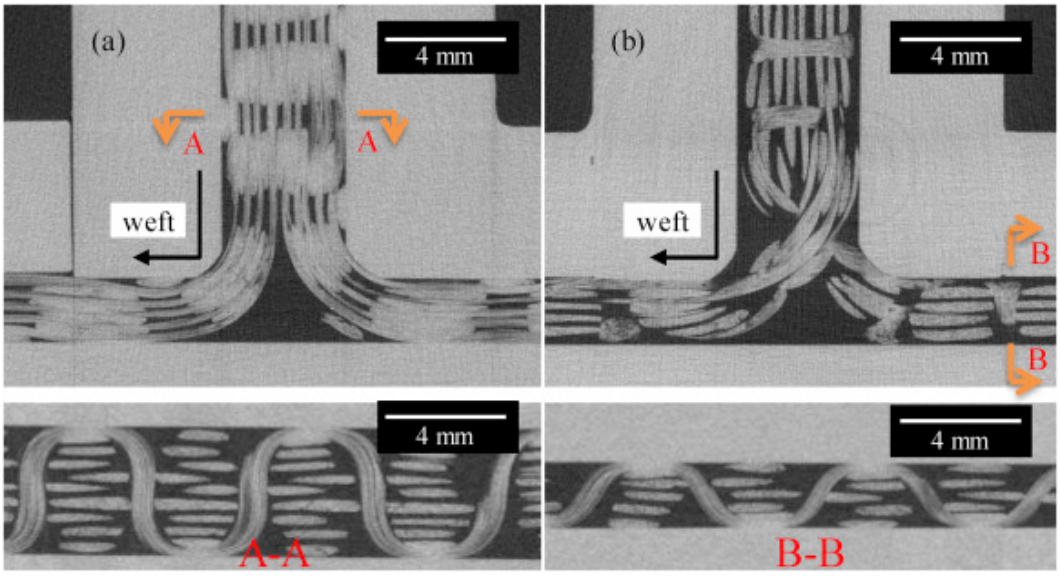

Figure 1-4 μCT scans of two 3D Woven T-Joints (a) T-Joint with wefts not crossing over, (b) T-Joint with weft crossover. Note the textile is fully bound by binder yarns in section B-B. Images taken from [12].

The binder yarns then bind the upper and lower flanges separately. This means that the woven fabric can be removed from the loom and the flanges opened out to form the net shape of a "T".

One of the barriers to entry into the industrial market for 3D woven composite T-joints is a lack of knowledge of how they behave under certain loading conditions, for T-joints in particular there is not a wealth of research into the effect of different weave patterns on the T-joint's failure mechanisms. This is due in part to the size and complexity of 3D weaving looms which make them expensive and require specialised training to operate. In addition, they require bespoke set ups to weave textiles with new weave patterns which is another source of expense.

1.3 Manufacturing Methods

1.3.1 Jacquard Looms

3D weaving on a standard Jacquard machine works by raising and lowering heddles attached to the warp yarns and inserting the weft yarns orthogonally through the gap created. This gap is also known as the shed. At the end of the process the loom has a beating action to push the weft yarns into vertical stacks between the warp yarns before restarting the process to create the next weft stack. Binder yarns are woven parallel to the warp direction to form the vertical interlacement and bind the weft yarns into the textile (see Figure 1-5).

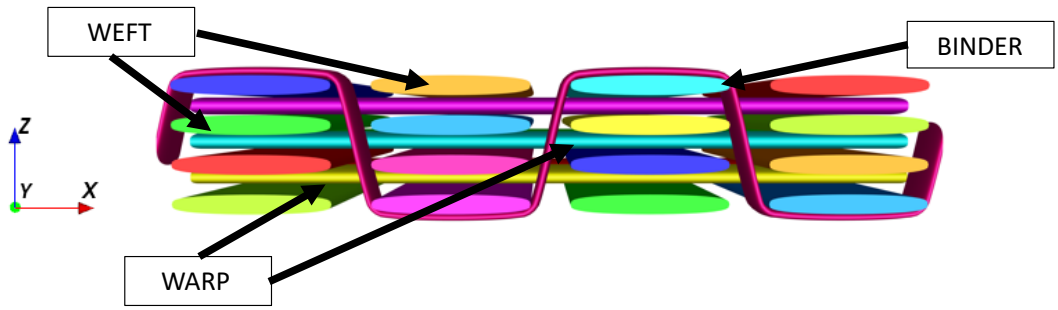

Figure 1-5 Orthogonal textile with the wefts into the page. The binder closest in pink travels along the same axis as the warp yarn. Model generated using TexGen.

There are three main types of 3D woven architecture: orthogonal, angle interlock and layer to layer weave patterns. Each varies by its binder yarn configuration. Orthogonal weave patterns have single binders transitioning from above one weft stack to below the next weft stack and vice versa resulting in a tightly bound weave. Angle interlock weave patterns have the binders transitioning between the weft stacks at different heights in the textile so that each binder traverses the thickness of the textile over multiple weft stacks (see Figure 1-6).

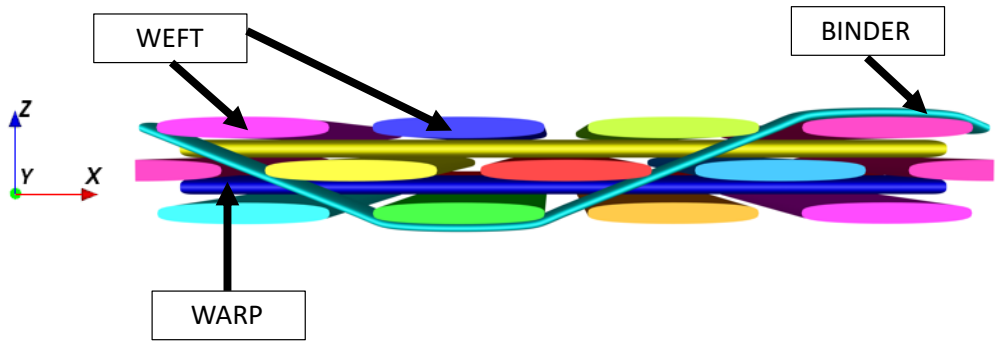

Figure 1-6 Angle interlock textile with weft layers staggered because of the binding configuration. Model generated using TexGen.

Layer-to-layer weave patterns are similar to orthogonal textiles but have multiple binder layers used to bind the weft yarns (see Figure 1-7). This leads to increased fibre volume fractions with more layers of binders leading to a denser textile.

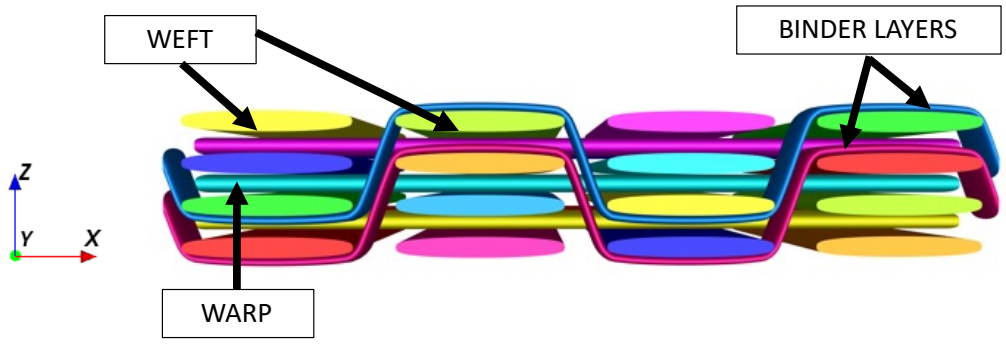

Figure 1-7 Layer-to-Layer textile with two binder yarn layers. Model generated using TexGen.

1.3.2 Placing Off-Axis Yarns and Multi-Weft Insertion

The traditional 3D weaving process can cause significant fibre damage as the weft yarns are inserted between the sheds. This is attributed to abrasion damage [13] between the yarns and the loom machinery. In addition to this, the slow manufacturing time means that woven textile composites can often be limited in their thickness to only a few layers. These issues and research into optimum off-axis yarn architecture for 3D woven composites [14] have driven manufacturing developments. Prototype looms developed as a result show some success in relaxing the usual manufacturing constraints by placing yarns along non-orthogonal axes and using multi-weft insertion which can speed up the weaving process with reduced fibre damage.

Multi-weft insertion machines such as the one developed at the University of Manchester, described in [15], are able to hold the sheds open and allow multiple weft insertions at the same time.

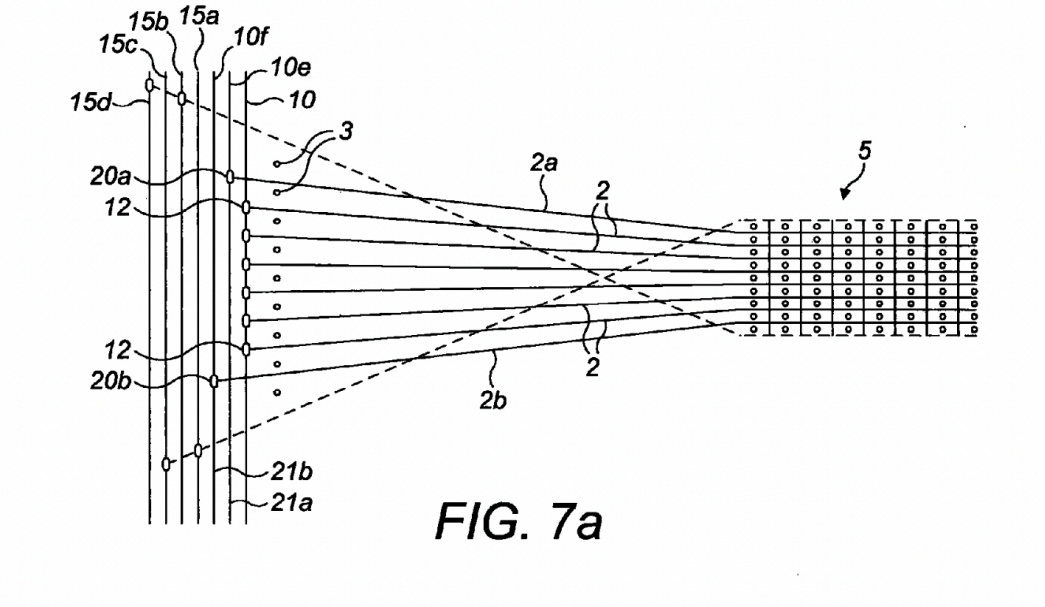

Figure 1-8 Diagram of a multi-weft insertion loom, taken from [15]. Each layer of warps are held apart to form multiple sheds so that the wefts, denoted here by the circles, can be inserted in the different layers at the same time.

This kind of loom has the advantage of the simultaneous insertion of multiple weft layers (see Figure 1-8) which reduces the shedding action and speeds up the weaving process with less preform damage. In addition, it is able to place the angle interlocking binder yarns so that they are not parallel to the warp yarns improving shear performance [16] and allowing further tailoring of the mechanical properties similar to laminate lay ups. Other prototype machines have been developed by GEMTEX [17] that are able to place off-axis yarns in a process similar to braiding.

Given the early stage of off-axis yarn placement technology, the work in this thesis will focus on weave pattern designs that can be produced on standard commercially available weaving looms. However, because the weft yarns are inserted straight across the loom the work contained in this thesis should still provide a framework to be able to automatically generate at least the weft yarn architecture for other types of weaving processes.

1.4 Modelling Advancements

TexGen [18], developed at the University of Nottingham, is used to generate and mesh weave geometry models as a pre-processor for finite element analysis. The code is written in C++ with a Python interface which is able to access the underlying core functionality using SWIG wrappers. The code is divided into several modules including the core with the main functions to model and mesh textile geometries (see Figure 1-9) and associated libraries including the VTK library to provide rendering, wxWidgets to provide the graphical user interface (GUI) as well as other libraries to facilitate meshing. Textile modellers can interact with TexGen using either the GUI or more flexibly via Python script which includes more functionality than is available from the GUI.

The TexGen core takes advantage of the C++ property of inheritance of classes. This allows further specialisation of functionality without the need to rewrite code. For instance, in TexGen this allows the different weave types to share code from the *CTextile3DWeave()* class while providing the bespoke code to

facilitate the building of the weave features specific to the weave type. During this work, additional features described will be added to TexGen as a combination of C++ code embedded in the TexGen core and Python scripts to further allow it to model and mesh the 3D woven T-joint geometry.

One of the challenges of virtual testing of complex structures is the generation of the finite element mesh. A fast and robust method for automatically generating this is required if the automatically generated T-joint textile geometry models are to be used in an optimisation routine. A conformal mesh can be difficult to achieve for woven composites due to the close proximity of the yarns. This can lead to poor quality matrix elements with high aspect ratios where the yarns come close together.

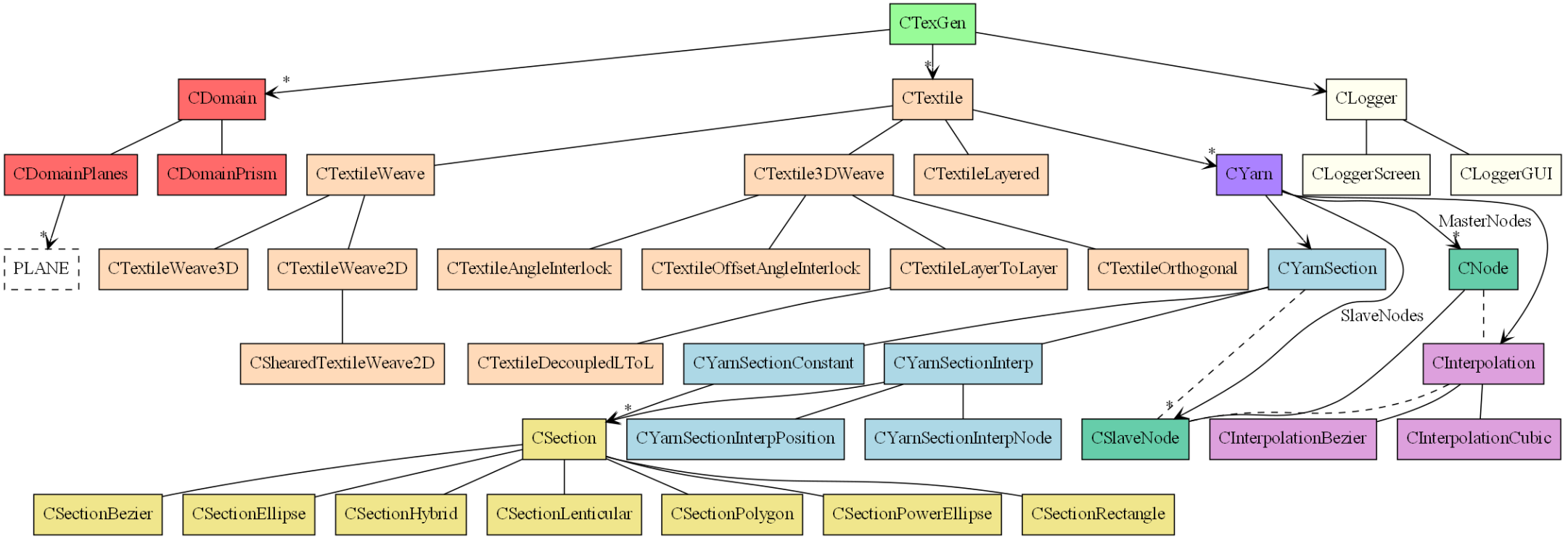

Figure 1-9 TexGen Core structure at the outset of the project start, showing the classes used to model textile geometry.

One method for creating the mesh is to use equally sized, brick-shaped elements called voxels [19]. This method has been used to good effect when used to find elastic properties of 3D woven composites with periodic boundary conditions. Voxel meshing results in jagged stepped interfaces between the yarns and matrix and can lead to stress concentrations when undergoing tensile tests.

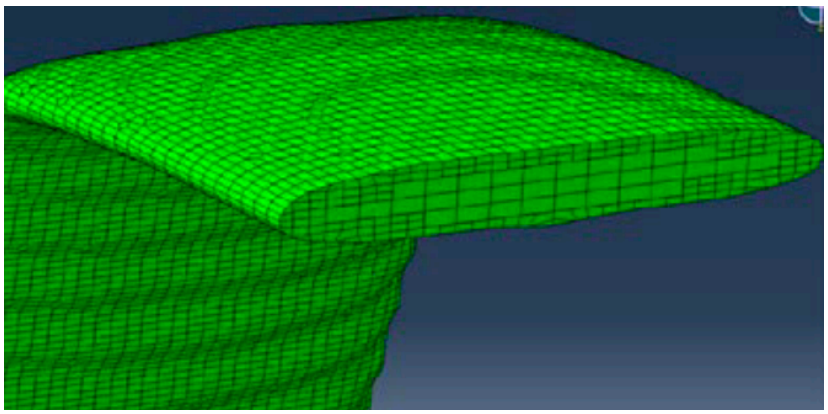

Figure 1-10 Smoothed and refined octree voxel mesh [14].

Further developments [20], have led to the ability to refine the elements at the yarn-matrix interfaces, storing the refined mesh in an octree structure. This octree voxel mesh can also be smoothed to create a mesh that closely approximates the conformed interface (see Figure 1-10). This method of meshing results in hanging nodes where refined elements meet less refined elements. This requires constraint equations in the finite element analysis, the large number of constraint equations results in a much longer simulation time.

1.5 Thesis Aims and Objectives

Under in-service loads, the woven architecture of 3D woven preforms leads to complex stress fields. This can make it difficult to know *a priori* the most appropriate weave pattern for a particular application. Virtual testing becomes important due to the time and manufacturing costs of producing and testing new weave pattern designs. However, with the large design space an exhaustive search is not possible.

For 3D woven T-Joint preforms, the specific geometry of weft yarns crossing over each other and entangling at the bifurcation/junction region has been shown to have an effect on the mechanical properties of the T-Joint [21]. For example, in ability to resist delamination under tensile loads. Historically, these geometries have been difficult to generate automatically using parameterised models because the order in which the weft yarns cross each other needs to be extracted from the weaving pattern information. Once this information has been obtained, careful modelling of the weft yarn geometry around the bifurcation area is required to prevent yarn intersections and replicate the nesting of the weft yarns for every weave design, which is a non-trivial task.

As will be seen in the literature review (Chapter 2), research into using optimisation methods has proven that optimisation algorithms are able to find the weave pattern designs most suitable for a specific objective function [22], [23]. Furthermore, experimental investigations and finite element modelling of 3D woven T-Joints have shown that their mechanical properties, including their stiffness and failure behaviour, are sensitive to changes in the weaving pattern [12]. The aim of this work is to determine whether it is possible to apply optimisation methodologies, namely algorithms, to finding the best weaving pattern for T-Joints. The research topic was broken into the following aims and objectives to achieve the overall thesis aim:

1) Experimentally investigating T-joint behaviour under the tensile pull-off test. This will include imaging T-joint fabrics using μCT machines. This will aid in setting up the finite element model boundary conditions

by providing experience in performing the test and informing the development of the geometry models.

2) Reviewing the current approach of 3D woven composite optimisation and seeing whether it is fit to apply to T-Joint fabrics. This information will be used to select the algorithm used for T-joints optimisations and to determine which modelling techniques, such as the use of cohesive elements and user subroutines for modelling failure, are appropriate for applying to T-joints.

3) Creation of a tool to automatically generate parameterised weave geometry models using a set of input parameters. This will be used as the basis of T-joint geometry generation in the optimisation algorithm.

4) A method of producing a good quality mesh automatically without user intervention. During an optimisation, potentially hundreds of weave designs will need to be meshed without outside input. Of key interest is the time taken to mesh each model and the accuracy of the mesh.

5) A method of scoring the weave designs, ie. an objective function and a means to evaluate it for each weave design. The total time to run the finite element analysis for each model and process the results to calculate the objective function value will determine the feasibility of the use of optimisation algorithms for 3D woven T-joints and other 3D profiled structures.

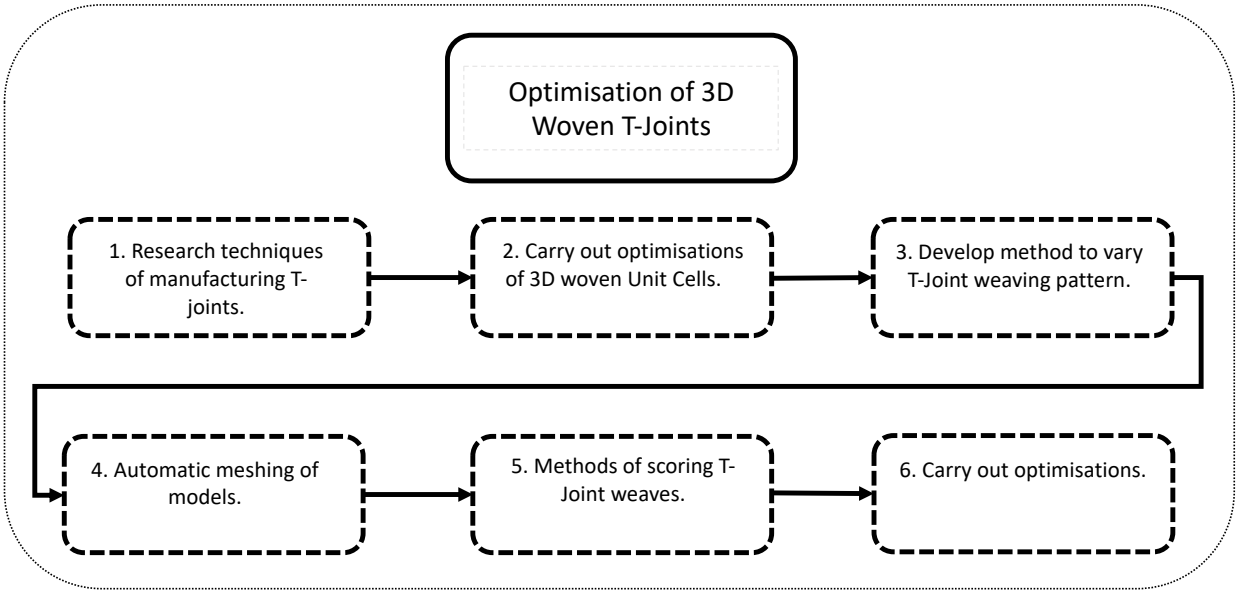

Figure 1-11 Breakdown of how the research aim will be achieved.

Completing an optimisation of the weaving pattern will be achieved by working through the aims and objectives above. A breakdown of the roadmap to achieving the research aim is provided in Figure 1-11. The optimisation will be followed by an analysis of the final optimised 3D woven textile architecture.

1. 6 Thesis Overview

Chapter 2 is a literature review of research into attempts to improve the interlaminar properties of composites, composite optimisation and the experimental and numerical investigations into composite T-Joints. This review is used to inform the research methodology outlined in subsequent sections.

Chapter 3 describes the methodology and results from the experimental work undertaken in this project to evaluate the mechanical properties of two of 3D woven composite T-Joint specimens, one with orthogonal warp and weft yarns and another with off-axis bias yarns. This section makes use of CT scans of T-Joint fabrics and experimental data from tensile pull-off tests to characterise

the effect the weaving patterns have on the mechanical properties of the woven preforms. In addition to this, the μCT scans are used to quantify the material variability. This data is used to validate the geometry models presented in Chapter 6.

In Chapter 4 methods to enhance the current state of the art for optimisation of flat 3D woven composites are outlined, including the optimisation of a flat 3D woven composite panel for delamination resistance. A basic set of feasibility rules are set out and implemented in a Python script. This allows weave pattern designs that do not satisfy the rules to be assigned dummy objective function values and then be skipped from the costly finite element analysis step. This makes optimisation of more complex objective functions possible. An optimisation routine to optimise flat 3D woven models for delamination resistance is used as a demonstrator. For this purpose, cohesive surfaces are applied and used in the finite element simulations to evaluate its applicability to the tensile test FE simulation for the full T-joints.

In Chapter 5 methods to automatically generate complex T-Joint weave geometries are set out. The first step is to extract the ordering of the weft yarn wrapping from the information in the weave pattern draft file. The μCT data from Chapter 3 is used to be able to generate more realistic weft yarn geometries in the junction region of the weave where the weft yarns nest as they form a compact shape. The nesting visible in the μCT data is replicated in the models.

A method of evaluating the objective function is set out in Chapter 6. The details of meshing the weave pattern designs and setting up the finite element models simulating the tensile pull-off test are discussed. Automatically meshing complex structures such as T-Joint weave pattern designs is a difficult process. Recent developments in TexGen's meshing capability allow the use of different meshes including voxel, octree voxel and smoothed octree voxel mesh. T-joint models are meshed with all three mesh types to compare the accuracy of the results. Element stresses are evaluated against the Hashin failure criteria in the yarns and the modified Von Mises pressure criterion for the matrix so that a load for initial failure can be determined.

In Chapter 7, methods to encode the design variables as binary strings are used to with a genetic algorithm to solve the permutation optimisation problem of finding the best weft yarn configuration to maximise the load at which initial failure occurs in infused 3D woven T-joints. The results from the optimisation of T-joints with weft yarn variations is discussed and used to provide information about optimal weaving patterns for tensile pull-off loading.

In Chapter 8 a holistic discussion of the work presented in this thesis is provided. Results are discussed and evaluated against the thesis objectives provided earlier in this chapter. Areas for future research are included as well as key outcomes.

Chapter 2 - Literature Review

2.1 Introduction

The purpose of this chapter is to review several fields relating to the different aspects of the work in the later chapters. This includes reviewing the current state of the art for the different methods of manufacture, testing and modelling of composite T-joints alongside the modelling and optimisation of more general composite structures. This is to identify areas where there are gaps in the literature and provide an overall context for the work in this thesis.

2.2 Composite T-Joint Testing

Laminates have high in-plane moduli and strength but are susceptible to damage in the form of delamination between the plies [1]. This occurs due to the cracking of the resin at the interface between two plies and is more likely to occur if the plies are at different orientations. This is due to the difference in mechanical properties between the two plies, created by their differing local fibre directions, when the part is loaded in one direction. This can result in in-plane strength properties of 500-800 MPa matched up with significantly weaker out-of-plane strengths of 20-30 MPa as reported by [24]. This makes them less than well equipped for applications where there is significant out of plane loading. This is a particular problem for 3D profiled structures such as I and T-joints which are commonly used as stiffeners [25] and joints in various applications in airplane fuselages and wings [26] where they undergo through-thickness loading. Research into alternative manufacturing methods to improve the delamination resistance properties of such components split broadly into two methods: the reinforcement of pre-preg laminates using stitching, tufting and z pinning and methods that use dry fibre tows to produce a near-net component before RTM infusion such as 3D weaving and braiding.

Mechanical testing of composite T-Joints most often includes the tensile pull-off and bending stiffness tests (see Figure 2-1). These seek to test the joint tolerance to the out of plane loads they are likely to sustain in-service. Testing of the flange plane under tensile load has also been carried out [27]. T-Joints generally contain a resin-rich region at the web-flange interface where the structure bifurcates to form the overall T-profile. This region is often referred to as the noodle region [28], the junction area [25], delta-fillet [29] or the bifurcation area depending on the context, T-joint manufacturing method and author. It often is filled with filler material to reduce the resin richness and add some stiffness, in these cases it is referred to as the noodle. In the following review, this region will be referred to as the junction region unless when mentioning filler material in which case the term noodle will be used.

In both the tensile pull-off and bending tests the flange is clamped while loads are applied to the web. Loading is applied until complete failure of the joint occurs. Much of the research into the properties of composite T-Joints involves either these mechanical tests or their virtual counterparts using finite element analysis.

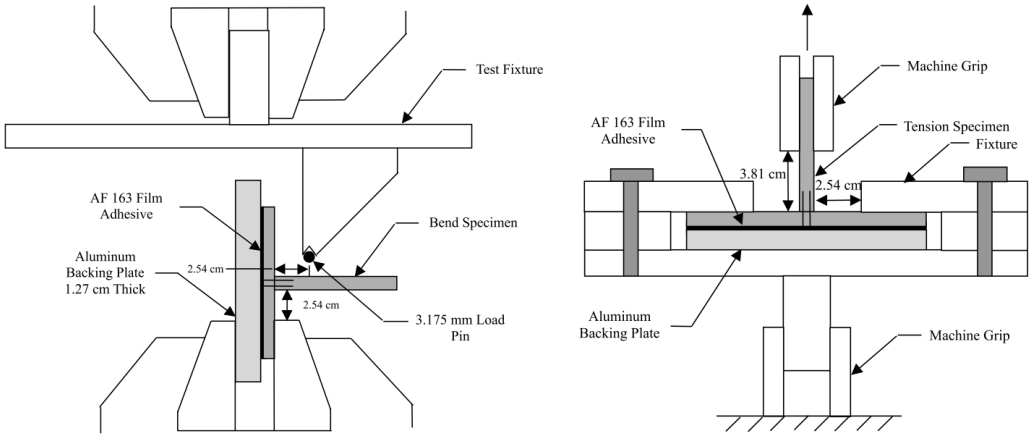

Figure 2-1 Schematic of Bending and Tension tests typically carried out on T-Joints from [30].

2.2.1 Stitched Composites

Stitching [31], [32], [33], [34] been researched as a method of improving the interlaminar fracture toughness of composites. A stitching needle penetrates through the layers of the material with the stitching thread providing the through-thickness reinforcement before either co-cure in the case of pre-pregs or resin injection and curing in an autoclave for RTM. It has been shown to improve the impact resistance [33] and interlaminar fracture toughness of composite laminates, with the bridging effect of the reinforcing thread providing increased resistance to crack growth. However, many studies, such as those reviewed in [24], suggest that fibre damage caused by the stitching needle can cause a degradation of the in-plane properties.

Stickler et al [26] attempted to characterise stitched T-joints mechanical behaviour by performing experimental and numerical T-joint bending tests on joints that were transversely stitched with a varying number of rows in the junction region. They found that for all samples tested, increasing the number of stitching rows into the junction region improved the failure strength. Initial failure occurred in the resin rich matrix corner where the web meets the flange where high stress concentrations occur. Final failure was due to fibre breakage and pull out. The force-displacement graphs for the specimens showed a linear portion up until the initial failure point, followed by a smaller gradient slope until the peak load was reached. This showed continued load resistance which was attributed to the ability of bridging stitches to arrest further crack growth. Unfortunately, no reference test was provided so it is difficult to determine the effect the stitching had on the mechanical properties. Finite element modelling with plane stress elements showed some agreement with the experimental data though no predictive failure modelling of the composite was included.

In a further paper [30], Stickler et al performed tensile and flexural bending tests on transversely stitched T-Joint samples to characterise the joints' failure modes. Post-test fractographic analysis of the tensile specimens with the symmetric loading through the flange indicated that they failed due to the cracking of the matrix at the interface between the web and flange. They found that the asymmetric loading of the inserted stitches during bending testing was

a cause of the initial delamination alongside delamination in the junction region. For both tensile and flexural tests, the stitched T-joints were able to continue to sustain load past the initial delamination failures, showing good agreement with their earlier results. The joints were adhesively bonded to aluminium plates to perform the tests and in some cases the joints cracked along the interface before failure occurred in the actual joint, affecting the results.

While investigating hybrid wing body aircraft at NASA, Lovejoy et al [35] added stitching rows to the web of the T-joints and performed tension and bending tests to determine the initial failure load and peak load. They compared T-joints with four and eight rows of stitches to the baseline design with one stitch close to the junction region. In addition, they tested the different designs with and without a stiffening rod passing through the top of the web. They found that for the samples without a stiffener passing through the web, the presence of additional stitching in the web actually decreased the initial delamination failure load under the tension-only tests when compared to the original design. The initial onset of delamination was reported to have occurred in the noodle region with load being transmitted from the web. One area that was not addressed was the effect of stitches on the flanges which see out-of-plane stresses in both bending and tensile tests.

Bigaud et al. [36] tried to reduce the difficulties associated with the need for stitching from both sides by comparing tensile pull-off tests of unstitched T-Joints to those stitched using a one-sided stitching (OSS) technique. The joints were stitched using a stitching head attached to a robotic arm. The OSS head inserted the thread at a 45° angle which was then picked up by a catching needle moving vertically through the dry preform. The authors reported an improvement of 25% in ultimate strength and 19% greater load recovery post ultimate strength in comparison to the unstitched T-Joint.

As can be seen from the literature surveyed, stitching is a well-established process. However, one drawback is that it typically requires access to both sides of the material because the stitching thread needs to be drawn back up vertically through the material. Specialised machines such as those reported by Bigaud

et al. are able to overcome that limitation. Further limitations from the damage to the load bearing fibres present an obstacle to the entry of stitched composites into industrial production.

2.2.2 Tufted Composites

An alternative to stitching is tufting [14]–[40] which uses a one-sided stitching process. The tufting needle draws its thread once through the material before releasing it, leaving a small loop on the material underside. Mechanical tests on specimens made using tufting again show an increase in delamination resistance but accompanied by a reduction in stiffness for similar reasons to z pinning [38].

Wang et al [41] performed numerical and experimental T-Joint tests on tufted and non-tufted composite T-Joint specimens designed for wind turbine structures. The T-joints where tufting yarns were introduced showed improved interlaminar fracture resistance when compared to the untufted T-Joints. This is very similar to the stitching process where the tufting thread bridges cracks and provides closure tractions and so more energy is required to promote further crack growth. Experimental observations for both tufted and non-tufted specimens showed continued damage tolerance after the peak load was reached but the tufted specimens had higher peak loads and saw less of a reduction after.

The tufting strategy is similar to that of stitching with the improved interlaminar properties provided by fibres that span the interlaminar interface. While both show improved interlaminar properties, tufting has the advantage of only needing access to one side of the component.

2.2.3 Z-pinned Composites

Z-pinned composites [42]–[47] seek to improve the interlaminar properties of pre-preg laminate composites by the insertion of rigid carbon fibre rods through

the lamina to hold the layers together. It is widely accepted that such a technique can lead to in-plane damage. The pins are inserted using a mediating foam to hold them steady and reduce buckling.

Cartie et al. [42] attempted to compare the effect of z-pinning and tufting T-joints on the interlaminar damage tolerance. T-joints manufactured using a lay up of five-harness satin weaves were z-pinned and cured in the autoclave while another set were tufted and RTM infused. The different manufacturing routes were a consequence of the different 3D reinforcement methods. A unidirectional pre-preg was inserted into the 'noodle' region for all samples. The samples were then tested under tensile pull-off load and separately compared back to base line T-joints with no through-thickness reinforcement. No method of ascertaining the optimum location for the reinforcement locations was described. Both types of samples showed improved damage properties with both achieving increased loads before initial failure and a reduced drop off of load after failure. Cracks initiated in the junction region before propagating outwards. Unfortunately, a like for like comparison between the two types of T-Joints was impossible due to the differing geometry and manufacturing routes used.

Koh et al. [44] investigated several parameters including the volume content of the z-pins and the angle of the pull-off load to assess their effect on the overall mechanical properties of the joints. This partly addressed the relative lack of literature covering variations in the loading conditions by varying the angle between 0° and 45°. This was able to generate combinations of through-thickness tensile and bending stresses. Initial failure occurred at the junction region, where stresses are highest due to the geometry of the joint. They found that post initial failure properties were improved such as the ultimate failure strength and failure displacement. However, the authors note that the stiffness and initial failure load were not improved by increasing the z-pin content.

Subsequently Bianchi et al [11] carried out finite element modelling of the z-pinned T-joints from [44], with the aim of accurately modelling the deformation and strength properties of the joints. The previous experimental observations of unpinned T-joints under tensile pull-off loading showed crack

initiation in the junction followed by horizontal delamination at the flange-skin interface and a vertical crack within the web. In comparison, the pinned joints saw improved resistance to crack growth along the flange-skin interface because of the closing force supplied by the pins. This provided continued load tolerance after the initial failure so that the pinned joints were able to reach a peak load of 3800 N in comparison to the 1800 N reached by the unpinned joints. A multi-scale modelling approach was used with a representative unit cell containing one z-pin used to find the closing tractions supplied by each pin. A cohesive zone formulation taking into account the earlier analysis was then used to model the macroscale effect of the pins on the overall T-joint. Finite element analysis showed shear mode II traction loads in the web and tensile mode I loads along the flange-skin interface. This showed good agreement with experimental results.

Z-pinning using metal arrow-head insertion rods has also been explored by Heimbs et al [48] where pull-off tests were performed with the loading at 0º and 30º. Furthermore, the loading rate was varied with quasi-static and dynamic loading used. It was found that the interlocking effect of the arrow head and higher plasticity of the metal pins were improvements when compared to the unreinforced joint. Unfortunately, no tests were performed on T-joints with z-pinning using carbon rods so no direct comparison was able to be made.

2.2.4 3D Woven and Braided Composites

3D woven composites [7], [49]–[52] have the through-thickness reinforcement provided by binder yarns. They have been studied extensively due to their improved resistance to interlaminar fracture. This method seeks to replace the standard approach of laid up pre-preg cured in an autoclave, with an integral weaving technique which can produce a near-net shape preform. Other advantages 3D weaving has over other forms of through-thickness reinforcement stem from its use of discrete yarns consisting of fibre bundles which are able to arrest cracks, with multiple fibre types possible [53]. Further improvement of properties is possible via the crimp level of yarns [54].

Improved impact resistance [7] has also been reported. Furthermore, the ability to apply weaving techniques such as varying the binder pattern to create bifurcations and changing the number of raised sheds along the width of the loom to change the weft height allows a wide array of possible textile architectures to suit the required application [55]. The periodicity of 3D woven composite unit cells, coupled with yarn homogenisation, allows the application of periodic boundary conditions as set out in [56] to predict elastic properties.

Similarly to 3D woven composites, braided composites make use of the ability to vary the processing parameters to achieve improved properties dependent on the application. Yang et al [25] compared a 3D braided T-joint to those made using 2D tape. It was possible to eliminate the resin rich junction region which was identified as a frequent site of initial damage of T-joints under pull-off loads. Speckle interferometry was used to measure the strain field distribution. The braided T-joint was able to sustain a higher load until the initial failure occurred. The strain distribution saw reduced strain concentrations in the braided sample. This was attributed to the uniform compliance given by the woven architecture of the braid. The majority of the yarns were not aligned with the load paths.

Sugun et al. [57] produced a novel design of a 3D woven ‘T-insert’ used alongside layers of laminate plies to produce full T-joints and compared them back to laminate T-joints without the inserts. The inserts were woven using a Jacquard machine and 3K carbon fibre tows. This produced a textile with the web bent over one of the flanges, that could be opened out to produce the full T-profile. Tensile pull off tests of both types of joint found that those with the insert had a 30% higher post initial failure ultimate load with final cracking occurring along the flange-skin interface of the joint. The increase in failure load from the insert was attributed to its ridges along the interlacements and the ability for the woven fabric to redistribute loads. The paper made no comment on the stiffness or initial failure load but visual inspection of the graphs reveal that they were unchanged by the inclusion of the insert.

Yan et al. [58] conducted CT scans on two different types of 3D woven T-Joint architecture, one with weft yarns that did not cross each other and another with

yarns that did crossover. Follow on experimental tensile pull-off tests showed that both types of samples showed an improvement when compared to 2D lay-up samples in terms of peak load and damage tolerance. The experimental test results were used to validate finite element analysis of the test. The geometry was modelled for each individual model type using TexGen, with the CT data informing the yarn placement and geometry. The samples with crossover showed improved damage properties compared with the T-joints made using 3D weave patterns without crossover under tensile testing. Only two 3D weave pattern designs were used, probably due to the time and cost involved in producing each textile.

Further work by Yan in [21] produced several T-Joint geometry models with different weaving patterns. These were then used in the same pull-off finite element analysis as before to evaluate the effect different weave pattern characteristics had on the mechanical performance. The textiles were categorised based on the crossover and entanglement of the weft yarns. Crossover referred to the number of yarns that crossed to the opposite side of the textile while entanglement was characterised as the number of yarns that did not stay parallel to each other in the junction region. The 3D woven textiles with maximal crossover and entanglement were able to reach a greater peak load and had a reduced drop off in performance after the peak load was reached. It was concluded that this was due to the crack arresting effect of the increased number of yarn-matrix interfaces where cracks travelling perpendicular to the yarn face were more likely to run into a boundary and be stopped. Due to the length of the time it took to produce the textile TexGen models and run the finite element analysis, only 8 weave pattern designs were evaluated.

There is limited research into 3D woven composite T-Joints, due in-part to the relative difficulty and slowness of creating new T-joint fabrics, and automatically generating high quality finite element models. The literature points to the weaving pattern influencing the final T-joint mechanical properties, however, the available literature on 3D woven T-joints is limited when it comes to evaluating different weave designs and why different weaves would perform better than others. This may be due in part not only to the long time it takes to generate geometry models but also the length of time it takes to

model failure behaviour with finite elements. Methods like cohesive surfaces and user subroutines to evaluate post initial failure behaviour are particularly time intensive. However, maximising the initial failure load of the T-joints is one of the most important aspects of T-joint performance so if an accurate failure load can be determined using another method, that may open the possibility to optimise this using optimisation algorithms.

2.3 Finding Optimum Composite Architectures

Optimisation algorithms have been used in engineering applications since the late 20th century [59] as a tool for finding optimum designs for cases where an exhaustive search of the design space is not possible due to its size. Optimisations are defined by an objective function which is the thing that is to be maximised or minimised subject to a set of constraints, and the design variables, the parts of the design the algorithm is varying to find the best solution. The best choice of optimisation algorithm is highly problem dependent and so needs to be investigated on a simpler problem before application to optimisations with more time and resource expensive objective function evaluations.

The use of optimisation algorithms to aid in the design of composite structures has become a popular topic for research due to a desire to maximise the advantages of composite anisotropy. Optimisations of composite laminate structures generally operate on discrete or a mix of discrete and continuous variables. The stacking sequence is most often made up from a discrete set of ply angles while continuous variables can include ply thicknesses. The discrete design space coupled with the fact that the objective function can contain local minima, which might trap a gradient based optimisation algorithm, means that heuristic algorithms which operate on a trial and error basis are well suited to composite optimisation. One example of a heuristic algorithm is the genetic algorithm, which has become the most popular optimisation solver in the last 30 years [60]–[66] for optimising the lay-up or stacking sequence of laminates. Objective functions for these optimisations can include minimising the laminate weight while maintaining laminate stiffness and strength properties.

Some reasons for its popularity over other solvers in laminate optimisation include its ease of implementation and robustness with implementations in MATLAB's global optimisation toolbox [67] and in Python libraries such as PyMoo [68] and PyGAD [69]. Other solvers such as the pattern search [70] and particle swarm [71] algorithms are less researched for composite design optimisation.

Inspired by the use of genetic algorithms applied to laminates, several efforts have been made to conduct optimisations of 3D woven weave architectures. Gommer et al. [72] [22] and Zeng et al. [23] conducted optimisations of 3D woven unit cells. Gommer et al. attempted to optimise the unit cell for a buckling coefficient formed of the flexural stiffnesses of the unit cell by using a genetic algorithm to vary the orientations of the warp and weft layers so that they were no longer orthogonal. This presented a problem for modelling binder yarn paths due to the reduced space between yarns for the binder yarn to pass through. They calculated the combinations of warp and weft yarn orientations that were able to leave a large enough gap based on the geometrical properties of the woven unit cell.

Zeng et al. made use of the same optimisation framework to optimise the yarn paths in a layer-to-layer flat woven unit cell for the buckling coefficient. They tested the genetic algorithm alongside a so-called μGA that uses a reduced initial population size with reinitialisation of the population after every generation. Using a parameter study to find the most efficient parameters for the genetic algorithms, they found that both algorithms were able to find the same optimum solution with the μGA being the more efficient of the two.

Matveev et al. [14] used a genetic algorithm framework where instead of running a finite element analysis to find the elastic properties of flat 3D woven composites, an orientation averaging method which uses the local yarn orientations and volumes to calculate the elastic properties was used. This resulted in a faster run time during the optimisation for the same optimisation problem as investigated by Zeng et al.

These optimisations have used analytical methods or finite element simulations of flat piece unit cells under loading prescribed by periodic boundary

conditions, as set out by Li in [56], to find the elastic properties of the unit cell. The objective function has then been formed from a combination of these elastic properties. While these works have developed methods to vary the parameters of 3D weaves, they are less applicable to more complex geometries such as T-joints where there is often limited periodicity.

3D woven composites are primarily used over laminated composites because of their improved through-thickness properties for preventing initial failure and then sustaining load post initial failure, therefore design optimisation of these properties is highly desirable, something that is not possible using the periodic boundary conditions technique.

2.4 Modelling Software

The ability to model textile composites has allowed much research to go into finding a deeper understanding of these materials. There are several different open source and commercial software that have been developed to generate textile models either for use as CAD or as pre-processors for finite element analysis.

TexGen [18], [73] was developed by the University of Nottingham's composites research group beginning in the late 1990s. It has existed in its current form since version 3 was released in 2006 [74] with continuous developments [52] adding further functionality to the software in the following years up to the present. It is an open-source software with over 45,000 downloads since 2006, making it one of the most popular textile modellers. It uses a kinematic approach to model yarns using splines to describe the yarn path and sweeping cross-section shapes along the interval to generate the yarn volume [74]. The cross-section shapes are interpolable allowing for them to be varied along the length of the yarn. This allows almost any textile geometry to be modelled given enough care and attention. A python scripting interface further facilitates fine control over model geometry.

Continuous developments to the software have resulted in several textile types such as 2D and 3D orthogonal, angle-interlock and layer to layer weaves to be

in-built so that users can quickly generate these models by supplying some parameters such as the number of yarns in each direction, the number of layers and binder pattern. These tend to differ from real geometries due to the inherent variability in textiles. Where possible CT data is used to inform the idealised geometry. In addition, several meshing libraries and methods are in-built including tetrahedral meshing with the TetGen library [76], voxel meshing and more recently a new octree voxel meshing method [20].

Another modelling software is WiseTex [77], [78] which was developed at KU Leuven and is commercially available with a licence. It provides a similar level of functionality to TexGen in that it can be used as a pre-processor for generating textile geometries for input into finite element solvers such as Ansys [79] and Abaqus [80]. While it shares a similar functionality to TexGen, the proprietary nature of the software limits its utility to users who may want to add to the code base without the need to go through the vendors. Another key difference is that where TexGen uses a kinematic approach of defined yarn paths with sweeping cross-sections, WiseTex uses the principle of minimum bending energy to calculate the shape of yarns on an elementary interval.

Researchers at NASA compared the two software packages alongside an in-house modeller in [81]. It was reported that both TexGen and WiseTex were able to recreate the geometry of a five-harness-satin weave. At the time of publication, it was noted that WiseTex had several in-built types of weave structures such as yarn nesting. In the time since, many of these have been implemented into TexGen including 3D textile structures including orthogonal, layer to layer and angle interlock weaves.

2.5 Meshing

The complex geometries of 3D woven composites present a challenge to the efficient automatic meshing of their models. The main types of meshing fall into two categories: conformal meshes where the interface boundaries align with the element surfaces and non-conformal meshes where the element surfaces do not align with the interface.

Conformal meshes make up what are generally considered to be the conventional way of meshing finite element models in commercial FE codes [82]. The heterogenous nature of textile composites means that there are often closely spaced interfaces between the matrix and yarns. Given that the nodes need to match on either side of the interface, this can cause in both structured and unstructured meshes distorted elements with poor aspect ratios. These elements can cause numerical errors in the resulting solution.

Wentorf et al. [83] automatically meshed textile composite models for finite element analysis using linear tetrahedral elements in a piecewise manner, first meshing the vertices, followed by the edges, faces and interior volumes. This allowed them to maintain the periodicity of the mesh for finite element analysis. It was found that when the number of nodes was increased by an order of magnitude, the error in the stiffness caused by the discretisation only improved by 2% whereas a 20% change in the volume fraction error, which can arise from poorly shaped elements, resulted in an 8% change in the stiffness. In other words, the effect of volume fraction errors was significantly higher than the error caused by the mesh coarseness.

Voxel meshing as set out by Kim et al. [84] is a non-conformal alternative to the type of meshing set out above. In a method borrowed from image-processing, three-dimensional pixel-like hexahedral elements called voxels are used to tile the domain space of the model. This produces a mesh consisting of equally sized and shaped blocks. In multi-material models, such as 3D woven textiles, each voxel is assigned to the material it lies within. This has the advantage of robustly meshing models with matching node sets across material interfaces and consistent element quality. A further benefit of the voxel meshing method is the guarantee of matching node sets on opposing faces, needed for the application of periodic boundary conditions for unit cell homogenisation analyses. The ability to capture the volume fraction accurately with a small enough element size means that voxel meshing is particularly good for finding the elastic properties.

Kim et al. found that voxel meshing was able to quickly mesh multi-material models such as textile composites, with the advantage of good accuracy in

obtaining the volume fraction of the individual elements regardless of mesh coarseness. It was noted that further improvements to the voxel method can be made by refinements of the mesh near the boundaries between materials.

One of the disadvantages to this approach is the step-like interface produced as described by Yan in [21]. This can cause stress concentrations at material interfaces which can cause early failure in strength analyses [85], a barrier to the use of voxel mesh for delamination analyses. In [21] Yan investigated the effect of the stepped interface on the ability to use cohesive surfaces. It was found that provided the primary stress in the model was direct tensile stress as opposed to shear then cohesive surfaces provided a good agreement with obtained experimental results. Voxel elements are typically encoded as 8 noded linear elements, so introduce shear stress errors under bending loads (known as shear locking) making them less well suited to evaluating the shear strength of a cohesive interface. To produce the cohesive surfaces, Hypermesh [86] was used for each model to generate the surfaces.

Matveev et al [14], [20] presented an octree voxel meshing method, implemented in TexGen, to refine the voxels at the boundaries between two materials by letting the user choose a minimum and maximum level of refinement. This greatly improved the ability of the voxel mesh to capture yarn cross section shapes while reducing the number of elements needed to generate the mesh. To reduce stress concentrations, a smoothing algorithm was used to reduce the jaggedness of the voxel surface which should improve the ability to apply cohesive methods to textile composites. Some of the advantages to this method are its ease of use and ready availability in open source code. Hanging nodes generated by the differing levels of element refinement are tied to neighbouring elements with multi-point constraints that constrain the nodes to the nodes of nearby elements. These take a long time to generate which can greatly affect the analysis time.

2.5 Discussion

Several methods have been employed to try to improve the through-thickness properties for 3D profiled composite structures such as T-joints. These include stitching, tufting, Z-pin insertion and 3D weaving. Stitching and tufting both involve passing reinforcing threads through dry carbon fibre textile laminate preforms prior to infusion using a process like RTM, Z-pin insertion reinforces laminate pre-preg using pultruded carbon fibre rods and 3D weaving produces integrally woven preform reinforcements. Nearly all the literature reviewed, with some exceptions, used either tensile pull-off loads or bending loads. Mechanical behaviours of particular interest to the researchers included the T-joint stiffness, initial failure load and post failure behaviour. Together these form a list of properties of T-joints that would be desirable to improve by design changes. T-joints in-service do not see only one type of loading at a time, future research should include new test methods to characterise combined tensile and bending behaviour.

Both stitching and tufting have the advantage of providing a relatively simple method of reinforcement which works with the current process of producing textile laminate T-joints. Areas for design optimisation include the location and number of stitching or tufting threads. For stitching in particular, the requirement of access to both sides of the T-joint and for both fibre damage caused by the stitching/tufting needle are drawbacks to its use.

Z-fibre pinning is the only method able to reinforce unidirectional laminates that do not have the ability to be interlocked by through-thickness fibres. They have the advantage of improving the interlaminar properties without adding too much weight. Some results were inconclusive about their ability to improve the initial failure point but found that the closing force from the pins can continue to sustain the load until final failure occurred later.

3D Weaving techniques, such as the weaving of bifurcations, can produce preforms in near net shape and have the advantage of a wide array of possible fibre architectures. While experience is often relied upon for producing the weave design, the complex weft interlacement at the junction region can generate complex stress states. Studies found that the multi-directional wefts at the junction of T-joints can arrest cracks, improving the fracture resistance of

the joint. The literature only shows one example where 3D woven reinforced composite T-joints made with different weave patterns were compared.

Research into modelling weave structures has been able to produce weave models on an individual basis using TexGen, though this takes a long time. Slow lead times for modelling make it difficult to characterise the effect the weave pattern has on the mechanical performance. As such there is limited research into finding optimum architectures for T-joint performance with manufacturer experience often relied on instead to guide the weave pattern design process. Further areas of research could include improving the creation of realistic geometry models including investigating the effect of tow waviness on mechanical properties.

Due to the long manufacturing process for 3D weaves, it is desirable to have some a priori knowledge of the best design. Borrowing from the use of evolutionary algorithms for laminate optimisation, there are several examples in the literature of optimisation algorithm use in finding the best woven architectures for flat panel unit cells for different objective functions. One gap in the literature is that the methods used by these types of optimisations are mostly limited to periodic fabrics where the in-plane stiffness is the design property being optimised by varying the binder yarn paths. Extending the use of these algorithms to 3D profiled structures such as T-joints is worthwhile to fully exploit the benefits of the 3D woven architecture.

The literature review has been able to identify the lack of 3D woven composite optimisation for non-periodic textiles as well as an inability to quickly model realistic T-joint textile geometries. The aim of this work therefore is to bridge the gap between new methods of automatic modelling and meshing for 3D woven composite T-joints and the use of optimisation algorithms to find better 3D weave designs to be able to explore the design space and find weave variations that maximise the design potential from the underlying woven architecture.

Chapter 3 - Experimental Investigations of T-Joint Weave Specimens

3.1 Introduction

The literature review in the previous chapter revealed there is limited research into the fabrication and testing of 3D woven T-joints. This may be due to several factors including the expense of 3D weaving looms and the long lead times required to set them up for bespoke weave designs. In this chapter, the designs and fabrication of two types of 3D woven T-joint specimen, the collection and analysis of CT images and finally their behaviour under tensile pull-off test is set out.

In the context of the work presented in this thesis, the best time to complete this experimental work would be after the final T-joint optimisation. The optimised weave designs could have been made and experimentally tested to directly validate the results of the finite element simulation. Unfortunately, the cost and time to produce weave variations meant that it was not feasible to manufacture the optimised weave designs. In its place two woven preform specimens were provided by Sigmatex ltd., alongside their weave pattern drafts, to be μCT scanned, infused using RTM and used in the tensile pull-off test. By request, one of the T-joint preforms from Sigmatex exhibited weft yarn crossover while the other did not. While the results from the T-joints made using these weave reinforcements are unable to directly validate the finite element work and the results of the optimisation, they can provide additional tensile pull-off test data to aid the interpretation of the results from the final optimisation of the T-joint weave design.

The literature review also revealed that earlier work has used μCT tomography to image geometrical features shown in T-joint reinforcement weaves. These showed that the weft yarns within the junction region will nest and their cross-section shape tends towards being circular. Further μCT data presented in this

chapter can provide further validation to that result, which will then be applied to the automatic geometry modelling in the later chapters.

3.2 Methodology

The experimental investigations into the T-joints were formed by two parts. The first part was to characterise the weave patterns of the two types of woven preform including their weaving patterns and yarn section geometries (described in section 3.3). The samples were μCT scanned to view the internal geometry of the weaves and observe how the yarn geometry changes within the junction region of the T-joint and whether there is any nesting effect of the weft yarns (section 3.4). The second part is the manufacture (section 3.5), and tensile pull-off testing (section 3.6) of the composite T-joints to determine their stiffness, initial failure load and ultimate tensile strength.

The woven preforms were supplied as 500mm long pieces of fabric with the width being the sum of the lengths of the preform web and flange before being unfolded to form the T-profile (approximately 150mm). To obtain good quality resolution μCT images, the woven preforms needed to be cut down from the supplied widths to more appropriately sized samples. The resolution of μCT images is inversely proportional to the volume of the sample being imaged. The final samples were mounted in Perspex containers to hold them in the opened out position. After the μCT images were taken, the image processing software imageJ was used to measure the yarn sizes at different regions of the T-joint. The images were also used to view the change in yarn cross-section shape and the nesting arrangement.

To prepare the composite T-joints for RTM, a mould tool was designed and made for the different preforms. The resin was then fed into the mould tool by gravity feeding. Curing occurred at room temperature and pressure.

The final T-joint samples for tensile testing were cut from the finished moulded parts and tested by displacement controlled loading in an INSTRON tensile testing machine. Due to time constraints Digital Image Correlation (DIC) was

unable to be used to view the strains on the profile face of the T-joint. The initial failure load can be seen from load drops in the load-displacement graph and the stiffness and ultimate tensile load can be calculated from the load curve's gradient and first maximum respectively. The following sections will set out how each of the above processes was carried out in more detail.

3.3 T-Joint Preform Weave Patterns

Two T-joint weave specimen designs were provided by Sigmatex Ltd, they were woven using Hexcel IM7 12k filament tows.

(a) (b)

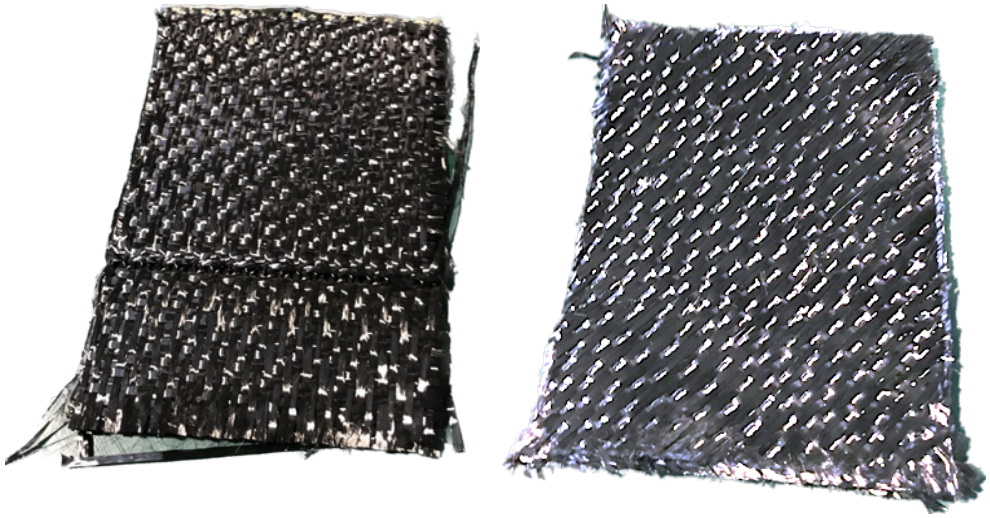

Figure 3-1 (a) Specimen 1 3D woven T-joint reinforcement textile exhibiting straight yarns. (b) Specimen 2 3D woven T-joint reinforcement textile exhibiting axial yarns.

The first specimen (specimen type 1) had a layer-to-layer weave pattern with 8 weft layers in the web of the T-joint, splitting into 4 weft layers in the flanges (see Figure 3-2). In the web the 6 binder yarn layers are grouped into a set of 4

layers with a layer spacing before a further set of two binder yarn layers. (see Figure 3-3).

(a)

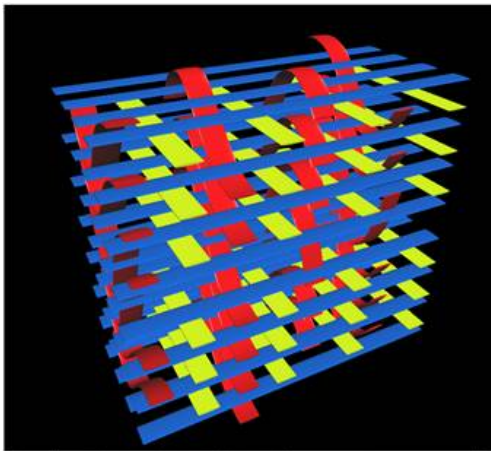

(b)

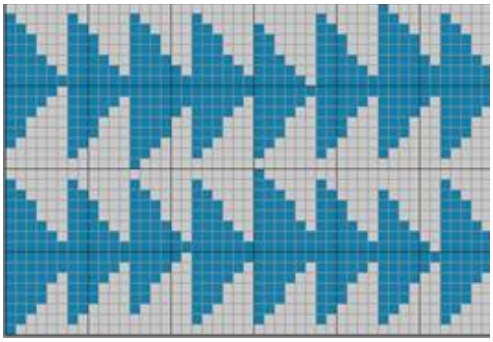

(c)

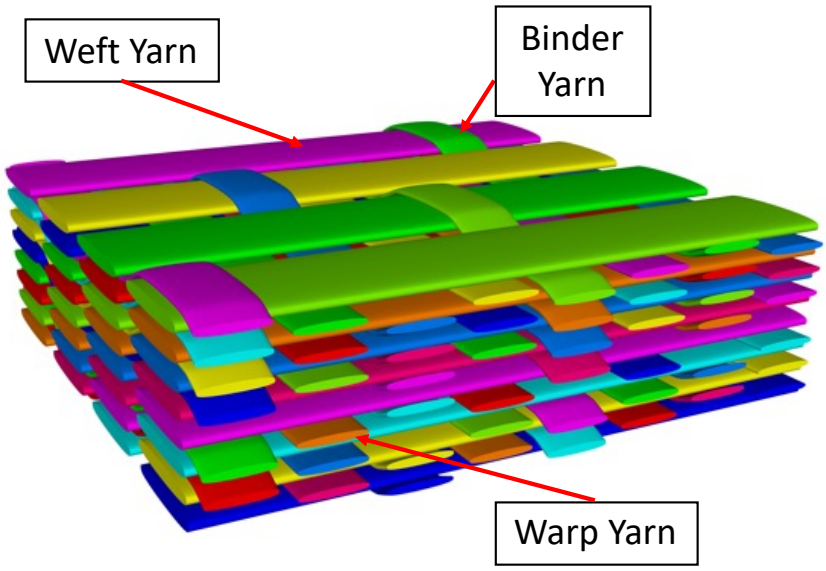

(d)

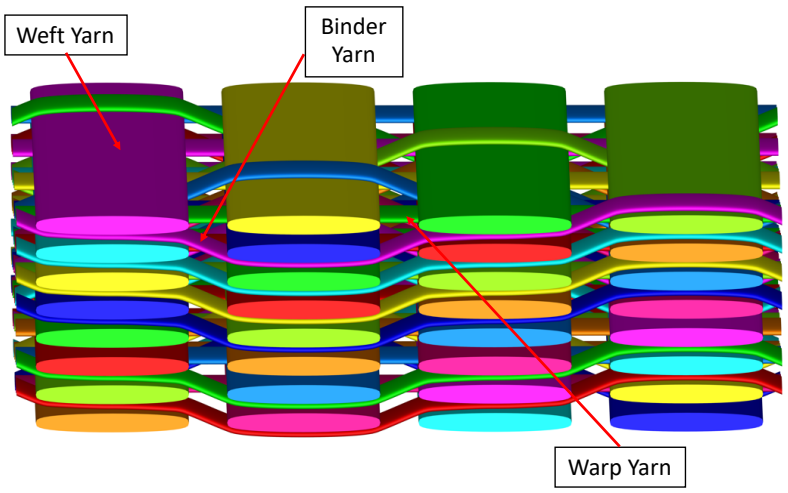

Figure 3-2 Pre-Bifurcation weave design for specimen type 1, forming the web of the T-joint. (a) Model of weave as provided by Sigmatex. (b) Textile pattern draft. (c) TexGen model of weave (d) Side view showing binder yarn paths with four binder layers, a space, then 2 more binder layers. Images (a) and (b) Provided by Sigmatex.

(a)

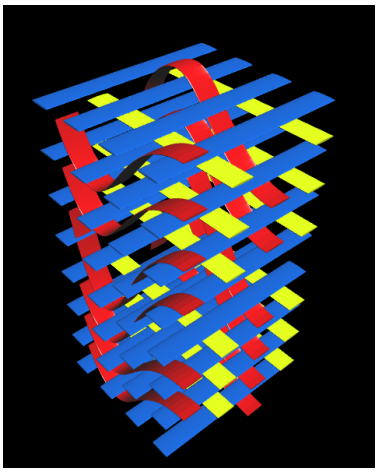

(b)

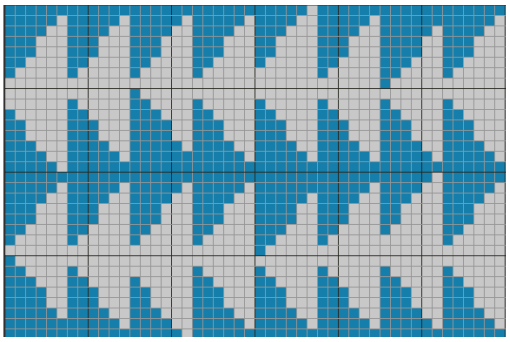

Figure 3-3 Post-bifurcation weave pattern for specimen type 1. (a) Model of the weave pattern. (b) Textile pattern draft. Images provided by Sigmatex.

A layer in the fabric is left unbound by the undulating binder yarns to form the bifurcation. The pattern draft, which shows the number of warp layers lifted for weft insertions, shows that before and after the bifurcation the weft yarns have shifted layers at the junction region by crossing over from one half of the textile to the other. For more information on reading pattern drafts see Chapter 5.

The second specimen (specimen type 2) was an axial layer-to-layer fabric with the warps and binders in the +45º and wefts in the -45º direction, again with 8 weft layers (see Figure 3-4). This gave the dry fabric a flexible feel when handling with the material able to shear easily. This would make it a good candidate material configuration for T-joints with curvature or where they need to drape over a curved part.

(a)

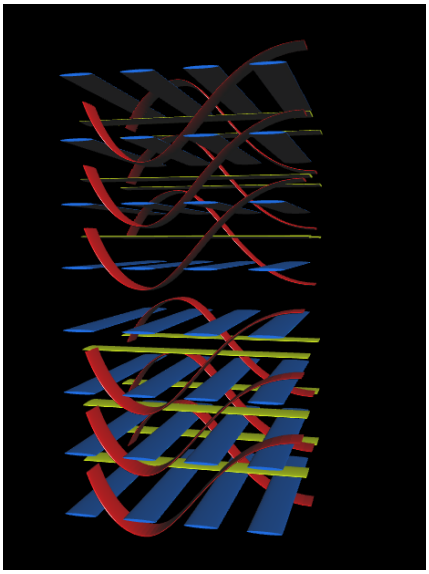

(b)

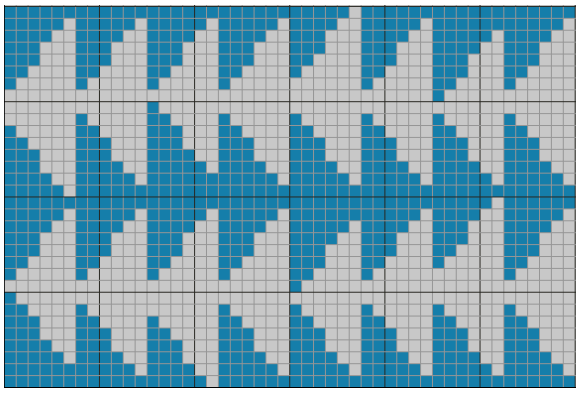

(c)

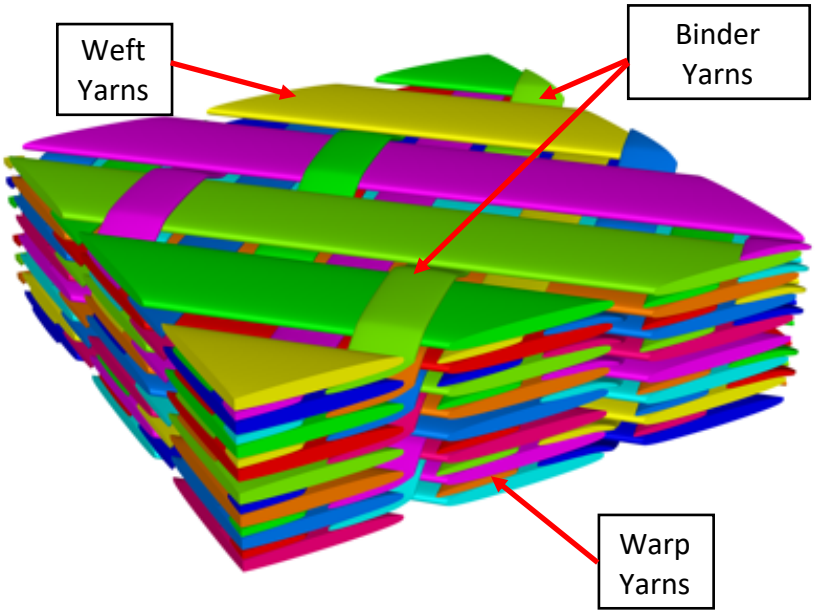

Figure 3-4 Weave pattern of the web for specimen type 2. a) Model of the weave pattern. (b) Textile pattern draft. (c) TexGen model of weave showing binders and warp yarns at +45.

3.4 T-Joint Specimen CT Imaging

Previous studies [58] have shown that the geometry of the weave along with weave pattern variations at the junction can have a strong effect on the mechanical properties of the final composite T-joint. To verify the geometry of the models generated later in this thesis, the weave specimens were CT scanned so that the internal geometry of the weaves could be used to provide more accurate measurements for the geometry models. Each weave specimen was encased in a Perspex fitting to be scanned in a µCT scanner, the purpose of this was to hold the material still in the opened out position. Dry fibre samples were cut using a pneumatic air cutter. Cutting the dry fibre samples was difficult because of the thickness and shearing of the material so longer lengths of fabric were used for scanning. This was to retain an unsheared region far from the cut textile edges. This limited the resolution of the scanned images.

CT slices were taken horizontally from the top of the T-joint weaves at intervals of 330µm. These were then loaded into the image processing software imageJ [87] for analysis.

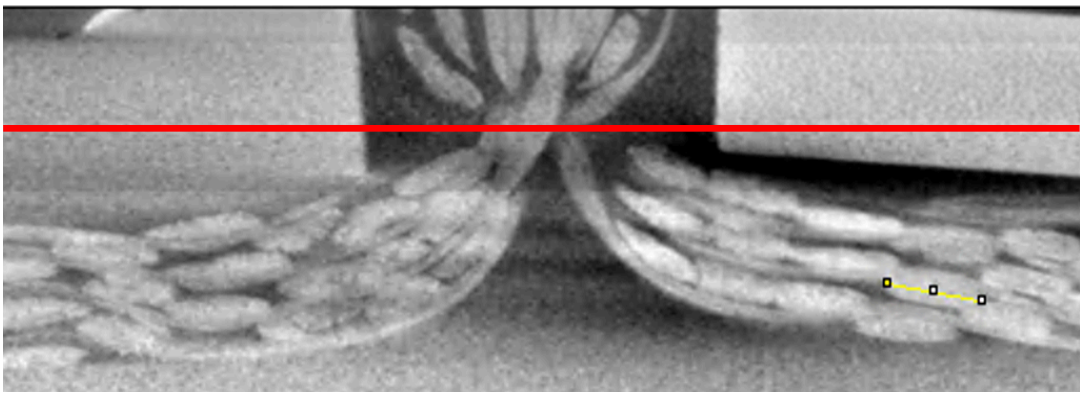

Figure 3-5 Orthogonal view of CT image of T-joint weave specimen 1, reconstructed using imageJ. Weft yarn crossover can be observed at the junction. The yellow line shows how the line tool is used to measure yarn dimensions. This yarn has a width of 1.42 mm. The red line is the slice in the x-z plane where the CT image in Figure 3-5 is taken.

Horizontal CT slices were used to measure the cross section shape and size of the weft yarns in the web portion of the T-joint weaves (see Figure 3-5). These will be used to provide yarn dimensions in the geometry models. Due to the inherent variability of the yarns, their cross section and shape vary along their length. To get a more accurate measurement, the wefts were measured across several slices, separated from each other by 5 slices, and the average taken.

A sample of yarns were chosen from the cross section to be measured. The size of each pixel was calibrated using the on screen ruler scale, and lines were drawn between each yarn boundary to find the width and height. The weft yarns at the top and bottom surfaces have different section shape and size compared to the internal yarns. From a visual standpoint, the internal yarns are narrower with an increased thickness, and this is reflected in the measurement data. This

is presumably because of the increased compaction force these yarns experience from the binder yarn layers and the surrounding yarns. To capture this difference, multiple internal and surface level yarns were chosen for measurement.

	Internal Yarn 1		**Internal Yarn 2**		**Internal Yarn 3**		**Top Yarn 1**		**Top Yarn 2**		**Bottom Yarn 1**		**Bottom Yarn 2**	
CT slice	Width (mm)	Height (mm)	Width (mm)	Height (mm)	Width (mm)	Height (mm)	Width (mm)	Height (mm)	Width (mm)	Height (mm)	Width (mm)	Height (mm)	Width (mm)	Height (mm)
280	1.47	0.65	1.35	0.53	1.45	0.46	2.28	0.35	2	0.48	1.59	0.43	1.87	0.37
285	1.39	0.44	1.3	0.48	1.42	0.42	2.34	0.36	2.07	0.48	1.89	0.5	1.99	0.4
290	1.59	0.51	1.46	0.44	1.41	0.39	2.28	0.4	1.99	0.44	1.5	0.49	1.81	0.42
295	1.48	0.5	1.64	0.4	1.41	0.49	2.22	0.44	1.99	0.48	1.69	0.53	1.87	0.31
300	1.48	0.57	1.7	0.45	1.52	0.43	2.34	0.4	1.98	0.44	1.74	0.46	2.06	0.4
mean	1.48	0.53	1.49	0.46	1.44	0.44	2.29	0.39	2.01	0.46	1.68	0.48	1.92	0.38
stdev	0.07	0.08	0.18	0.05	0.05	0.04	0.05	0.04	0.04	0.02	0.15	0.04	0.10	0.04

Table 3-1 Weft yarn dimensions in the flange

Another area of interest from the CT data is the weft positioning at the junction region (see Figure 3-6). CT scans of other T-joint weaves [55] showed that weft yarns crossing over at the junction region showed two interesting geometric features: (a) The weft yarn sections become more circular at the junction region and, (b) The crossing over weft yarns arrange themselves in a nesting pattern as they wrap around each other.

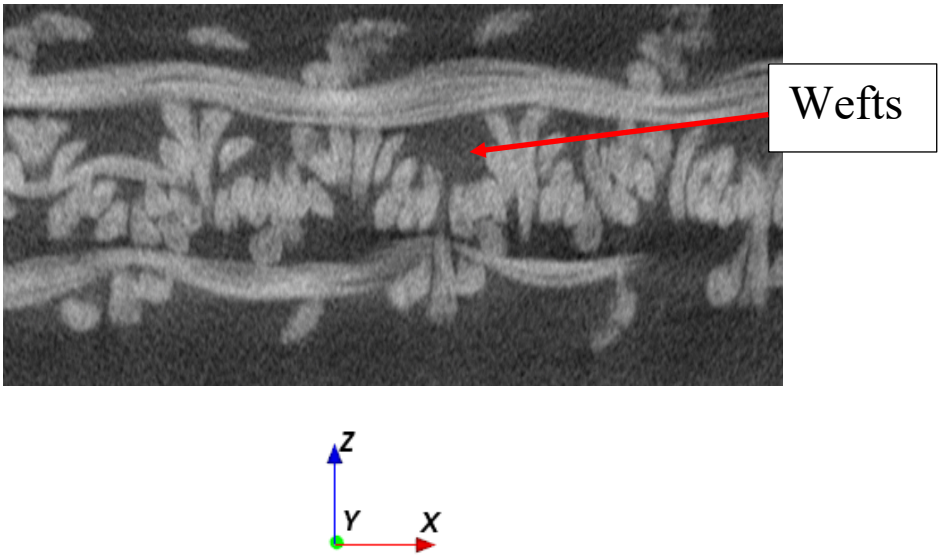

Figure 3-6 CT image of the weft yarns at the junction as they cross over each other as they move from one half of the textile to the other. Wefts crossing over move from top to bottom and vice versa. See Figure 3-4 for location of the CT image slice.

The wrapping moves a portion of the yarns into the junction or noodle area that would otherwise be a part of the bulk matrix region, this has the effect of increasing the overall fibre volume fraction in the local region. This is believed to improve the resistance of the T-joint to failure as this is where stresses in the T-joints are highest. The yarn distribution in the junction region is multi-

directional, this means that on average the crack pathways available are reduced.

3.5 Composite T-Joint Sample Preparation

The samples were moulded in an aluminium mould tool using gravity fed RTM, see appendix A for 2D drawings of the tool. The tool comprised two L shape components, a mould tool cap, a flat plate and spacers (see Figure 3-7). Due to some small differences in the sample sizes, two tools were made using the same base plate.

(a) (b)

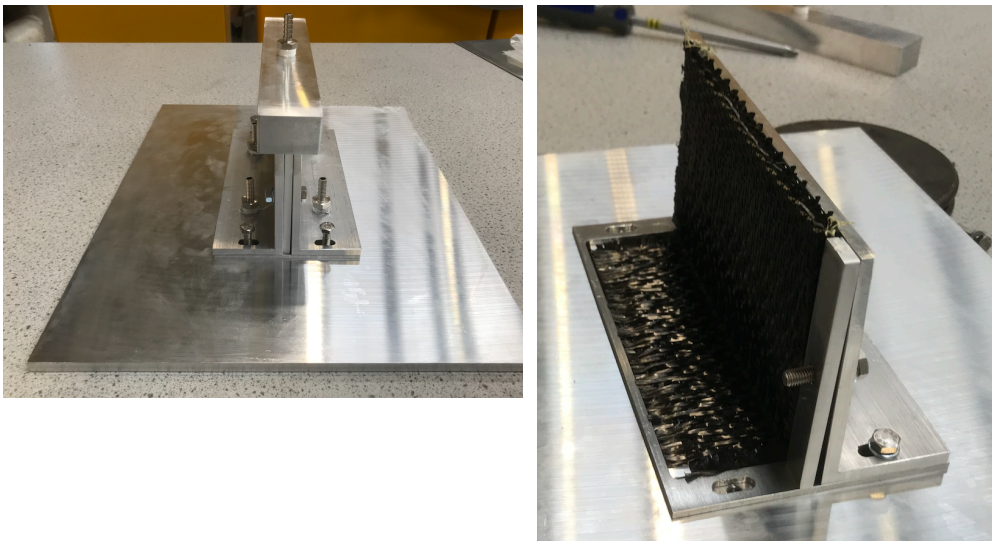

Figure 3-7 Aluminium mould tool for RTM. (a) Mould tool as assembled. (b) Mould tool with the cap and corner piece removed, illustrating how the woven preform sits inside inside.

In preparation for moulding the mould surfaces were cleaned using acetone before application of Frekote-700NC mould release agent using a fibre cloth. This was to ensure that the samples were easier to demould at the end of the process. Each surface was brushed with mould release agent four times

according to the manufacturer's instructions. This process was repeated between mouldings.

The mould was assembled using M3 screws to fasten the spacers and mould surfaces together. The mould was sealed using a mould cap and tacky tape. A vacuum test was performed to ensure that the mould could hold vacuum pressure without leaking. Any gaps that formed in the tacky tape were plugged with the addition of more tape.

The resin used was Gurit Prime 20LV epoxy mixed with extra slow hardener to the manufacturer's instructions. This was chosen so that the resin would be able to infuse the entire fabric without hardening in the resin lines. Before and after mixing both the resin and hardener were degassed using a vacuum pump to remove any dissolved air. The resin bucket was connected to the mould lid via piping and hoisted using string over a high beam to generate the pressure to push the resin into the mould tool's inlets.

As the resin entered the mould, the displaced air caused bubbles to flow from the mould into the resin lines. After a short time, the resin was seen bubbling at the outlet before it started flowing more fluidly with the pressure from the incoming resin forcing it through the mould. Once it was seen that the bubbles stopped flowing in the lines, the mould was tilted to make sure any pockets of trapped air were able to escape through the outlet. The resin inlet was tied off just below the bucket and the mould left overnight for the resin to harden.

Once hardened, the moulded composite was demoulded and placed in the oven to post-cure for another hour at 70º C. Any rough edges or extra resin was sawn off with a hacksaw and filed down with a metal file. Test samples were cut from the length of the demoulded composite, these were chosen to be 30mm wide to ensure they would not slip from the clamps of the testing rig.

3.5 Composite T-Joint Material Characterisation

The T-joint samples prepared using the above process were weighed and the fibre volume fraction calculated. Good wetting of the fabric could be visually observed particularly in the flange and junction region. From weighing the sample composite T-joints, specimen 1 had a fibre volume fraction of 41% and the samples from specimen 2 had a fibre volume fraction of 36%. This is likely to be a low estimate of the true fibre volume fraction across the central part of the T-joint as the preforms generally underfill the mould, leaving resin richness at the flange and web extremes. The second specimen's volume fraction is low because of higher resin richness at the flange ends than for the first specimen (see Figure 3-8). This was not a problem for conducting the tensile tests because these regions were well outside of the span of the tensile testing clamps.

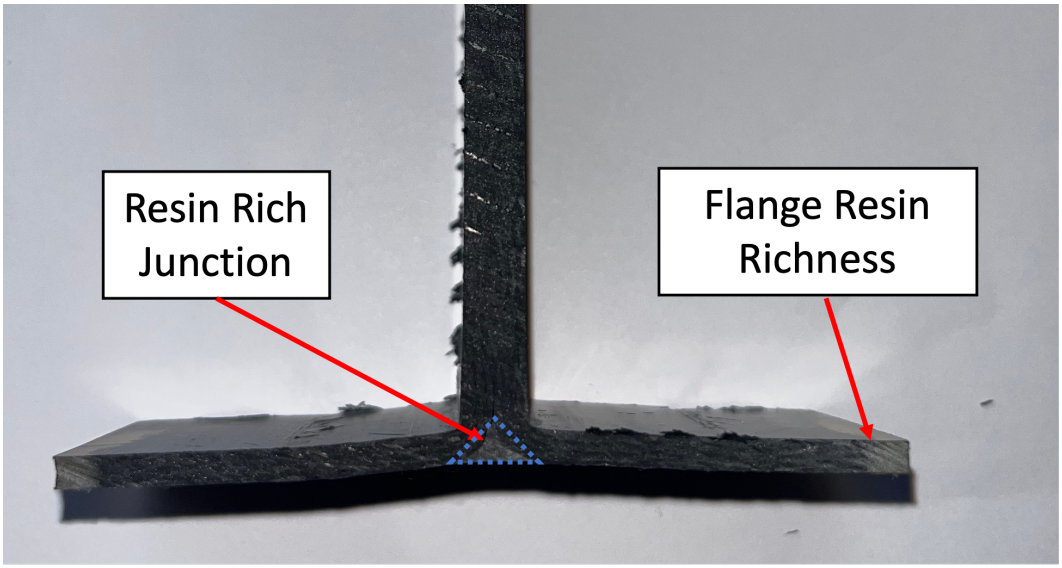

Figure 3-8 Specimen 2 composite T-joint showing both mould underfill and triangular shaped resin rich region at junction base.

The specimen 1 samples had a thickness of 6mm in the web and 2.5mm in the flanges, while specimen 2 samples were 5.5mm thick in the web and 2.5mm thick in the flanges. The T-joint samples made from both specimen weave types

had a triangular shaped resin rich region at the base of the junction. Measured along the base and height of the resin rich region using a ruler, the specimen 1 samples had an average base length of 1mm and a height of 1mm while specimen 2 samples had a much larger average base length of 5mm and height of 2 mm (see Figure 3-8). This corresponds to cross-section areas of 1mm^2 and 5mm^2 respectively. This discrepancy between the two samples was because of the lack of crossover wefts in the specimen 2 samples which resulted in a larger volume of the junction region unfilled by reinforcing fibre.

3.6 T-Joint Pull-Off Testing

The T-Joint samples were tested using a INSTRON tensile test machine to perform the tensile pull-off test. This is a test that is commonly used to characterise the properties of T-joints under tensile loading.

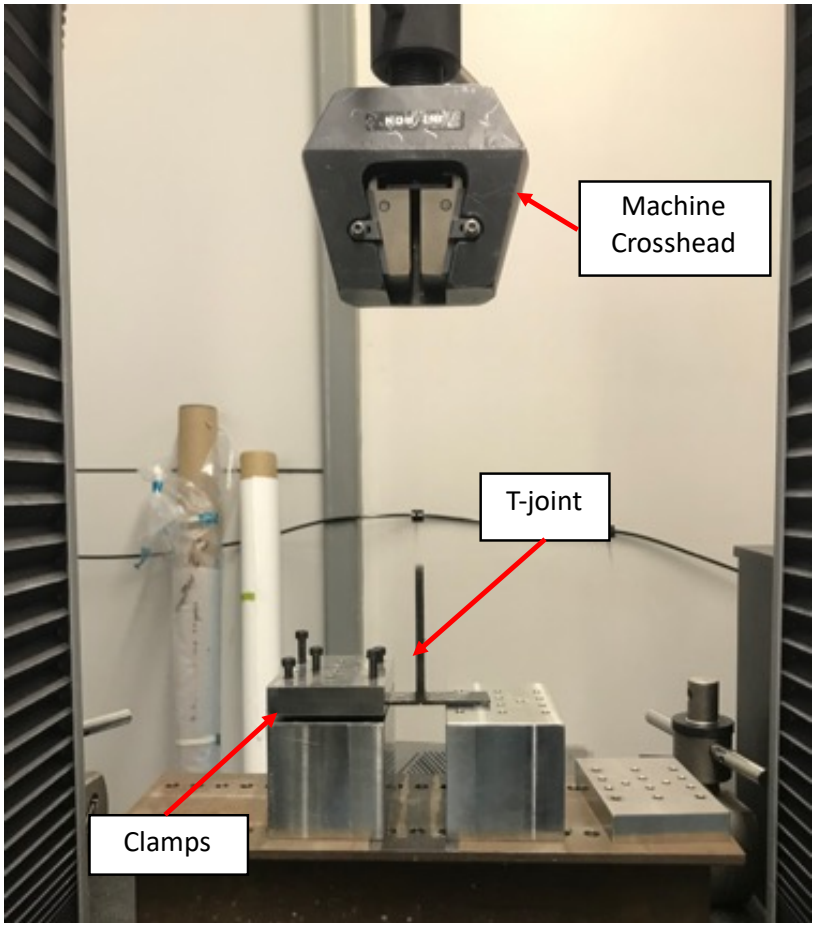

Figure 3-9 T-joint specimen pull-off test set up – T-joint clamped below INSTRON tensile test machine crosshead.

The T-joint flanges were clamped so that the T-joint had a support span of 40mm between the clamps (see Figure 3-9). The web was then clamped to the machine crosshead. The crosshead applied displacement controlled loading to the web of the T-joints, moving at a rate of 1mm/min. The force and displacement at each increment were written to the testing rig computer. Three samples of each joint type were tested.

3.7 Results and Discussion

In this section, the results of the T-joint tensile pull-off tests for both specimen types will be discussed separately before comparing them. The INSTRON testing rig wrote the force-displacement data to the file at intervals of 0.1s. The data was then plotted. The data for the two specimens is analysed separately to compare the results between the sets of coupons from the same specimen. The specimens from the two types are then compared together to draw conclusions about the effect of the variation in weave design had on the mechanical behaviour.

3.7.1 Specimen 1 – Straight Wefts with Crossover

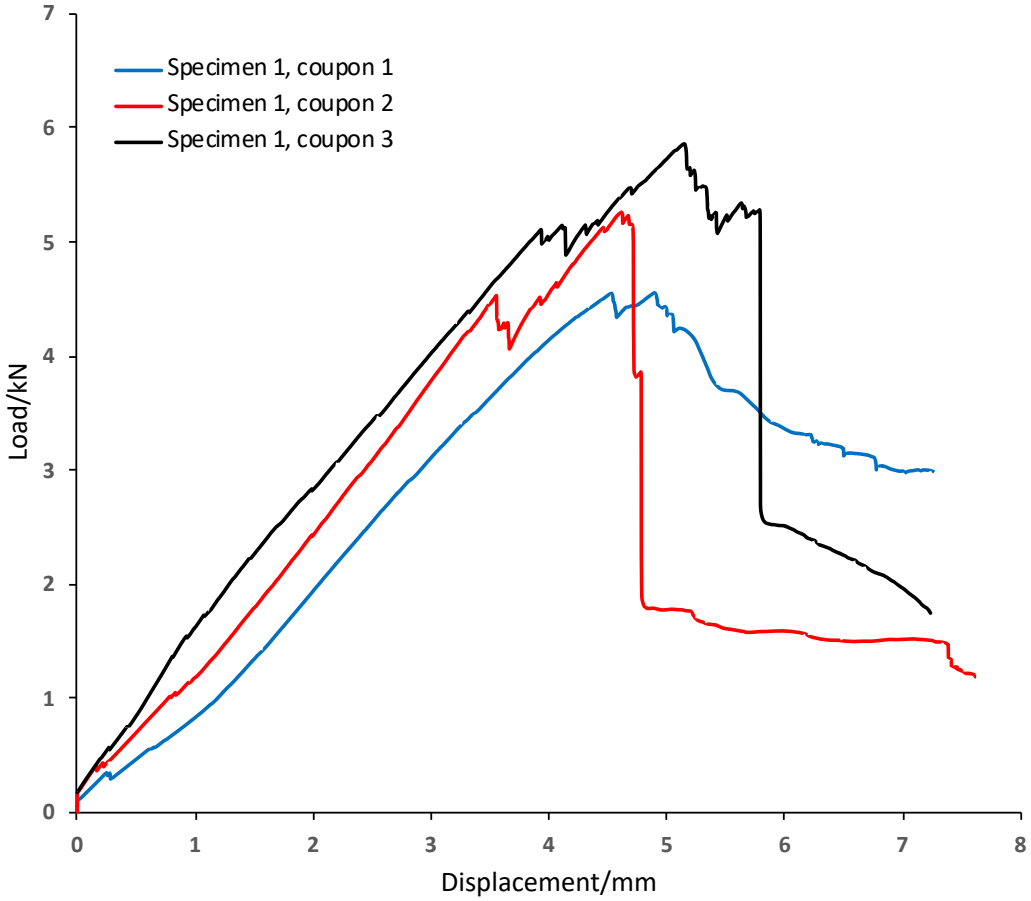

Figure 3-10 Load-displacement graph of specimen 1 coupons (straight wefts) under tensile loading.

For specimen 1, (see Figure 3-10) the T-joint coupons deform elastically until initial failure by matrix cracking in the junction region at a displacement of approximately 3.5-4.5 mm, corresponding to a load of above 4000N for all three specimens. Prior to the initial failure, small drops in the load were accompanied by audible acoustic emissions suggesting the initial formation of cracks. However, because the load reduction is small and there is no appreciable change in the load-displacement gradient these can be discounted as initial failure points.

All samples continued to deform until the peak load is reached. The samples reached measured peak loads between 4560 and 5862N. At this point large matrix cracks could be observed at the junction region, both internally and at the 90º angles between the web and flanges. For coupon 1, the load reduced until the test was stopped. Final failure for this coupon was determined to be from matrix cracking which was visible in the sample (see Figure 3-11).

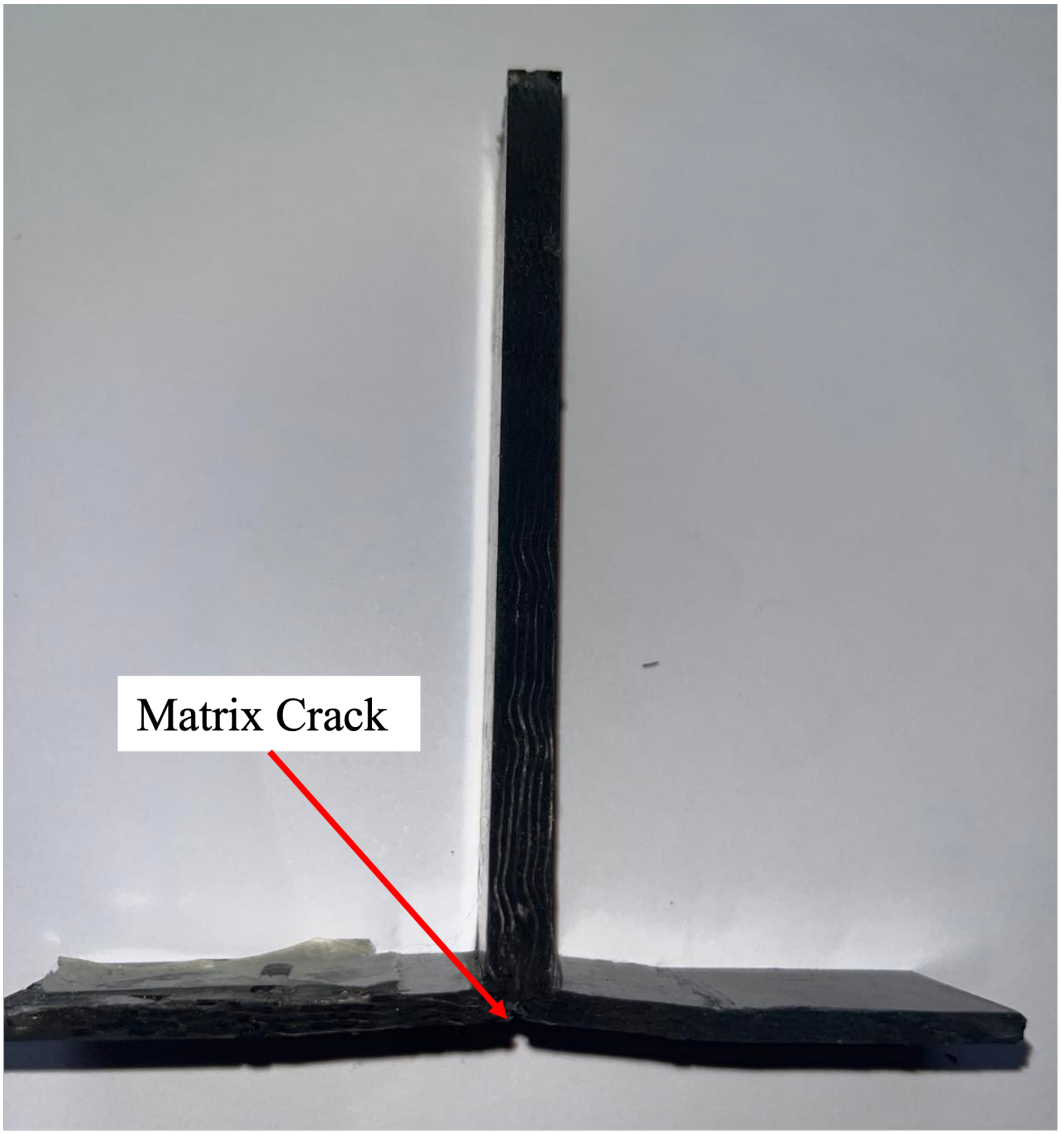

Figure 3-11 T-joint specimen 1 coupons after tensile pull-off test. Coupon 1 showing matrix cracking from base of junction region.

For coupons 2 and 3 some different behaviour can be observed after the peak load was reached. Matrix cracks were also observed at the junction region until the peak load was reached but the ultimate failure of these joints was due to the failure of the flanges at the clamps (see Figure 3-12).

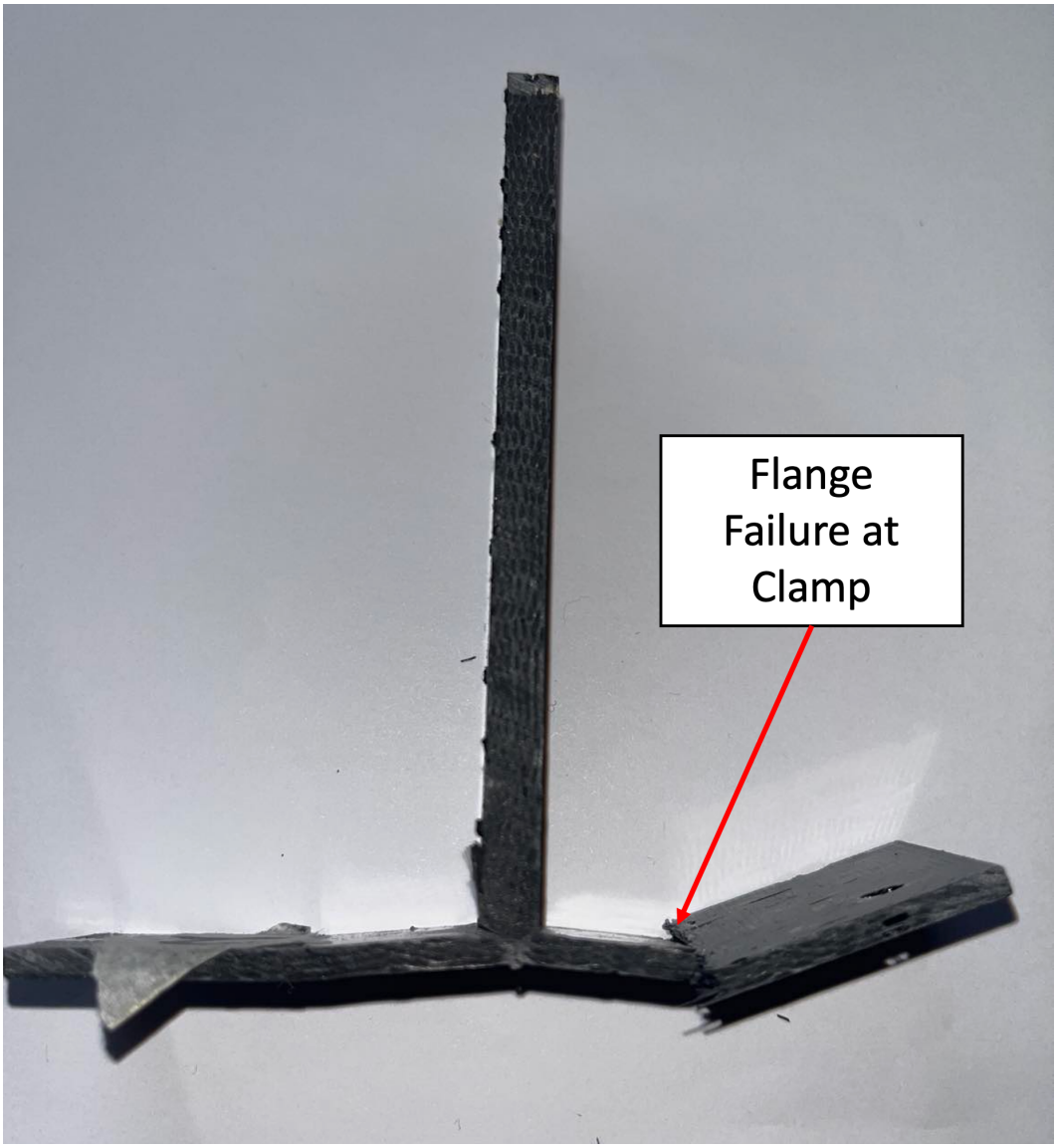

Figure 3-12 T-joint specimen 1, coupon 2 after tensile pull-off test. Coupon 2 showing failure at flange.

This was probably due to the clamping force being too high, compressing the flanges and weakening them. This may also account for the disparity in peak loads reached between specimens, with slippage changing the angle the load was being applied to the junction. This is substantiated by the fact that coupons 2 and 3 both reached peak loads greater than that achieved by coupon 1.

3.7.2 Specimen 2 – Axial Fabric with no Crossover

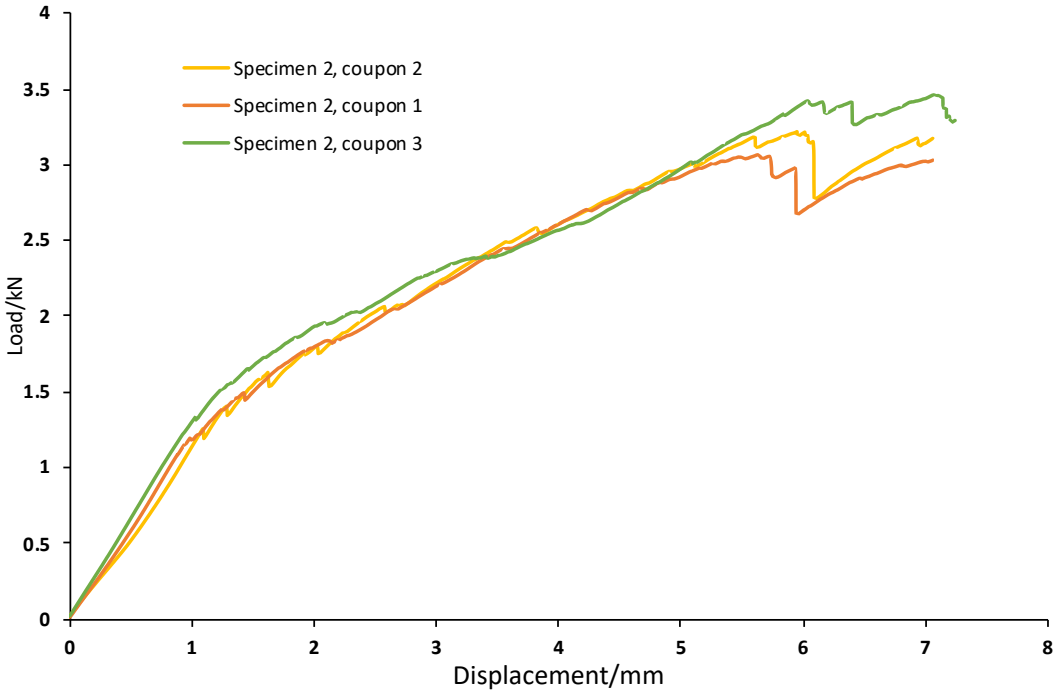

Figure 3-13 Load-displacement graph for specimen 2 coupons under tensile pull-off load.

The behaviour of the specimen 2 T-joints under tensile load was more consistent than Specimen 1 and initial failure occurred at a displacement of about 1 mm (see Figure 3-13). However, after this they displayed a reduced stiffness and were unable to sustain the same levels of load as the Specimen 1 coupons, reaching values between 2944 and 3309N. Large matrix cracks were

visible extending from the base of the resin rich junction region into the web for all three coupons (see Figure 3-14).

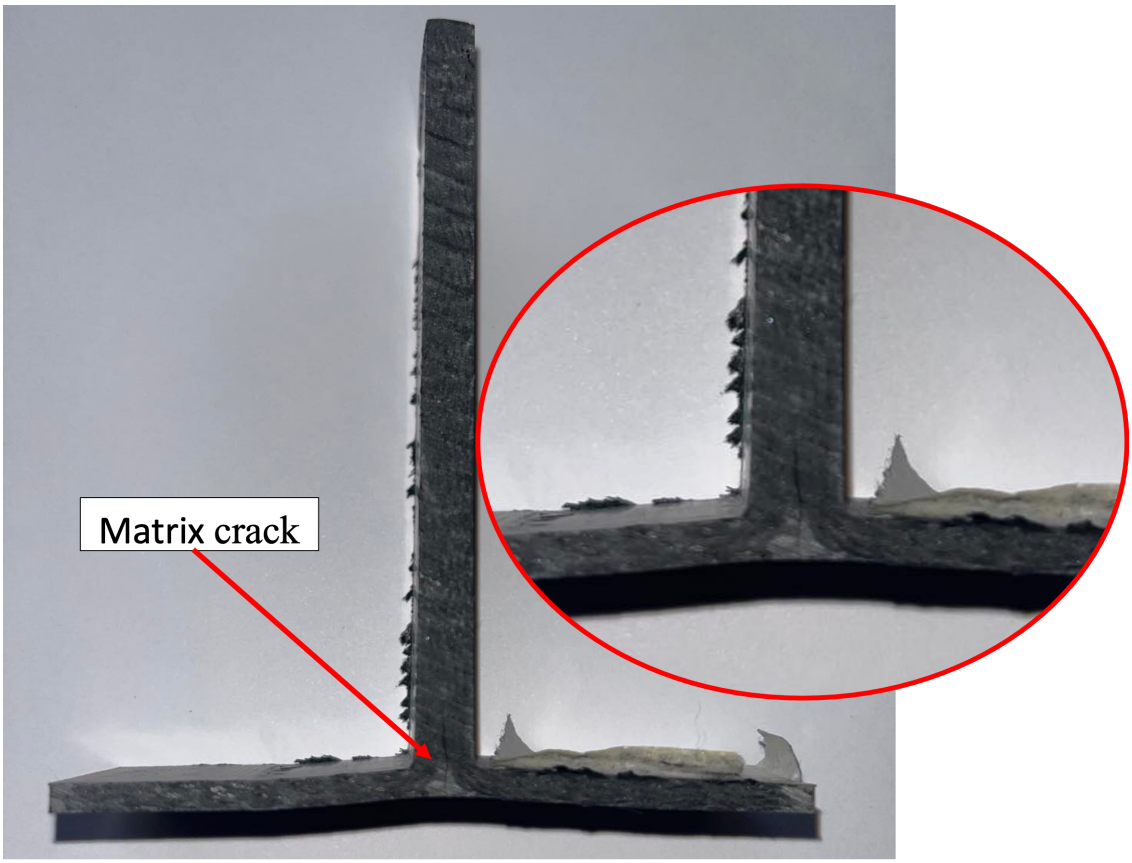

Figure 3-14 Specimen 2 coupon showing visible crack from base of resin rich junction region.

Several factors are responsible for the reduced stiffness and lower strengths: (a) There was no yarn crossover for this specimen resulting in a much larger resin rich region at the junction and (b) The axial yarns mean that there are fewer yarns aligned with the loading path. Final failure occurred by cracking at the junction.

3.7.3 Comparison of Specimen Types

Both T-joints were similarly thick specimens with similar volume fractions but produced different behaviour under tensile loading. Even though the two

specimens were different in terms of the directions of the warp and weft yarns, it could be noted that the weft crossover provides significantly increased overall resistance to the ultimate failure of the T-joint (see Figure 3-15). The initial failure loads from the T-joints made from specimen 2 with the axial weft yarns were lower than those of specimen 1.

The force-displacement behaviour between the specimen 2 samples was uniform where there was no failure at the flanges. This provides further evidence that the disparity between the specimen 1 types was due to the slippage and failure observed in coupons 2 and 3.

It was noted that the main failure mode for the coupons from both specimens seemed to be matrix cracking that began in the resin rich junction. It is relevant, therefore, that the resin rich regions of the specimen 2 coupons without any junction crossover are 5 times larger than the resin rich regions of the specimen 1 coupons. The reduction in the strength for the specimen 2 coupons suggests that the larger resin rich junction region acts as an inherent stress raiser. This, combined with the fact that the load bearing axial yarns are non-aligned to the load path, would explain the lower initiation load for the specimen 2 coupons.

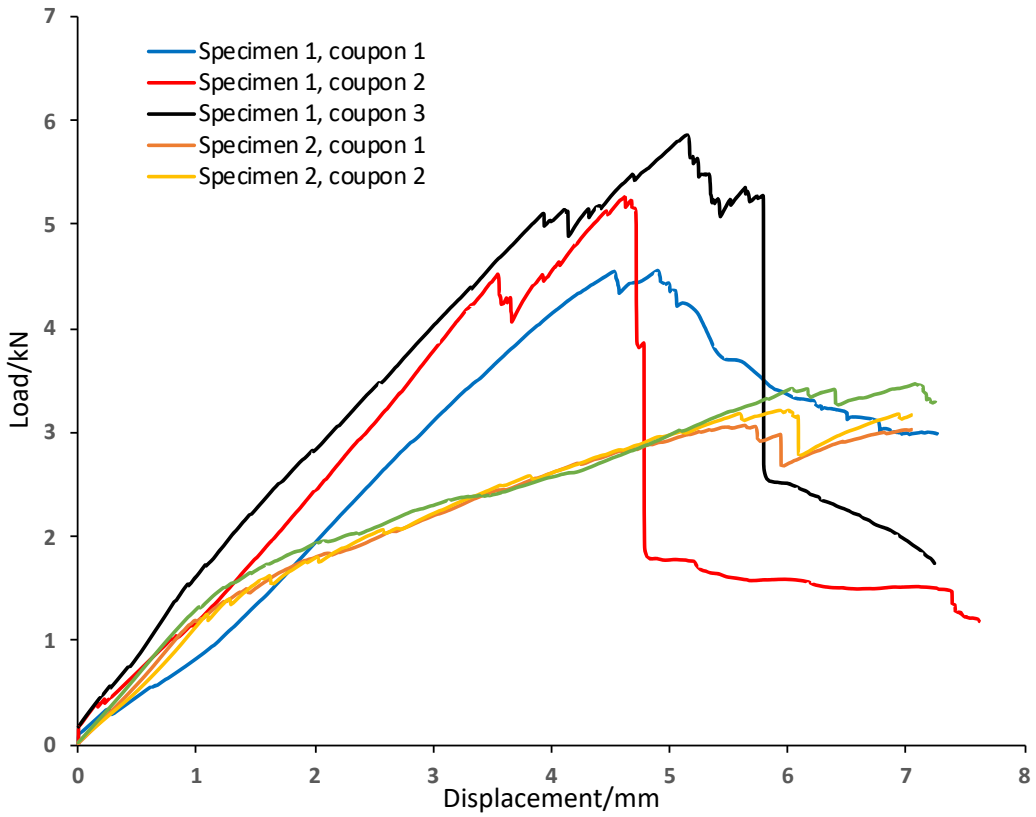

Figure 3-15 Load-Displacement graphs combined for specimen 1 and 2 coupons under tensile pull-off load.

Furthermore, the results from both specimen types would suggest that the level of displacement that the joints can sustain before the initial formation of cracks is low, though this is offset by the high initial stiffness.

The results from this chapter will contribute to the analysis of the optimisation by providing further information on how 3D woven T-joints made with weave patterns of different types behave under tensile pull-off load, in particular the location of the initiating cracks. It established that the size of the resin rich junction region is an important factor in determining the initial failure load of T-joint specimens. Furthermore, it will aid in understanding the role of weft yarn crossover on tensile pull-off behaviour.

3.8 Conclusions

This chapter discussed the experimental investigations into the behaviour and geometry of two weave pattern designs. First, CT scanning was performed to evaluate the internal geometry of the two 3D woven reinforcements. The CT scan of the straight yarn weave pattern, specimen type 1, showed the features of weft yarn nesting and circular sections at the junction region where crossover occurred. Weft yarn sections were measured using imageJ. The information obtained here will be used to inform the geometry modelling in Chapter 5.

Next, composite T-joint specimens were prepared before undergoing the tensile pull-off test in an INSTRON tensile testing machine. The results of the testing was presented. It was found that for specimen 1 with the straight weft yarns, initial failure began at a displacement of approximately 4mm, corresponding to a load of over 4000N for all samples. With ultimate failure caused by matrix cracking in the junction for the first coupon and a combination of matrix cracking and flange breakage for the second two coupons.

For specimen 2, with axial yarns and no weft yarn crossover, initial failure was caused by matrix cracking in the junction region at a displacement of approximately 1mm corresponding to a loading force of 1200N, significantly weaker than the specimen 1 weaves. With final failure occurring because of matrix cracking in the resin rich junction.

Chapter 4 - Optimisation of 3D Woven Textile Weave Patterns considering Delamination

4.1 Introduction

The purpose of this chapter is to evaluate the effectiveness of several optimisation techniques including the choice of algorithm and modelling methods, specific to 3D woven structures. Flat panel unit cell models of 3D weaves were chosen as case studies because of their relative simplicity in design and problem size in comparison to 3D woven T-joint models and because the web and flanges of T-joints are each made up of periodic flat weaves. The periodicity of the flat woven parts of the T-joint means that the methods of evaluating flat weave designs for feasibility developed here could be applied to the web and flanges of T-joint models in optimisations.

The objective function of an optimisation is the property to be minimised subject to constraints. In this work, this function is evaluated using finite element analysis. The meshing of the model, load application, analysis submission and post-processing of the results all need to happen automatically without user input. A drawback of this approach is the computational cost of each function evaluation call.

Matching node sets are required for the application of periodic boundary conditions to find elastic properties. When meshed using voxels, this is a straightforward process as all the elements are the same shape throughout the mesh. The first part of this chapter will deal with optimisations of 3D woven composite elastic properties. Different types of heuristic algorithms are used to compare their suitability to 3D woven optimisation. These algorithms are chosen over gradient based algorithms due to their ability to escape local minima and applicability to the discrete design space. An additional outcome of this work is a tool implementing new rules to evaluate the binder yarn configuration for weave feasibility. This tool can be used to reduce the number of weave designs that do not meet the feasibility criteria from being run through the finite element part of the objective function evaluation.

Binder yarn path can affect the in-plane elastic properties of woven textiles, with the volume of yarn oriented in the z-direction the dominant factor in through-thickness properties [10], [34]. However, the yarn path can also have a significant impact on the delamination [88] properties of composites made with 3D woven reinforcements. The finite element analysis time for models using cohesive surfaces to model delamination is much longer than the models using periodic boundary analysis to find elastic properties. As a result, 3D woven models have not been optimised for their resistance to delamination in the past. The first part of the chapter will inform the selection of the algorithm used in the second half along with the new methods using the feasibility constraint tool to mitigate for the longer finite element analysis time. The purpose will be to optimise 3D weave unit cell models for their peak load under through-thickness load.

In this chapter, three optimisation algorithms will be implemented to optimise a flat woven textile using the binder yarn paths and the number of binder layers as the design variables. This is due to their effect on the volume of yarns oriented in the z-direction. Details of the implementation will be found in section 4.3 along with the results which will be used to select the optimisation algorithm to use for more expensive function evaluations. Details of the delamination optimisation will be given in section 4.5. The best performing algorithm will be used to demonstrate optimisation of an idealised subcomponent of a T-joint, the flange, for resistance to yarn delamination under an idealised uniform through the thickness loading. A High Performance Cluster (HPC) will be used because of the high computational cost of generating and running the finite element models.

4.2 Optimisation Algorithm Comparison

Global search algorithms including the genetic algorithm, particle swarm and the pattern search algorithm will be implemented and compared for best

performance. The optimisation is implemented using the Matlab optimisation toolbox [67].The optimisation problem is posed as:

$$Minimise\ f(\boldsymbol{x}) < 0$$

where the objective function 'f' is the through-thickness stiffness of the 3D woven composite and the vector of design variables '$\boldsymbol{x}$' is the binder yarn offsets from the top textile layer that define the binder yarn path. The optimisation is subject to linear constraints:

$$c.(\boldsymbol{x}) \leq 0$$

where the constraints 'c' are the linear constraints that must be satisfied at every interval. In this case they are combinations of the yarn offsets that when satisfied rule out the case where the binder yarns lie floating above or below the textile, not interlacing with the wefts. See section 4.3.3 for more details.

The design parameters in the optimisation for the geometry are integer valued, the positions of the binder yarns in the weft stacks. This means that any optimisations must be mixed integer optimisations. An initial investigation showed that through-thickness stiffness was sensitive to changes in the binder path and therefore was an appropriate candidate for the objective function.

Each of the following algorithms generate a set of design variables which are written as a set of parameters to a simple .dat file (see Figure 4-1). The *GenerateTextile* Python script reads these values and, using the University of Nottingham's textile geometry modeller TexGen [18], builds the geometry of a parameterised weave and then meshes it using a voxel mesh [84]. These models are then automatically submitted to Abaqus for finite element analysis, the output from which is used to calculate the objective function value. Constraint checking is done by the *CheckBinderPaths* Python script. If there is constraint violation, the objective function value is assigned to a value based

on the level of violation. These objective function values are then used by the algorithms to decide which weave designs to evaluate next, based on the internal methods of each algorithm.

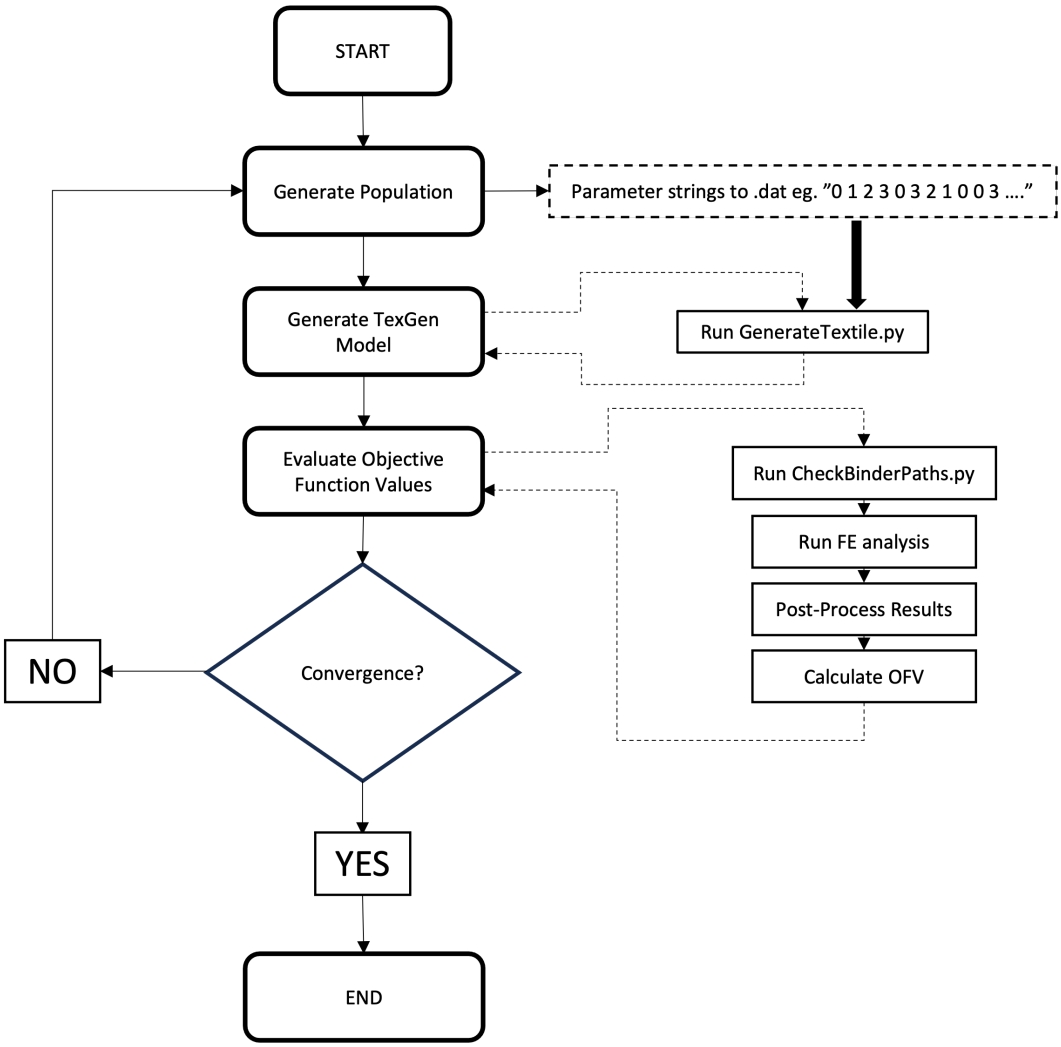

Figure 4-1 Flowchart showing the optimisation process. Subprocesses are denoted by the dashed arrows.

4.3. Optimisation Implementation and Performance

4.3.1 Generating the Geometry and Meshing

In this chapter, the geometry being modelled is the meso-scale fibre architecture in the flange of the T-joint. This part of the T-joint is analogous to a flat woven textile made up of the warps and binders and the wefts inserted orthogonally to the warp/binder direction. The warp and binder yarns are aligned with the local material x-axis and so can be grouped together as X yarns.

A Python script is used to read in the parameters from the "parameter.dat" file. The Python script uses the parameters to set the binder yarn offsets and the number of binder layers which are used to generate a parameterised model using the TexGen CTextileLayerToLayer() base class (see Table 4-1).

Parameters of CTextileLayerToLayer Class	
Number of Warp/Binder Yarns	6
Number Weft Yarns	6
Number of Binder Layers	1
Warp/Binder Spacing	3.8
Weft Spacing	3.8
Warp Height	0.5
Weft Height	0.5
Warp Width	3.0
Weft Width	3.0

Table 4-1 Geometric properties of the parameterised textile used as inputs to the *CTextileLayerToLayer* class.

The Python script used to generate the textile and its mesh can be found at the link contained in appendix B.

One of the challenges of the optimisation of structures with complex geometries, such as 3D woven textiles, is automatic creation of the finite element mesh. Due to the complex geometry, it is difficult to create a conformal mesh that does not generate highly distorted elements along yarn-matrix boundaries, especially where yarn boundaries come close together. Voxel meshing [84] is particularly useful for predicting the elastic properties of woven composites and has been shown in [21] to be effective for delamination analysis where normal stresses are the dominant factor, but less applicable in the presence of large shear stresses.

A sensitivity study to find the best voxel size for the elastic property models was conducted using the periodic boundary conditions analysis discussed in the next section (see Table 4-2). Using the geometry parameters for the yarns in Table 4-1, the maximum mesh size was found by experimentation to be 0.12mm or 110 voxels before the binder yarns failed to be fully captured with gaps in the mesh along the length of a yarn. Cubic voxel elements were used before trying double the number of through-thickness elements to capture the yarn cross-sections more faithfully, resulting in cuboidal elements with a 2:1 length to through-thickness height aspect ratio.

NumXVoxels	Ex/Pa	Ey/Pa	Ez/Pa	Vxy	Vxz	Vzy
110	2.465E+10	6.463E+10	6.909E+09	0.031	0.417	0.043
120	2.741E+10	5.926E+10	6.883E+09	0.033	0.422	0.048
130	2.748E+10	6.229E+10	6.997E+09	0.032	0.418	0.045
140	2.693E+10	5.980E+10	6.935E+09	0.033	0.422	0.047
150	2.579E+10	6.193E+10	6.961E+09	0.032	0.420	0.045
160	2.680E+10	5.960E+10	6.953E+09	0.033	0.422	0.047
170	2.564E+10	5.926E+10	6.910E+09	0.033	0.424	0.047
110Zx2	2.715E+10	6.167E+10	6.910E+09	0.032	0.422	0.046
120Zx2	2.668E+10	6.116E+10	6.912E+09	0.032	0.422	0.046
130Zx2	2.625E+10	5.969E+10	6.873E+09	0.033	0.424	0.047

Table 4-2 Results of the periodic boundary condition mesh sensitivity study.

For obtaining elastic constants it seems from the results in the Table that there is not an effect from increasing the mesh density at these mesh sizes. Therefore, a mesh size with 140 voxel elements along the length of the model was chosen for speed of simulation and to be sure yarn geometry would remain continuous regardless of the binder configuration. Each finite element analysis using this mesh takes 13 mins on a desktop PC.

4.3.2 Periodic Boundary Condition Finite Element Models

At the microscale, each carbon fibre tow is made up from resin impregnated bundles of fibres. It is too computationally expensive to model each fibre individually in mesoscale models so in TexGen the yarns are considered to be homogenised with transversely isotropic effective material properties and an intra yarn volume fraction. The effective material properties can be obtained from a microscale finite element analysis where the input is the individual constituent properties or from measured values [89]. This means that each yarn can be modelled at the mesoscale as an individual, transversely isotropic

unidirectional composite. The constitutive equations governing the stress-strain relationship for the yarns are:

$$\begin{bmatrix}\varepsilon_{11}\\ \varepsilon_{22}\\ \varepsilon_{33}\\ \gamma_{12}\\ \gamma_{13}\\ \gamma_{23}\end{bmatrix} = \begin{bmatrix} \frac{1}{E_1} & \frac{-\upsilon_{21}}{E_2} & \frac{-\upsilon_{31}}{E_3} & 0 & 0 & 0 \\ \frac{-\upsilon_{12}}{E_1} & \frac{1}{E_2} & \frac{-\upsilon_{32}}{E_3} & 0 & 0 & 0 \\ \frac{-\upsilon_{13}}{E_1} & \frac{-\upsilon_{23}}{E_2} & \frac{1}{E_3} & 0 & 0 & 0 \\ 0 & 0 & 0 & \frac{1}{G_{23}} & 0 & 0 \\ 0 & 0 & 0 & 0 & \frac{1}{G_{31}} & 0 \\ 0 & 0 & 0 & 0 & 0 & \frac{1}{G_{12}} \end{bmatrix} \begin{bmatrix}\sigma_{11}\\ \sigma_{22}\\ \sigma_{33}\\ \tau_{12}\\ \tau_{13}\\ \tau_{23}\end{bmatrix} \quad (4\text{-}1)$$

where the E_i are the normal elastic moduli, the G_i are the shear elastic moduli and the υ_{ij} are the Poisson ratios. Continuum voxel elements are used to model matrix and yarn regions. Yarn elements are also assigned fibre volume fractions as well as elastic properties.

To compare the performance of the different optimisation algorithms, a periodic boundary finite element analysis is carried out using the methods set out in [56]. This analysis method is in-built into TexGen and works by producing an Abaqus input file implementing the periodic boundary conditions that the user can then run. The ease of finding matching node sets on either side of the model is another reason why voxel meshes are well-suited to periodic boundary conditions analyses. Once the Abaqus job has finished, TexGen is then able to post-process the results in the .odb file and return the elastic properties.

Properties of the weave that are dependent on elastic properties can be calculated by combining them in the necessary manner. This forms the basis of the objective function evaluation in the optimisation.

4.3.3 Textile Feasibility Rules

3D woven textiles have some design constraints to ensure the integrity of the weave. During optimisations, it is likely that weave designs are generated that would not be possible to weave. This is partly because the multiple design variables that describe a yarn path are treated individually by the algorithm framework. This section describes some rules on textile feasibility that were formulated and used to rule such spurious weave designs out of the optimisation process where they take up significant finite element analysis time.

In TexGen, each binder yarn path is described as an integer list of its z-axis offsets from the top of the weave for each weft stack/cell (see Figure 4-2). Binder yarns must bind every warp and weft yarn in a stack, meaning that a binder yarn needs to loop over and under at least once somewhere along the length of each weft stack.

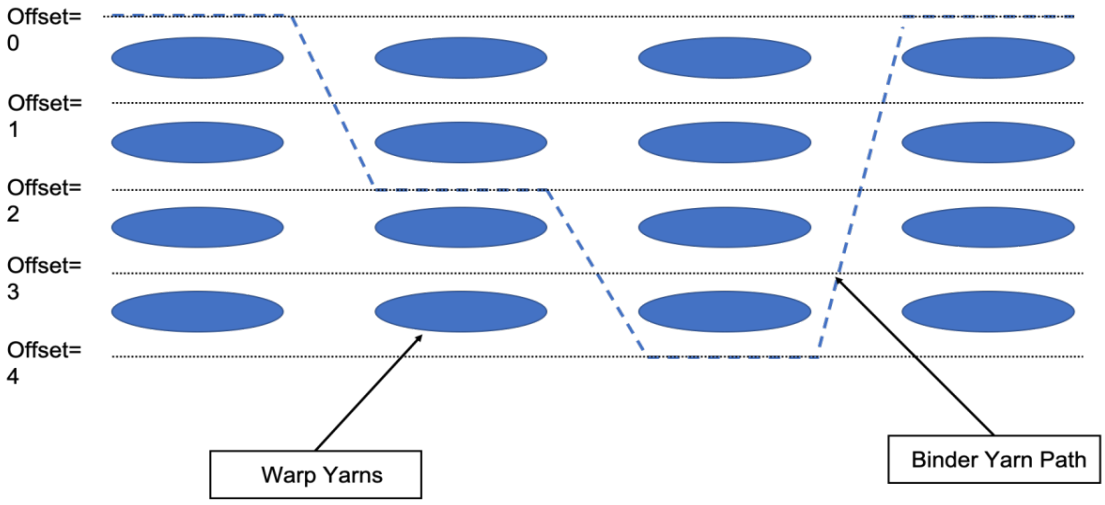

Figure 4-2 Diagram of binder yarn path through the textile, with offsets taking values between 0 and the number of layers=4. The dotted binder yarn path would be described as “0 2 4 0” in the parameter.dat file.

The physical constraints on binder yarn paths will in general apply to all the paths collectively (see Figure 4-3). It is posited that they are:

1) All yarns must be bound. At least one binder should pass over the top and another should pass under the bottom of each weft stack.

2) No unbound binder yarns floating or running flat above or below weft stacks.

3) There must be at least one binder yarn crossing all horizontal planes between weft layers within the unit cell to interlace with wefts to prevent the textile separating between them (remove this constraint to generate weaves with bifurcations).

(a)

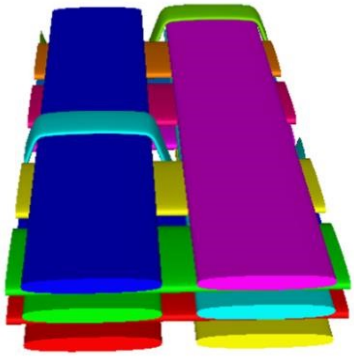

(b)

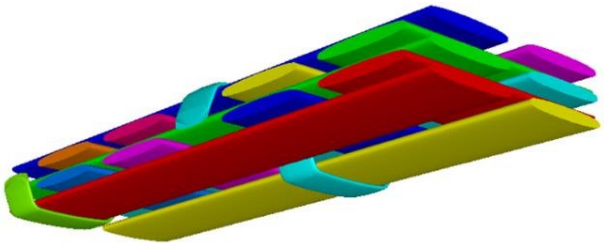

Figure 4-3 TexGen model (a) showing binders looping above and below each weft stack (wefts into the page) (b) Each binder crosses both internal horizontal planes between the weft yarns.

4.3.3.1 Implementing Constraint 1 and 2

Constraint 1 can be written in a mathematical form. For example, if there are 3 yarns **a, b, c** then in a weft stack there will be three offset values for each of the three yarns. A list of these can be written as:

$\{a_i, b_i, c_i\}$ for $a_i, b_i, c_i \in \{0, nly=4\}$

where the index 'i' labels a particular weft stack and nly is the number of weft layers in the textile.

To satisfy constraint 1, one of the elements of the set has to have a value of 0 - the binder goes along the top of the weft stack - and one of the others has to have a value of nly - it goes underneath the weft stack. This must be the case for each weft stack. This can be written:

Constraint 1: $0, nly \in \{ai, bi, ci\}$

There is a special case where this constraint is not enough to ensure that all weft yarns are bound. If the binder yarn path lies across the top or bottom of the weave and does not interlace with any of the wefts, then constraint 1 will be satisfied but the yarns will not be binding the textile. This can be avoided simply by implementing the following:

Constraint 2: $if\ x = \Sigma\, a_i$ then require $0 < x < nly * NumWeftStacks$

Here x is the sum of the yarn path offsets for a yarn. In Figure 4-2, x=6, nly=4 and NumWeftStacks=4. This forces the binder yarns above and below the weft stacks to interlace at least once with a weft.

This second constraint coupled with constraint 1, confines the possible yarn paths when there are two binders so that the only valid weave pattern is an orthogonal weave. The third constraint is clearly automatically satisfied by the

first two constraints as both binders will have to cross all horizontal planes between weft layers. A new algorithm was developed to be able to implement constraint 3.

4.3.3.2 Formulating Constraint 3

The third constraint will not be automatically satisfied by the first two when there are more than four binder yarns. With four binders, it is possible that there will be two pairs of binders with both binders in each pair only interlacing with each other and not with any of the yarns of the other pair. This will satisfy constraints 1 and 2 but will leave an uninterrupted plane throughout the midlevel of the unit cell. This will cause the textile to split along this plane.

An algorithm (see Figure 4-4) was formulated to determine if the binders interlace with each other:

1) Find the offsets of all the binder yarns at the weft intersection points.
2) Compare the z position of each node to see whether there is a yarn with a z position below and above a certain z position (midway between weft layers as in Figure 4-2).
3) Move onto the next plane and repeat by recursively calling the function.
4) If all planes satisfy the constraint and all the other constraints are satisfied, return 0.
5) If not, return 1 and apply a penalty parameter.

If the presence of horizontal planes without a binder yarn crossing is allowed, bifurcations can be created.

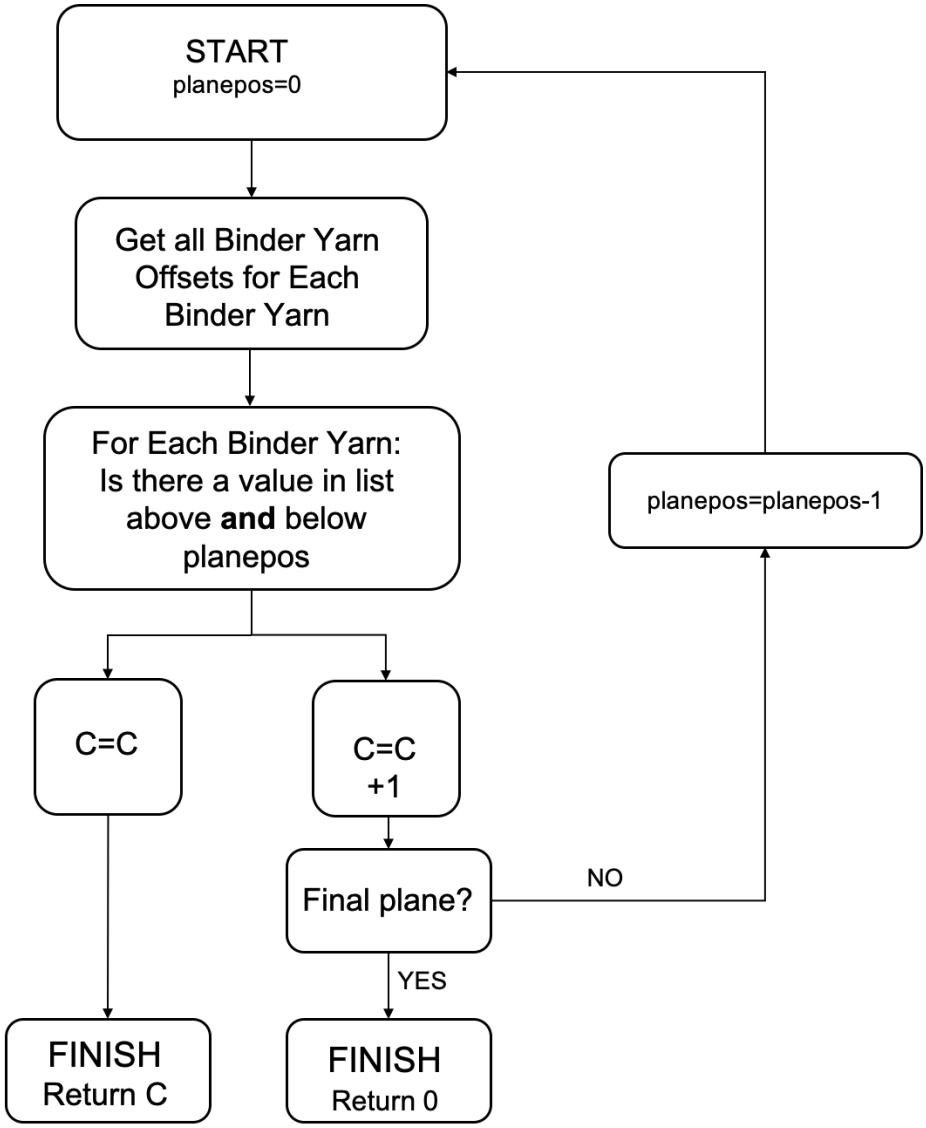

Figure 4-4 Algorithm flow chart for implementing constraint 3.

4.3.4 Implementation within optimisation framework

Constraints can in general be categorised as linear and non-linear with respect to the design variables. The algorithms will only generate members that are feasible with respect to the linear constraints and bounds and so these constraints will be satisfied at each generation. Non-linear constraints do not have to be satisfied at every point in the optimisation but must be satisfied for convergence to be reached. This can be achieved by penalisation of members that violate the non-linear constraints. Penalisation is applied by assigning

objective function values to the weave dependent on the level of constraint violation.

The algorithm *CheckBinderPaths* was implemented in Python to evaluate the level of constraint 2 and 3 violation. A dummy variable based on the extent of constraint violation is assigned, and the finite element analysis can be skipped. This drives the optimisation algorithm to find the feasible design space.

4.3.5 Comparison of Optimisation Time Against Literature

Previous studies, for example Zeng et al [23], employed optimisation algorithms to optimise the binder yarn path and number of layers of 3D woven composites for a formulated dimensionless buckling coefficient. These studies were able to find feasible weaves within a narrowly defined design space. The bulk of the time taken in the optimisation set out in that work is taken up in running the finite element analysis on the different weave designs. One of the disadvantages of the optimisation process is the use of loosely defined constraints used so that many the weave designs produced, while satisfying the linear constraints, do not constitute producible designs with respect to the feasibility constraints set out above. This results in running the time and computationally expensive finite element analysis even for weaves that are not producible.

Matveev et al [14] employed an orientation averaging approach to finding the elastic properties of weave designs. The orientation averaging approach yielded elastic properties below that of finite element analysis and can only be used to optimise objective functions based on those elastic properties. When used in an identical optimisation to Zeng et al, the authors reported a function evaluation 7 times faster than running the finite element analysis.

Zeng et al reported an optimisation time of 420 minutes on a desktop PC with 5 working CPUs able to evaluate 20 generations in 2100 CPU minutes. Using the same set up, Matveev et al were able to find the same weave design in 70 minutes resulting in 300 CPU minutes. For the optimisations taking the approach of ruling out infeasible weaves as set out above, a desktop with 4

CPUs performing 5 repeats of the same optimisation with different starting populations took a mean time of 30 mins or 120 CPU mins and produced the same optimum weave design as the other two methods. This speed up is due to being able to skip the costly mesh generation and finite element analysis. This results in the optimisation taking 50% of the time of the orientation averaging approach and 6% of the time of the finite element analysis only approach (see Figure 4-5).

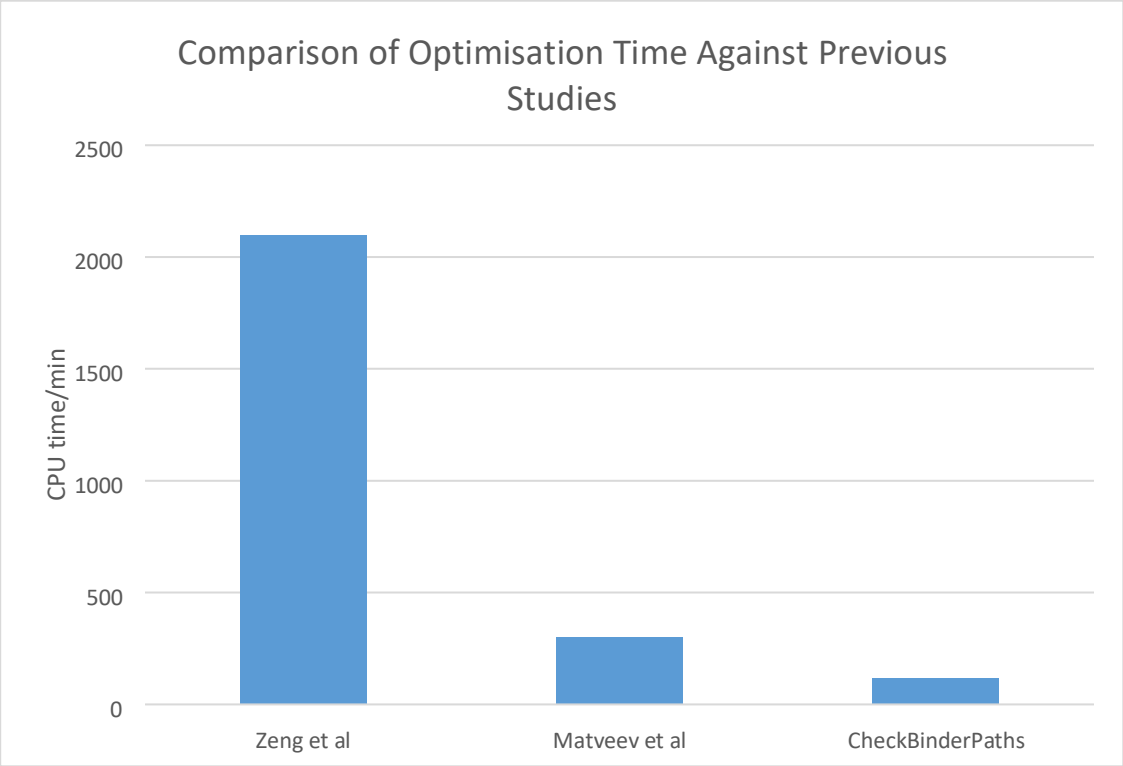

Figure 4-5 Comparison of the length of time it takes to optimise for buckling coefficient, all times scaled to CPU minutes for side by side comparison.

By employing the *CheckBinderPaths()* algorithm a significant speed up can be achieved while retaining the flexibility to optimise using function evaluations based on finite element analysis.

4.4 Optimisation Algorithm Performance Results

The genetic algorithm, particle swarm and pattern search algorithms were used to optimise a flat woven textile using periodic boundary conditions. The design variables were the yarn path of the three binder yarns in the unit cell with the objective function being through-thickness stiffness, E3. There was one binder yarn layer. The dummy values assigned to non-feasible weave points have been omitted from the graphs.

The genetic algorithm was able to reach a minimum after evaluating 185 weaves. The algorithm stops iterating after the change in the best function value is less than the prescribed function tolerance. The optimum weave can be described using the following design variable string describing the binder yarn paths:

Yarn 1: 4 0 0 4 0 4

Yarn 2: 0 4 4 0 4 0

Yarn 3: 0 0 4 0 4 0

The TexGen model of this weave is below in Figure 4-6, with yarns ordered 1, 2 and 3 into the page:

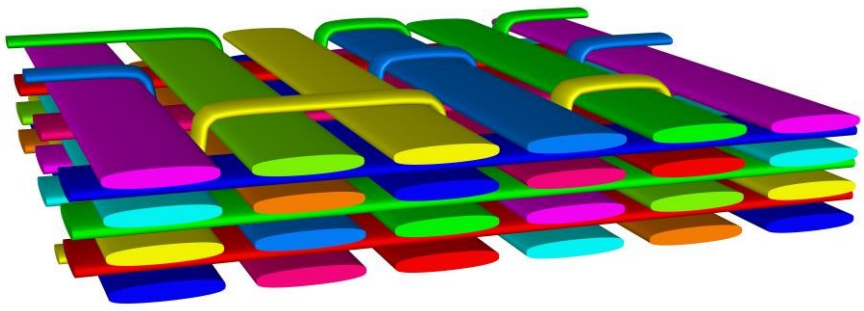

Figure 4-6 TexGen model of optimum weave selected by genetic algorithm.

This satisfied the constraints.

A graph of the optimisation iterations against objective function value is shown in Figure 4-7. On the y-axis the objective function value is the through-thickness stiffness.

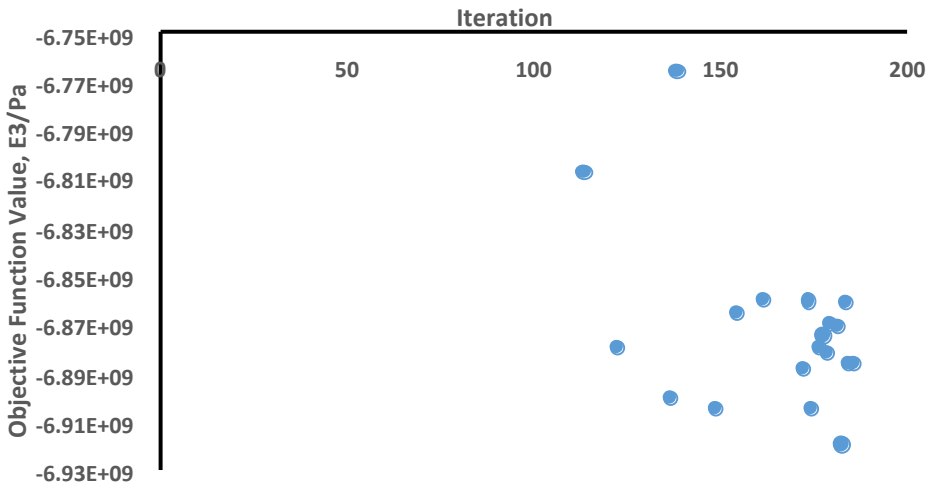

Figure 4-7 Graph of genetic algorithm for optimisation of flat woven geometry with three binders.

The particle swarm algorithm was able to find a minimum after evaluating 405 weaves, requiring 522 evaluations to reach the stopping criterion. The optimum weave was found to have binder paths:

Yarn 1: 4 0 4 0 4 0

Yarn 2: 0 0 4 0 4 4

Yarn 3: 0 4 0 4 0 4

The TexGen model of this weave is shown in Figure 4-8:

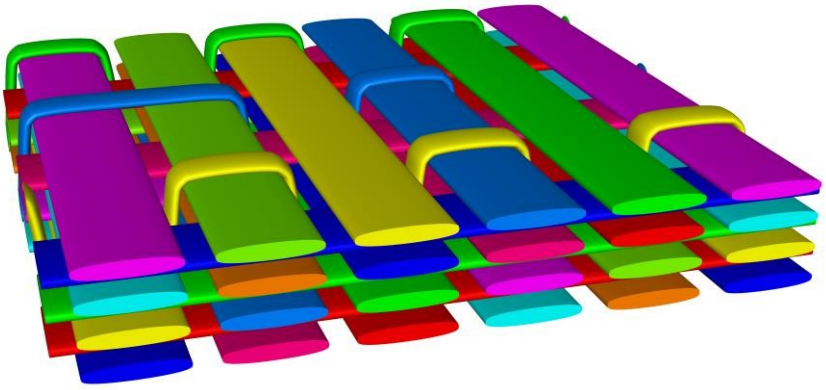

Figure 4-8 TexGen model of optimum weave selected by particle swarm algorithm.

A graph of the particle swarm optimisation's objective function against iterations in Figure 4-9

.

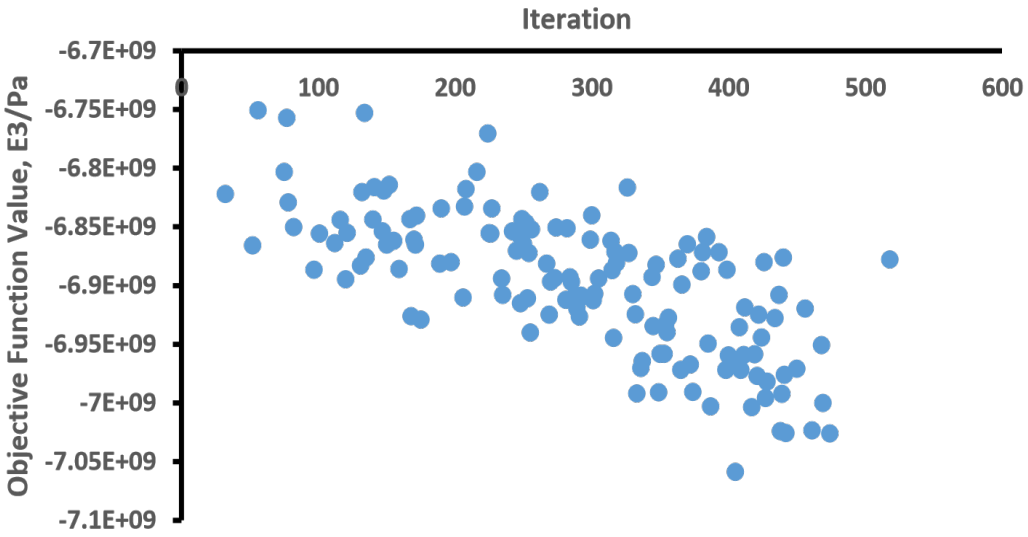

Figure 4-9 Particle Swarm Algorithm results.

The particle swarm algorithm and genetic algorithm both employ heuristic searches of the design space with a set of new designs generated and evaluated before moving on to the next design set. This leads to the scattered appearance of the graphs between iterations. This is usually why these algorithms are often

presented with the results of each generation or the results from all the members of the swarm at each point in time, plotted against the objective function value. However, in the interest of comparing the algorithms' performance, these are presented on a per function evaluation basis to be able to directly show how many evaluations it takes to reach convergence.

The pattern search algorithm was able to find a minimum after evaluating 607, requiring 653 weave evaluations before the stopping criterion was met. The optimum weave was found to have binder paths:

Yarn 1: 4 0 4 0 4 0

Yarn 2: 4 0 4 0 4 0

Yarn 3: 0 4 0 4 0 4

The TexGen model of the optimum weave selected by the pattern search algorithm can be found in Figure 4-10.

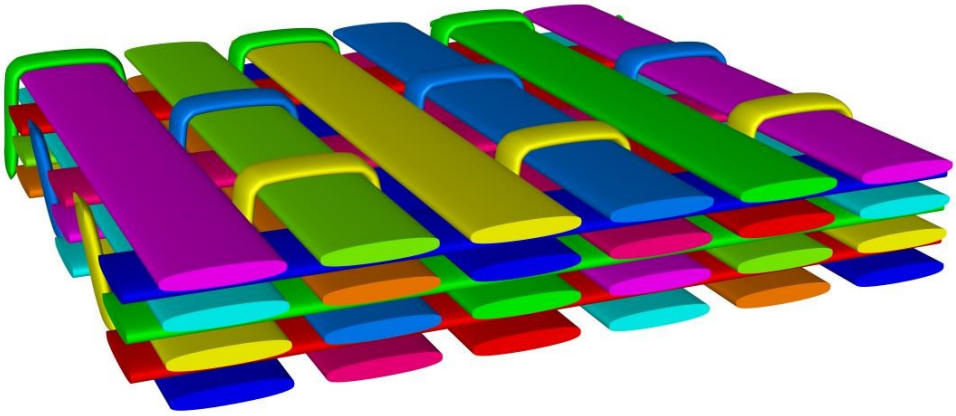

Figure 4-10 TexGen model of optimum weave selected by pattern search algorithm.

A graph of the pattern search algorithm's objective function value against iterations can be found in Figure 4-11.

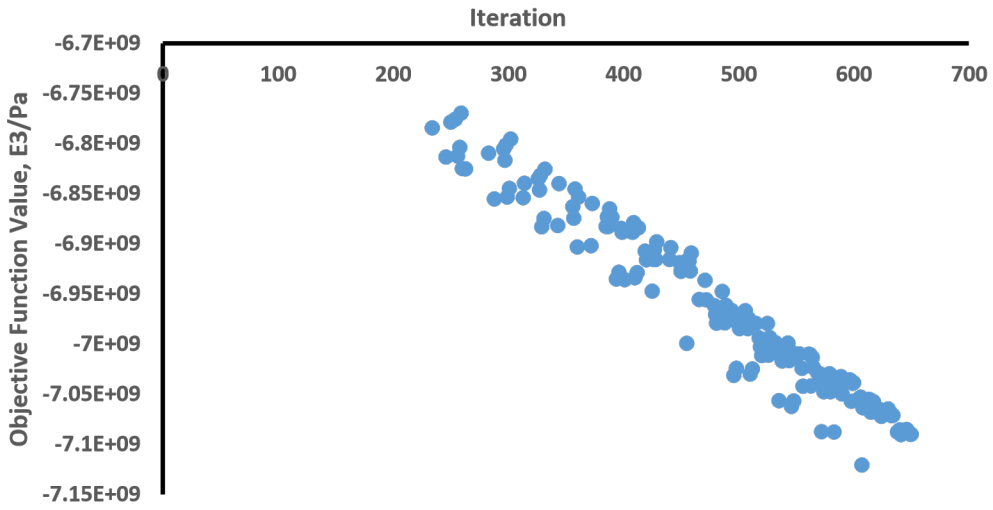

Figure 4-11 Pattern Search algorithm results.

The pattern search algorithm graph clearly has a downward trend as the algorithm begins to follow the objective function slope. This trend is clearer with the pattern search algorithm than with the previous two algorithms because of the more direct method of searching the design space. A smaller pool of designs is generated and evaluated in each set before moving on to the next set of weave designs.

Usually the algorithms spend a great deal of time evaluating non-feasible weaves. This problem is reduced by employing the CheckBinderPaths algorithms which allows the optimisation to assign an objective function value to the non-feasible weave and move on to the next design without running the finite element analysis. This allowed each of the algorithms to finish within two days on a desktop PC. Using the CheckBinderPaths algorithms to skip the finite element analysis stage for weaves that do not satisfy basic constraints saves time to make optimisation of more computationally complex textile properties such as damage resistance possible.

Algorithm	**Optimum Value, Stiffness E3/GPa**	**Stiffness Percentage Difference/%**	**Total Function Evaluations**	**Total Function Evaluations Percentage Difference/%**
Genetic Algorithm	6.92	-2.8	185	0
Particle Swarm	7.06	-0.8	522	+182
Pattern Search	7.12	0	653	+253

Table 4-3 Comparison of optimisation algorithm performance results.

Even though the particle swarm algorithm and pattern search were able to find more optimum textiles, the genetic algorithm was faster in converging, evaluating fewer textiles using the computationally expensive finite element analysis. The final weave selected by the genetic algorithm was not the optimum textile, with the difference being 3% between its optimum weave and the weaves selected by the pattern search and particle swarm (see Table 4-3). However, it took only 185 weave evaluations to reach this value and for the stopping criterion to be reached, compared to 522 and 653 function evaluations for the Particle Swarm and Pattern Search algorithms respectively. The genetic algorithm's process of generating a diverse population and iterating from one generation to the next allows it to find a minimum value faster than the other two algorithms but also prevents it from being able to easily narrow the search leading to early convergence. The trade off in computational time versus optimum value led to the choice to use the genetic algorithm for optimisation of delamination resistance where more computationally expensive function evaluations are required. This was deemed sufficient for applying to the optimisation of the delamination where the use of cohesive surfaces can increase the computational cost of the function evaluation.

4.5 Optimisation of Delamination Resistance

Avoiding delamination with through-thickness reinforcement is a key reason to use 3D woven composites. In this section the flange of a T-piece is modelled as a flat woven composite and subjected to pure thickness loading to assess the peak load. Cohesive zone modelling using cohesive surfaces are used to model damage at the yarn/matrix interfaces. This finite element model is used to evaluate the objective function value using the genetic algorithm to optimise the peak load.

4.5.1 Parallel Optimisation Framework

Each evaluation of the objective function takes longer for delamination because of the increased complexity in generating and running the finite element model in addition to the higher mesh density required. This would usually preclude this type of analysis being used in optimisations. However, using a High Performance Computing (HPC) cluster enables parallel computing to be utilised.

Multiple MATLAB workers can generate design variables and submit jobs in a parallel system (see Figure 4-12).

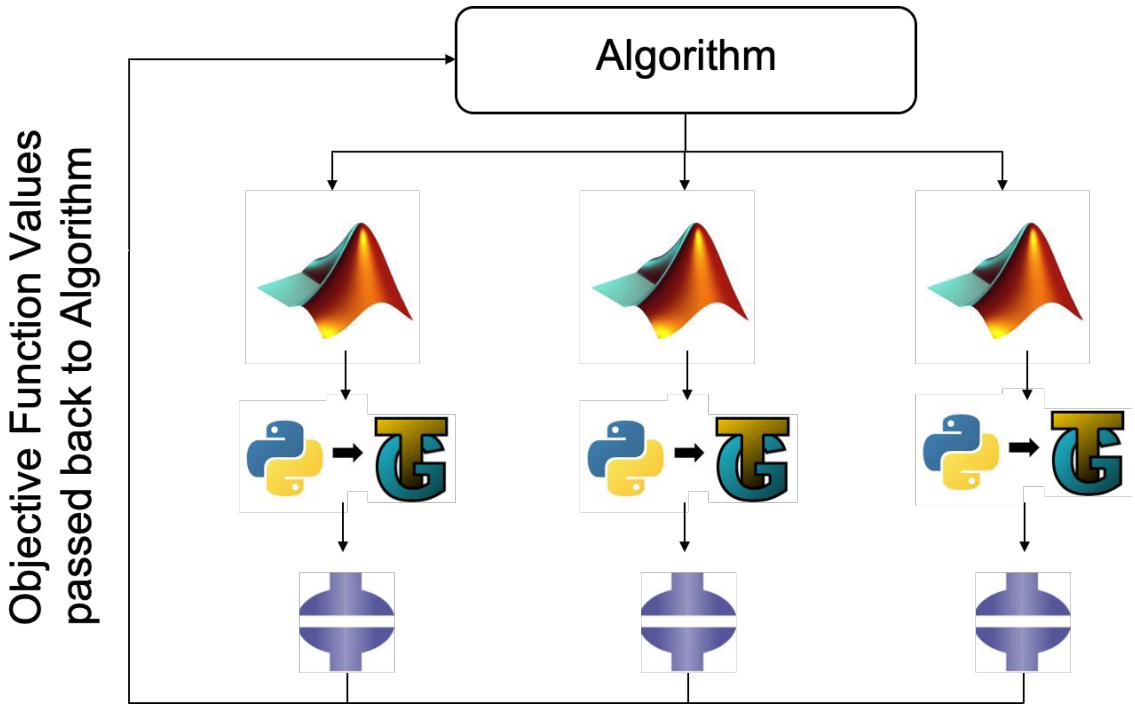

Figure 4-12 Parallel algorithm system.

This allows multiple weaves to be evaluated at the same time. If three workers are running at the same time, each evaluation takes about an hour. This gives an equivalent time of 20 minutes per function evaluation when comparing with running the algorithm in serial.

4.5.2 Loading

Displacement loading of all the nodes on a surface is applied through the thickness of the composite model by applying displacement boundary conditions to a dummy node which transmits the loading via homogeneous linear constraint equations to the top surface nodes in the finite element mesh. The bottom surface is similarly connected via linear constraints to a dummy node, to which encastre boundary conditions are applied. The nodes are constrained in degree of freedom three, the through-thickness direction.

The linear constraint equation for each surface node takes the form:

$$u^{dummy\ node} - u^{surface\ node} = 0 \qquad (4\text{-}2)$$

where $u^{dummy\ node}$ is the displacements of the dummy node and $u^{surface\ node}$ are the displacements of the nodes on the model face that the displacements are applied. This means any displacements applied to the dummy node are applied to the surface nodes. This allows the loading and boundary conditions to be applied to the surface nodes in a straightforward manner (see Figure 4-13).

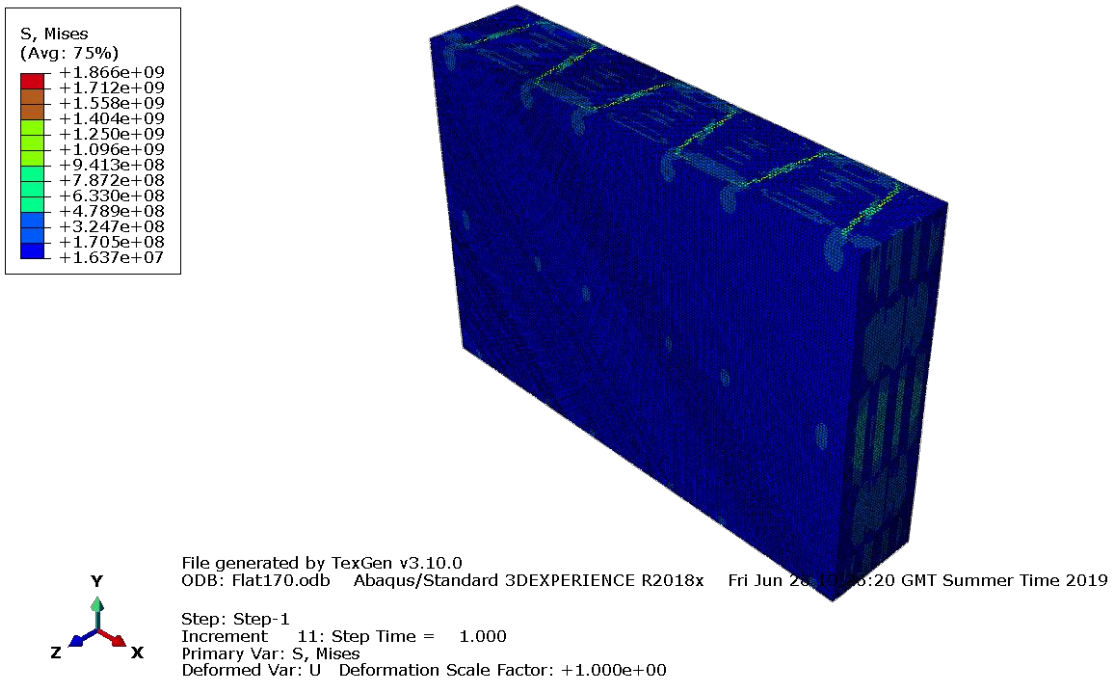

Figure 4-13 Model after tensile loading along z-axis, perfect bonding between the yarns and matrix.

4.5.3 Voxel Mesh

While voxel meshing was found to provide good results for finding elastic constants using periodic boundary conditions, they are less suitable for modelling damage initiation and progression. This is because of the step-like yarn interface that is generated where the yarns are not aligned with the

orthogonal axes. This has been found to produce shear stress concentrations in tensile finite element models which can lead to early damage initiation. However, they have been successfully used in [21] to model the tensile pull off test because of the low levels of shear stress.

To assess the level of shear stress concentrations caused by the stepped yarn/matrix interface at different mesh densities, the tensile delamination model presented in earlier sections was used with perfect bonding between interfaces. The results for shear stresses S13 and S23 show similar correlations to the S12 case.

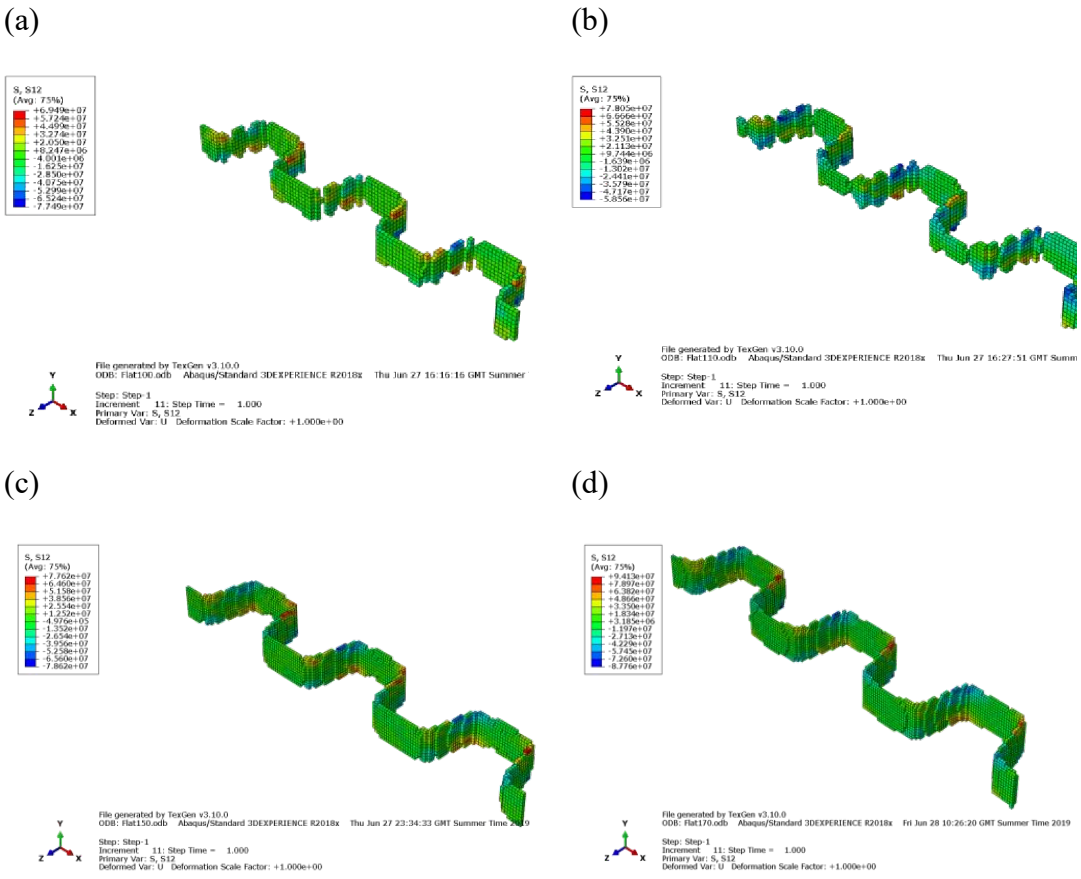

Figure 4-14 Shear stress concentrations (S12) along binder yarn/matrix interface for voxels of size (a) 0.12, (b) 0.117, (c) 0.086 and (d) 0.07mm

As the mesh density increases (see Figure 4-14), the continuity of the binder yarn mesh significantly improves. A reduction in the size of shear stress hot spots can also be seen as the mesh density increases. The normal stresses (S33) along the loading direction for the same yarns are shown in Figure 4-15.

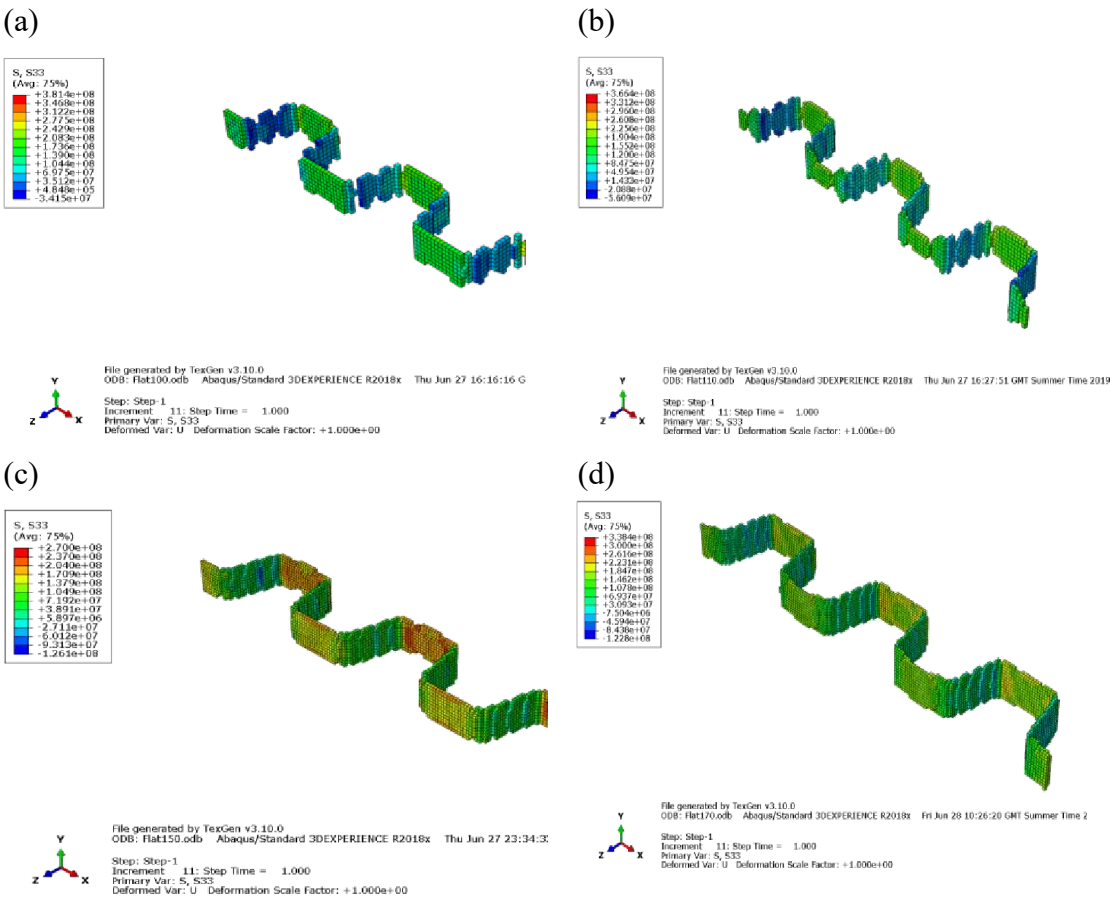

Figure 4-15 Normal stress concentrations (S33) along binder yarn/matrix interface for voxels of size (a) 0.15, (b) 0.136, (c) 0.122 and (d) 0.115mm.

The maximum S33 stress is approximately 30% higher than the maximum S12 shear stress across all models making it more likely to initiate interface debonding (see Figure 4-15). Furthermore, the S12 shear stress concentrations are located along the yarn edges while the S33 stresses are more centrally located.

The finite element model was run for different voxel mesh densities between 150-200 elements with mesh size between 0.15-0.115mm along the model's x direction (see Figure 4-16).

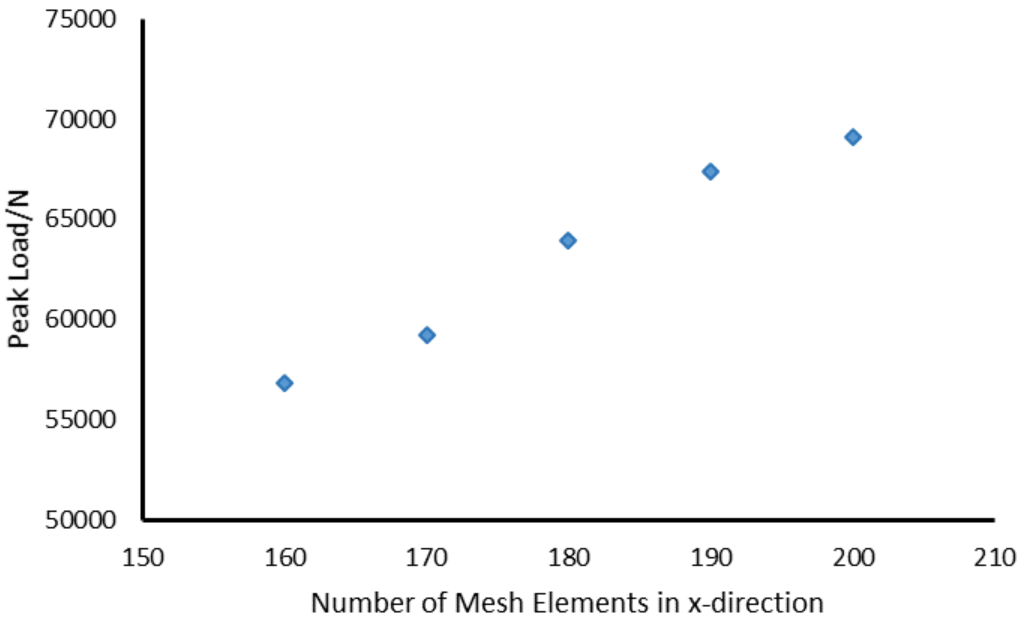

Figure 4-16 Mesh sensitivity results for peak load reached for flat weave models.

The peak damage load before damage initiation increases linearly with mesh density. It was concluded that the higher mesh density leads to lower stress concentrations leading to delayed onset of damage in the model. The voxel mesh was deemed to be appropriate because the shear stress was not the dominant factor at these mesh densities.

It can be reasonably expected that the weave which is the best at resisting delamination will be an orthogonal weave with binder path offset values at 0 and 4, ie. over the top directly through to the bottom of the textile and vice versa. The algorithm, however, has no such knowledge of the problem. The aim is to demonstrate that the algorithm can find a design that is equally good if not better than this.

Generation of the input files took a long time to complete because the generation of surfaces for the cohesive zone formulation requires each element

to be looped through several times. TexGen is usually run on one CPU and the large number of surface elements was too great for the iterative process. To reduce this time, the OpenMP API was implemented allowing the process of surface generation to be split across multiple CPUs on the HPC. This reduced the time from 6 hours on one CPU to 30 minutes when split over 12 on the HPC. With this addition each finite element function evaluation on one worker thread took 1 hour with 3 workers running concurrently.

4.5.4 Results of delamination optimisation

The final optimised weave design had periodic binder paths:

Yarn 1: 4 0 0 4 0 4

Yarn 2: 0 4 4 3 4 4

Yarn 3: 0 0 2 0 4 0

This clearly satisfies all the constraints. This weave is different from the orthogonal weaves that were expected to form the optimum solution.

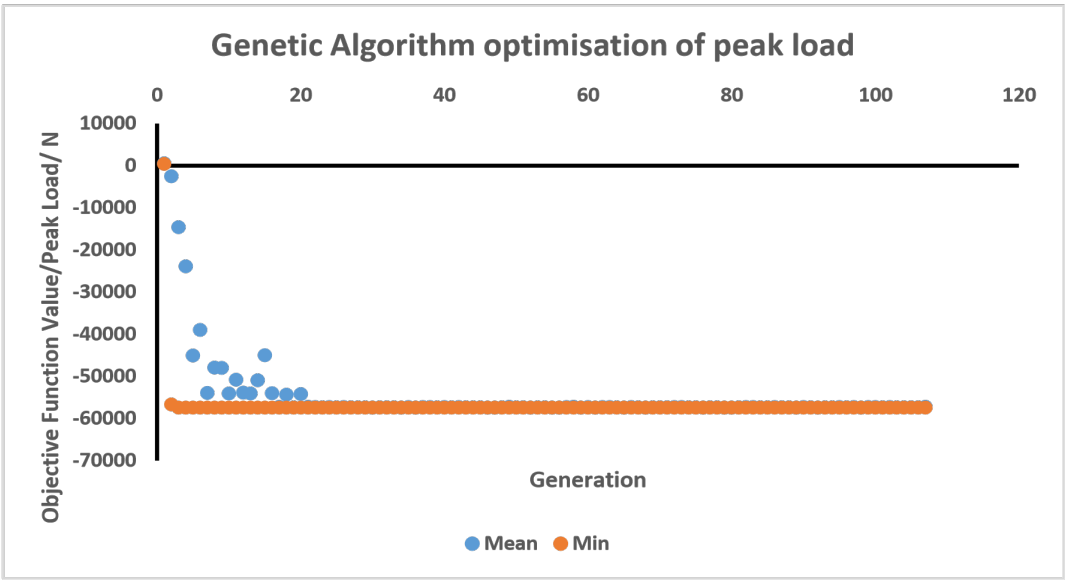

Figure 4-17 Optimisation results from the delamination models.

There were 1104 weaves evaluated using the algorithm taking 39 hours, with convergence reached after 23 generations after which no improvements were found until the algorithm reached the stopping criteria (see Figure 4-17).

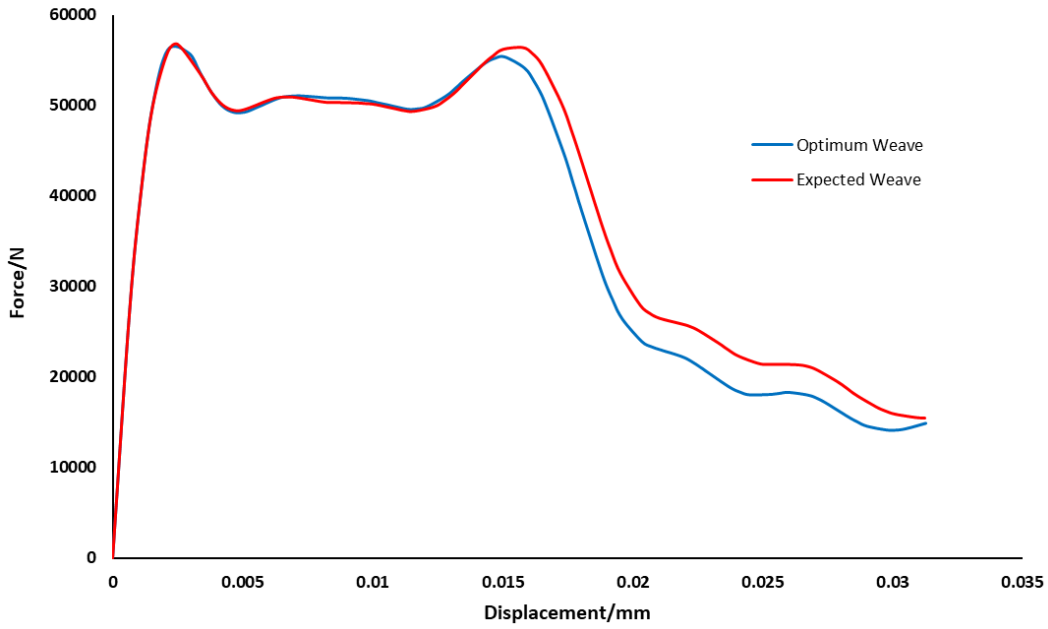

Figure 4-18 Force–Displacement Graphs for optimised weave (blue) and the expected optimum weave (red).

The force-displacement graphs of the expected and optimised weaves are similar, with both weaves having identical stiffness before reaching a peak load within 500N of each other at the same displacement (see Figure 4-18). The expected weave has a slightly higher peak load before a slower degradation in material stiffness. This is due to its increased through-thickness reinforcement (see Figure 4-19).

(a)

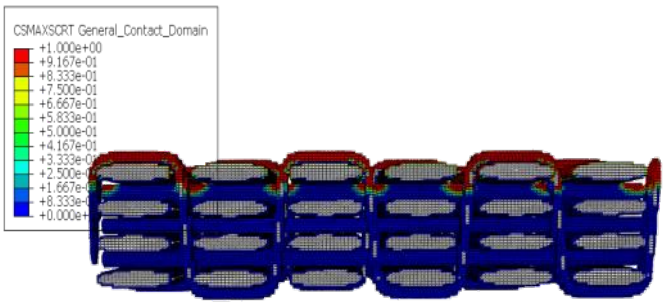

(b)

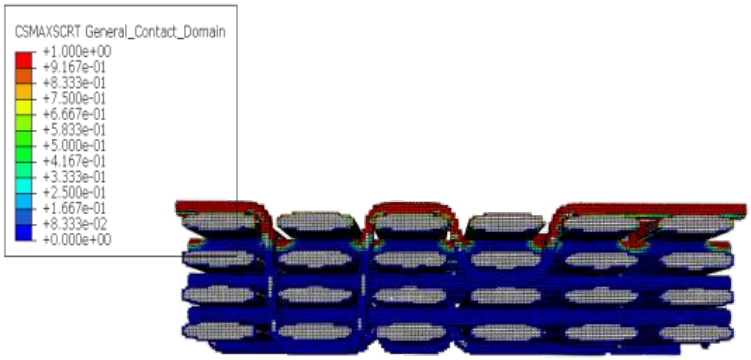

Figure 4-19 Interface damage on the finite element models of (a) the expected weave and (b) the optimised weave.

From the above results, it is concluded that the orthogonal pattern of two of the yarns in the optimal weave was sufficient to provide a similar peak load and therefore resistance to delamination initiation to the expected weave. The optimisation was able to find a weave close to the expected weave, it can therefore be concluded that the process is suitable for use in more complex optimisations such as the weaving patterns of T-Joints. However, the

behaviour after this load was reached suggests a faster degradation. This can be seen in Figure 4-19, where the binder yarn in the expected weave passes above two consecutive weft stacks, but the interface has failed completely.

4.6 Conclusions

Flat woven textiles have been optimised for their through-thickness stiffness using the genetic, pattern search and particle swarm algorithms. Using the *CheckBinderPaths* algorithms to bypass the finite element analysis stage for weaves that do not satisfy basic constraints shows significant improvements on previous optimisation efforts. This, in addition to speeding up input file generation in TexGen, makes optimisation of more computationally complex textile properties such as damage resistance possible. The genetic algorithm was used to optimise for delamination resistance because it represented the best trade-off between the speed of finding the feasible function space and finding optimum values. Optimisation of the flat weave for delamination resistance demonstrated this ability. The parallelisation of the input file generation and the optimisation framework alongside careful selection of the objective function opens up the possibility for the further optimisation of more complex weaves and objective functions than can be achieved using the classic elastic constants obtained from periodic boundary condition analyses.

Chapter 5 - Automatic Generation of T-Joint Geometry Models

5.1 Introduction

One of the key components to optimising the weave architecture of 3D woven T-joints is the automatic generation of accurate geometry models. As discussed in the literature review, current geometry model generation methods for these types of woven structure that contain weave bifurcations are slow, manual processes unsuitable for optimisation algorithm routines where many models need to be generated without direct user intervention. The current modelling process is not only unsuitable for optimisations but also restricts other design processes where the automatic generation of individual geometry models could be beneficial for weave designers. Often weave designers must rely on previous knowledge and experience to design woven reinforcement architectures that aim to produce the required material properties without having any way to prove that they have successfully managed this before manufacture.

The difficulty in automating the modelling process is due to the complex arrangement of the weft yarns within the T-joint junction region where they can crossover and interlace with each other. The order in which these yarns wrap around each other is determined by a combination of the order in which they are inserted, the beating direction of the loom and the change in layer position on either side of the bifurcation.

The current method of T-joint model generation in TexGen starts with reading in the pattern draft. The data within the pattern draft can be used to populate the relevant *CTextile3DWeave* class. The models initially generated have flat, idealised geometries. The weft yarns intersect with each other as they transfer heights on either side of the bifurcation, (see Figure 5-1).

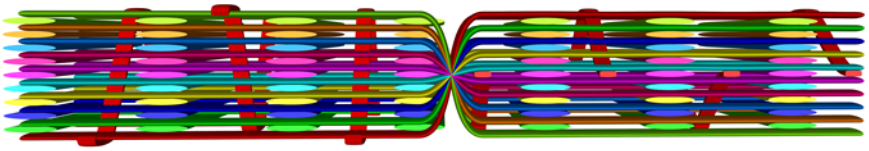

Figure 5-1 Idealised flat woven textile generated from a pattern draft using the *CTextileOrthogonal* TexGen class. As weft yarns enter the bifurcation, they cross through each other.

The pattern draft gives information about the order of weft yarn insertion and can therefore be used to find the order that these weft yarns need to be moved to wrap around each other. Nodes then need to be added to the weft yarns along the length, within the bifurcation region, to be able to shape the yarns as they wrap around each other. Cross sections of the yarns may need to be altered to prevent intersections of the yarns before the bifurcation transforms set out in [90] can be used to simulate opening the fabric to its final T-shaped profile (see Figure 5-2).

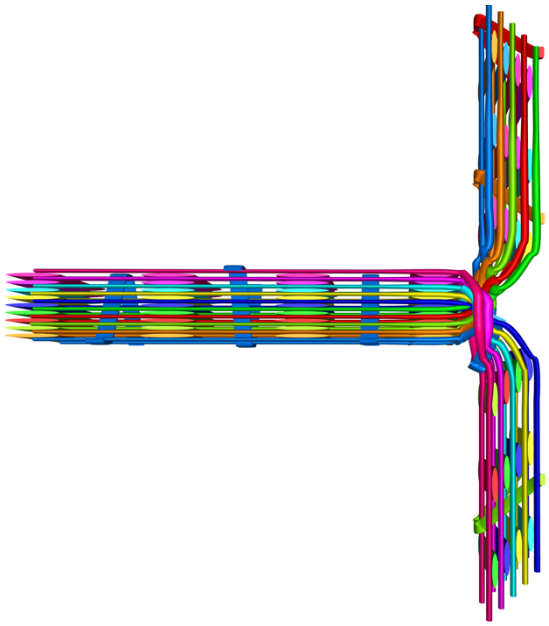

Figure 5-2 Final woven architecture TexGen geometry model generated using the new method. The direction of beating of weft yarns is into the page.

This chapter will demonstrate that by using TexGen, the University of Nottingham's textile geometry pre-processor [18], T-joint weave geometry models can be automatically generated by reading in the pattern draft, using the information contained within it to calculate the ordering of the weft yarns as they wrap around each other and automatically add nodes and translate them to the correct positions. To prevent intersections of the yarns, their sections can be altered and this chapter will describe how μCT data can be used to inform the geometry choices in the junction region of the T-joint. This novel methodology will allow models to be automatically generated for optimisations of properties and other design purposes. This chapter focusses on the woven architecture of T-joint reinforcements, but the principles contained within it should also be applicable to other weave structures that contain bifurcations.

In section 5.2 near net shape preforming is discussed to give an overview of the preforming process. This is followed by a description of the method used to read a pattern draft in section 5.3. This is important to be able to understand how the 3D woven T-joint architectures are designed and how TexGen produces the initial models. Next in section 5.4 is a description of how the ordering of the weft yarn interlacement is determined automatically from the pattern draft. This is used in section 5.5 to carry out the necessary yarn level movements and section changes to automatically generate the models. A simplified example is given in section 5.6 to illustrate the process before demonstration models are presented in section 5.7 to give examples of some of the weave geometries that can be produced using the new method.

5.2 Near Net Shape Preforming

3D weaving on a standard Jacquard machine works by raising and lowering the heddles attached to the warp and binder yarns and inserting the weft yarns orthogonally to cause the required interlacement. At the end of the process the loom has a beating action to push the weft yarns into place before moving further down the textile.

One of the major advantages of 3D weaving is the ability to produce weaves in near net shape. In the case of T-Joints, a plane within the textile that no binders cross is used to enable the creation of a bifurcation. This means that the woven piece can be removed from the loom and the end opened out to form the net shape of a “T”.

For standard orthogonal weaves, a constant number of the warp yarns that create a layer are raised as the weft is inserted. This creates the standard interlacement pattern with straight warp and weft yarns and binders looping over the top and bottom to create the interlacement. However, different numbers of warp yarns can be raised for a given insertion to cause the weft yarns to shift their height as they transition between warp stacks.

The placing of the yarns at different heights can cause the yarns to cross over each other. This, along with the beating action of the loom, causes the yarns to wrap around each other so that they end up at the correct height. The part of the textile where this occurs is called the junction region. Predicting the order of the wrapping from the information in the pattern draft is important to being able to automatically generate models.

5.3 Reading the Pattern Draft

Weave designs are produced based on pattern drafts. These are a set of instructions to the loom, directing it to raise and lower the sheds as the wefts are inserted. Pattern drafts can be represented by a block of white and black tiles.

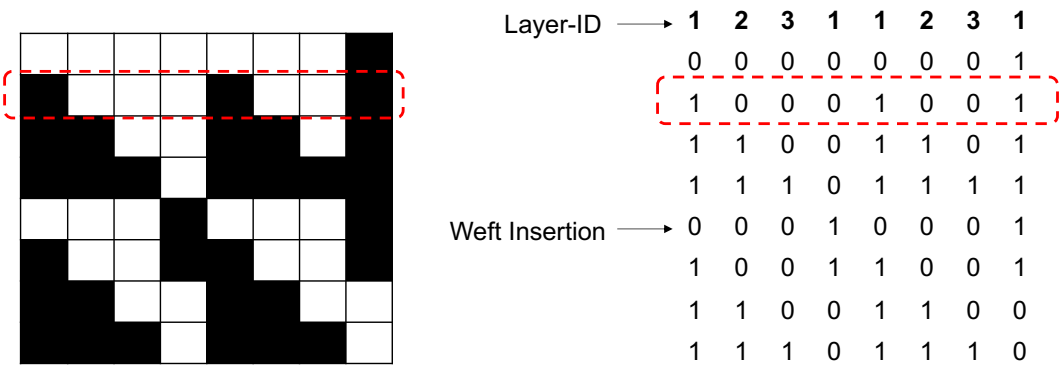

Figure 5-3 (a) Weave pattern draft. (b) Converted to matrix of 1's and 0's with Layer-ID. A row representing a weft insertion has been highlighted on each image.

These can be replaced with a matrix of 1's and 0's where a 1 means the warp or binder, is lifted up and a 0 means that it is down when the weft yarn is inserted across. For TexGen to be able to keep track of how many warp/binder yarns need to be raised, the first line of the weave pattern contains the layer ID information. Each number in the layer ID gives TexGen the layer in the warp stack, counting down from the top of the textile, so that the largest number along that row is the number of warp layers in the textile. In the weave represented by the pattern draft in Figure 5-3, there are three warp layers. The number returning to a 1 denotes the next warp stack or binder. Each line in the weave pattern is a weft insertion.

TexGen functions called from a Python script can take this information and a string of numbers identifying the which of the yarns are binders and which layer they are in and produce an idealised flat model of the weave. This is described in detail in [9] and can be found in the *WeavePattern* module included in TexGen. In the course of this work, the *WeavePattern* module was modified so that any binder yarn pattern could be read in for orthogonal type weaves. This allows the binder yarns to be placed so that they form the bifurcation necessary to form the T-Joint. This was achieved by relaxing the constraint that the binder yarns in orthogonal textiles must be in the top or bottom position as well as altering the input parameters so that it can read in

the necessary information. This idealised model (see Figure 5-4) is the starting point in the automatic generation set out in section 5.5.

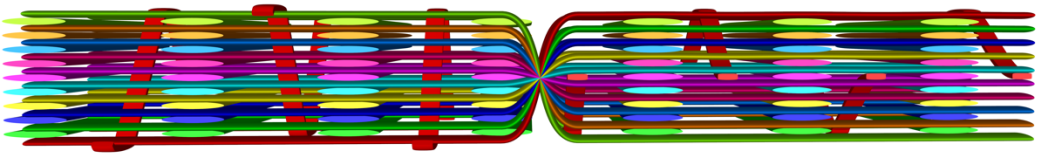

Figure 5-4 Idealised flat model produced by TexGen.

If no weave pattern file is provided but the final positions of the weft yarns are known, these can be used to generate a weave pattern using the new *WeftInsertion* module to create the weft insertions based on the number of warp layers and stacks. This is necessary for an optimisation process to be able to vary weaving patterns based on varying the final weft yarn positions after the bifurcation.

5.4 Automatically Determining the Order of Weft Yarn Interlacement

Depending on the weave pattern design, as weft yarns enter the junction region of the T-Joint, they may cross over and entangle with each other before leaving. Sometimes this also leads to them crossing from one half of the textile to the other as they move vertically between the warp stacks on either side of the junction region. The yarns in the model generated pass straight through each other and need moving laterally at the junction so that they no longer intersect (see Figure 5-5 (b)). To determine the order in which to move the weft yarns laterally out of the textile, in other words the way they interlace, requires the vertical location of the yarns to be tracked. Using the information found in the weave pattern draft, this can be readily achieved.

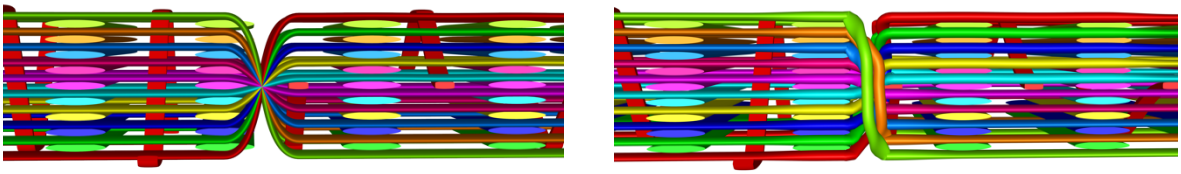

Figure 5-5 (a) Initial geometry with weft yarns passing through one another. (b) Final flat geometry with interlacement order resolved.

From the layer ID and the weft insertion information from the weave pattern, it is possible to obtain the start and end positions of the weft yarns in the warp stacks either side of the junction. This information is found for each weft insertion, or row in the pattern draft, by counting the number of warp ups in the stacks either side of the junction. For example, in Fig 4., the yarn at the top of the textile, in green, with no warps up as it is inserted, will have a position of 0 and transitions to the bottom after the junction with all the warps up and a new position of 9.

If it is assumed that the order of weft insertion by the loom follows a “top down” approach, whereby the first weft insertion in the weaving pattern is at the top of the textile, and that the beating direction of the loom is known, then counting the number of warp ups for each yarn on either side of the junction and then comparing the number to previously inserted yarns will return the distance which they need to be moved. Switching to a “bottom up” approach or reversing the direction of beating, will yield the mirror twin of the textile with the same geometry but viewed from the other side.

The key principle to determine the order of weft interlacement is whether subsequently inserted weft yarns cross and end up in higher positions than the weft that is being inserted. Each yarn that is inserted after the current yarn and crosses above it will push and displace the current yarn further in the direction of the loom beating (see Figure 5-6). When these crossing yarns are counted

for each yarn, the numbers are used to order the displacement of the yarns by creating a mapping between the yarn index and the displacement. A map in this case is a key-value pair, also known in Python as a dictionary, which can be used to store linked information.

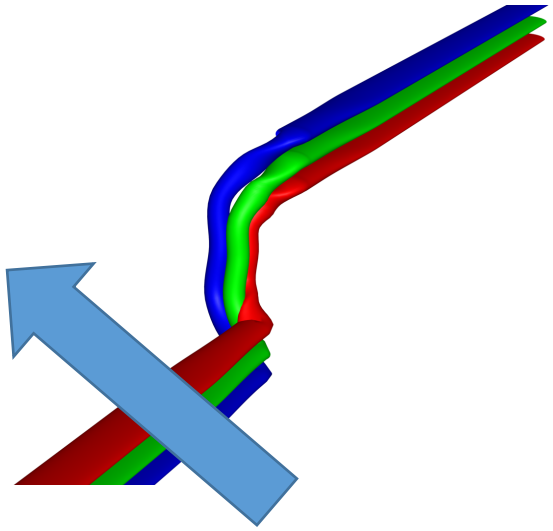

Figure 5-6 Three yarns wrapping each other. The arrow points in the direction of the loom beating. The blue yarn is inserted first, with the yarns following crossing above and pushing it in the beating direction.

Using a map between the initial yarn positions and the final positions, it is possible to count the number of yarns that finish above the current one. The displacement of each yarn is then stored in another map along with the yarn index as a key.

5.5 Model Generation

Models are generated by making use of TexGen's Python scripting interface to create the model and perform the adjustments needed to produce the final T-Joint weave. All the information required to create the initial geometry including the tow size and spacing are read in from the TexGen pattern draft

file. In an idealised model automatically generated by one of the TexGen 3DTextileWeave classes, nodes are generated at the points where the warp and weft nodes cross. An interpolation function then generates a yarn path between the nodes. Where the weft yarns pass through the textile thickness, in the junction region between subsequent nodes, this can result in interpolated paths which cause intersections with the warp yarns (see Figure 5-7).

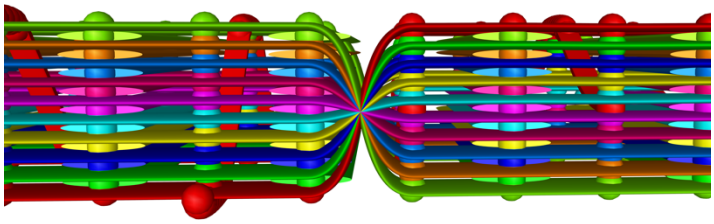

Figure 5-7 Textile model produced showing the weft yarn intersections with the warps as they transition in the junction region. Yarn nodes also shown.

Starting from this idealised model, using the Python scripting, nodes are automatically added along the weft yarns at the junction region so that these intersections are removed (See Figure 5-8). The position of the junction along the weft is determined for each yarn by checking whether the next node along is at the same height in the textile.

(a)

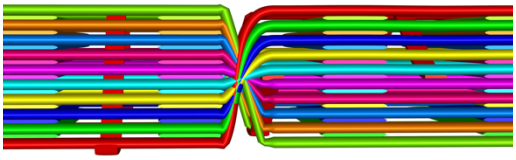

(b)

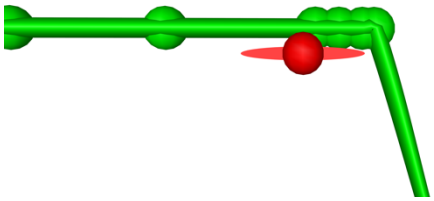

Figure 5-8 (a) Weft yarns shaped over warp yarns in the junction region. (b) Magnified image of the added nodes shaping over the warp.

Extra nodes are added to the weft yarns at the mid-section of the junction region, which are then used to assign a new position based on how far out the yarn is pushed by subsequent weft yarn insertions. This new position can be read from the map created in section 5.4. These nodes are assigned circular cross sections to approximate the deformation of the yarns which can be seen in CT data slices where they appear significantly squashed when compared to those slices taken further from the junction in Chapter 3 (see Figure 5-9).

Figure 5-9 CT slices from woven T-Joint, showing the weft yarn configuration at the junction region as they crossover.

The yarns can also be seen to arrange themselves in a zigzag pattern at the junction region. This is replicated in the model by slightly offsetting the

position of odd and even numbered yarns from each other when viewing along the y-axis (See Figure 5-10).

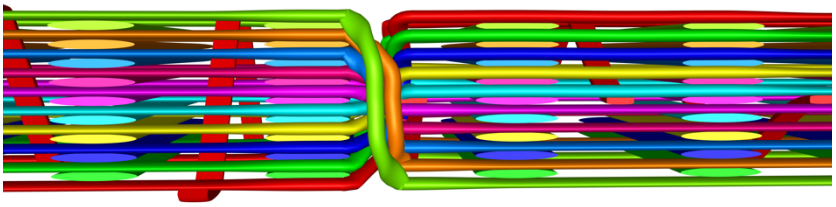

Figure 5-10 Weft yarns offset from each other so that they nest in a more realistic pattern.

Using the above methodology means that all the yarns that are pushed out in the direction of the beating. In reality, they would be centred with the tension in the yarns causing them to distribute themselves symmetrically either side of the central yarn path axis. The yarns are re-centred into the correct position by a translation of the nodes.

Finally, a bifurcation transform as set out in [21] is used to translate the nodes so the weave reflects the final T shape form. From here a domain around the model is created and the model can be meshed for finite element analysis.

5.6 Simplified Model

In this section a toy model of 4 weft yarns will be used to demonstrate the above modelling process. The first model will have no crossover but will be used to demonstrate the reading in of the pattern draft before the next model will demonstrate how yarns that change height in the textile at the junction region wrap around each other.

First the pattern draft is read for the straight weft yarn model (see Figure 5-11).

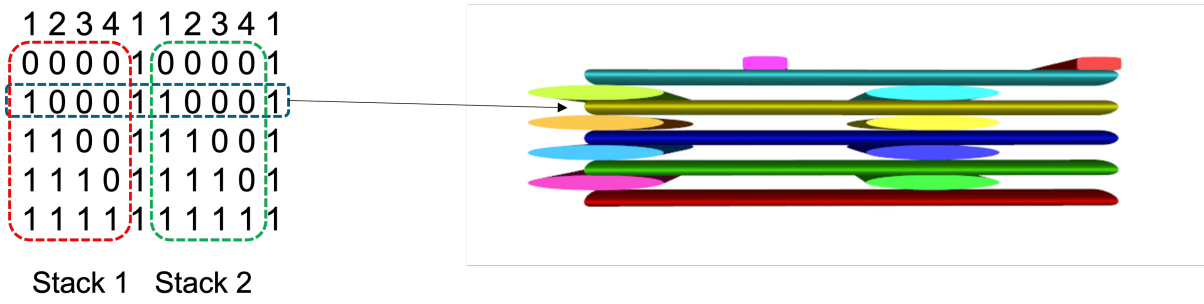

Figure 5-11 – Straight weft textile model with its pattern draft. Pattern draft has been grouped into its warp stacks.

The highlighted weft is the second inserted. For weft stack 1, the highlighted weft is at z-offset 1 which is determined by the last number in the layer ID for that stack that has a 1 (reading from left to right). For weft stack 2, the weft is still at z offset 1 so no change in weft height. This is the same for all weft insertions, no wrapping of yarns occurs.

For the model where the wefts change height between warp stacks.

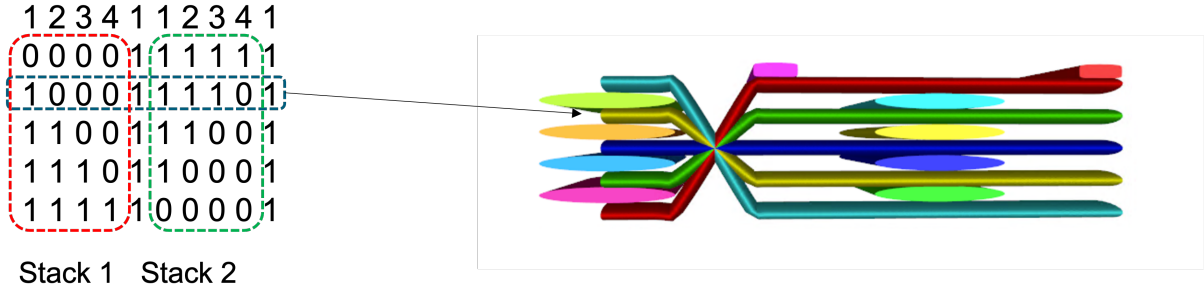

Figure 5-12 Crossover weft textile model. Second weft insertion highlighted.

For warp stack 1, the highlighted weft is at z offset 1 as before. For warp stack 2, from the weaving pattern it can be seen that the weft is now at z offset 3 as the weft has changed height in the textile. In the model, the yarns crossover and intersect as they move height. To automatically generate the interlacement in the models, we need to know the order in which the wefts are inserted and any change in weft positions between the stacks. The blue weft (see Figure 5-12) is

the first inserted, any subsequently inserted yarns that are positioned above it in the second stack will have to cross over it, in this case all three yarns. These yarns will push the yarns inserted before them in the direction of the beating action. Counting the number of yarns inserted after the current weft that cross above will give how far the yarn will be pushed out by the beating action (see Figure 5-13). Yarns that do not cross above do not contribute to pushing the yarns above them in the direction of beating. The information is stored in another Python dictionary.

(a)

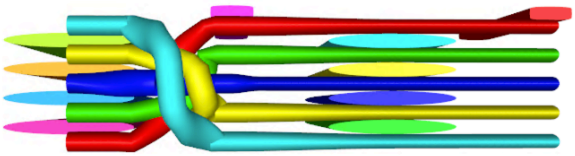

(b)

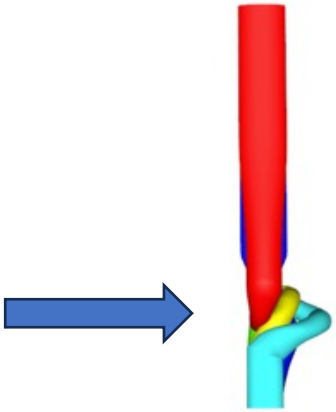

Figure 5-13 Modelling the beating action pushing the yarns inserted before into position. Beating direction indicated by arrow.

The dictionary table for the above crossover model is shown in Table 5-1:

Weft Insertion Number	Positions Pushed out by Beating
0	4
1	3
2	2
3	1
4	0

Table 5-1 Table representing the contents of the dictionary with the key-value pairs being the weft insertion number and the number of positions it is pushed out by the beating action of the loom.

The python script then adds nodes along the length of these yarns between the two warp stacks and moves them into the correct position to capture the nesting effect as set out earlier in the section.

5.7 Demonstration Models

To demonstrate the capability of the method described above, several models were automatically generated and are included below. Each has 10 weft yarns and 9 warp yarns in a stack.

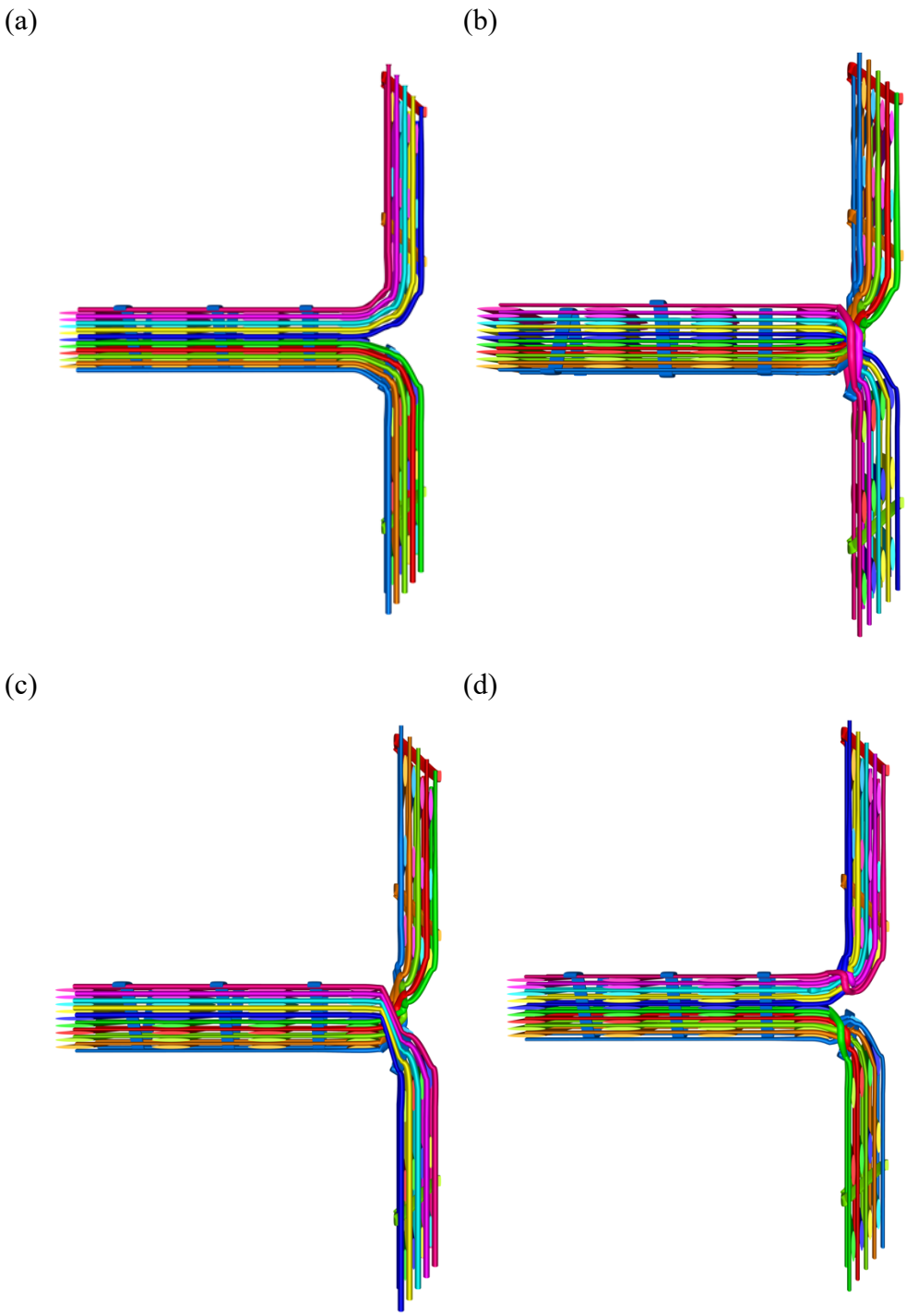

Figure 5-14 Four automatically generated T-Joint models.

As can be seen from the images (see Figure 5-14), a wide range of weave architecture can be modelled using this method. The first weave, in Figure 5-14 (a), has no crossover between the yarns and no transitioning over at the junction region. The second, in Figure 5-14 (b), has total crossover between the yarns and every yarn transitions to the opposite half of the textile. The third

weave, in Figure 5-14 (c), has one half of the textile crossing each other with the yarns all transitioning across the junction. The final weave, in Figure 5-14 (d), has all the yarns crossing each other but none of them transition into the other half of the textile.

5.8 Conclusions

New methods to model the geometry of 3D woven T-Joint reinforcements were developed. These include an implementation in TexGen that improves the ability to read patterns of orthogonal weaves by being able to place the binders to form the bifurcation, and the scripts that take the information from the weave pattern and generate the final woven geometry of the T-Joint including the rearrangement of the yarns in the junction.

The tool to automatically generate complete T-Joint models from weaving patterns provides the ability to quickly produce high quality geometric models from weave pattern designs. The first step in an optimisation process. The aim, therefore, is to use the ability to automatically generate T-Joint models to find optimum weaving patterns. In the next chapter, the automatically generated models will be meshed, surfaces between the yarns will be inserted automatically and validated finite element analyses will be carried out as part of an optimisation process.

Chapter 6 - Analysis of Automatically Generated T-joint Models for Optimisation

6.1 Introduction

In Chapter 5, a description was provided of how meso-scale 3D woven T-Joint geometry models were automatically generated using TexGen's Python scripting interface. The next requirements for using this to find optimum weaving patterns for the woven reinforcements are automatic mesh generation and a method of scoring each weave or evaluating an objective function value.

In this chapter, the tensile pull-off test that was performed in Chapter 3 is simulated using finite element analysis. Meshing of a non-cuboidal weave domain that conforms to the T-joint profile is discussed. A novel adaption for using the octree voxel mesh with the new domain type is presented in section 6.2. Details of the finite element analysis are contained in section 6.3. Parameter studies are performed on the voxel, octree and smoothed octree voxel meshes and compared before one is chosen to be used in the optimisation in section 6.4. Key considerations include the accuracy and time it takes to run the analyses. The post-processing used to calculate the objective function value is set out in section 6.5. This will be used in the optimisation routine presented in the next chapter.

6.2 Meshing of T-Joint 3D Woven Textile Models

Once the meso-scale geometry models are produced, a domain is created using the *CPrismDomain* TexGen class, which has been included in a recent release of TexGen, v3.13.1 [18]. This allows the domain of the model to be specified to conform to the outline of the T-shape (see Figure 6-1). This domain can then be meshed. Before this work, only voxel meshes could be generated on prism shaped domains. The *COctreeVoxelMesh* class was originally designed to mesh rectangular block domains and so it was necessary to adapt it to be able to mesh the outline of the T-profile. This was achieved by checking whether

each element's nodes were in the bounds of the specified prism outline, which in this case was the T-profile.

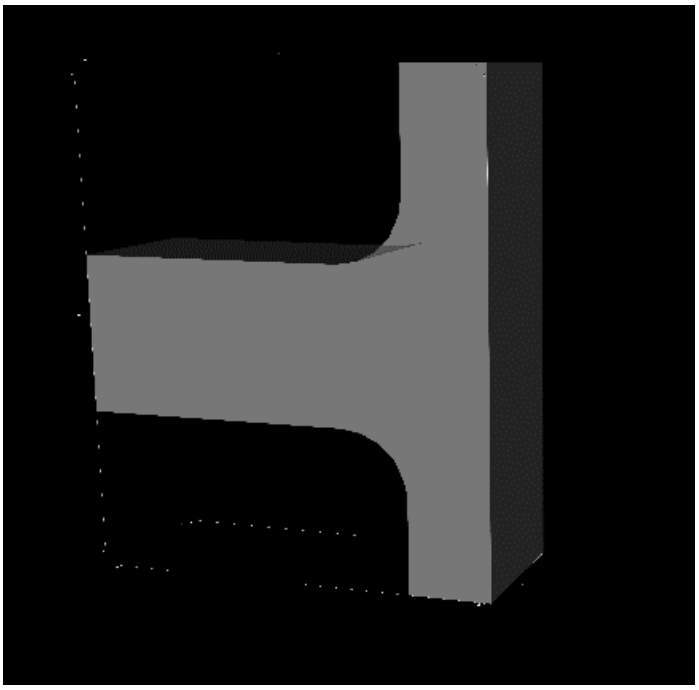

Figure 6-1 TexGen prism Domain with T-joint outline. The T shape is defined as a set of points and then provided with a length to form the full 3D shape.

This allows any prism shaped domain to be meshed with the octree voxel mesh in TexGen, allowing the possibility for users to use it to mesh complex domains such as I and Pi shaped domains, among others. In this work, this allows the octree voxel mesh to be applied to the T-joint geometry models discussed in Chapter 5.

6.2.1 Voxel Mesh

Models of composite textile structures have often been meshed with voxel meshes which provide a robust solution to the problems associated with the automatic generation of conformal meshes, namely their inability to capture

the yarn geometry with elements of sufficient quality. Additionally, matching nodes on opposite surfaces allows for easy application of periodic boundary conditions evaluating unit cell textile models. Conformal meshes have been shown to produce distorted elements upon meshing yarns in close proximity to each other with the solution in [91] to be the reduction of the cross sections to provide contact clearance. This is because of their rigid constraints of conformity to, and displacement continuity across, the interfaces between the yarns and between the yarns and the matrix.

One of the disadvantages to voxel meshes is the jagged, stepped interface between the yarns and the matrix elements formed when the interface is not aligned along any of the three global cartesian axes in which the model was meshed. This can cause stress concentrations and requires the user to be selective in the uses for voxel meshes. One such area where it is unclear the voxel mesh is suitable is when cohesive surfaces or elements are employed.

The effect of the interface depends on the stress state of the elements on either side. If tensile stress normal to the interface dominates then the effect is reduced. Conversely, shear stresses along the stepped interface can cause stress concentrations, as was seen in Chapter 4. A check should be made that the shear stress should be low compared to the normal stresses at the interfaces between the yarns and matrix elements.

Another disadvantage of rectangular voxel meshes is their relative inability to capture the yarn cross section geometry accurately. They require many more elements than those required in conformal meshes to approximate the cross-section geometry.

6.2.2 Octree Voxel Mesh

Matveev et al. [20] proposed and implemented in TexGen an improvement to the standard voxel mesh that addresses the problems caused by the step-like interface. It uses the dual methods of octree refinement, where the elements that straddle the material interfaces are divided and stored in an octree, and smoothing, where the element boundary nodes along the interfaces are moved

so that the mesh elements better approximate the interface boundary and is closer to a conformal mesh. The combination of refinement and smoothing improve the performance of the voxel mesh. Hereafter, this method shall be referred to as the octree voxel mesh and it will be specified as to whether the smoothing algorithm has been applied.

Each mesh element straddling the boundary is divided and the process is repeated with straddling elements divided until the user-specified maximum level of refinement is reached. The memory structure in C++ that holds the node structure information is called an octree. The mesh is "balanced" so that there is a gradual change in the level of refinement at further distances from the material interfaces (see Figure 6-2). Using this method can result in fewer elements being needed to discretise the entire model when compared to the voxel mesh, as not all the elements need to be as refined to fully resolve the model geometry.

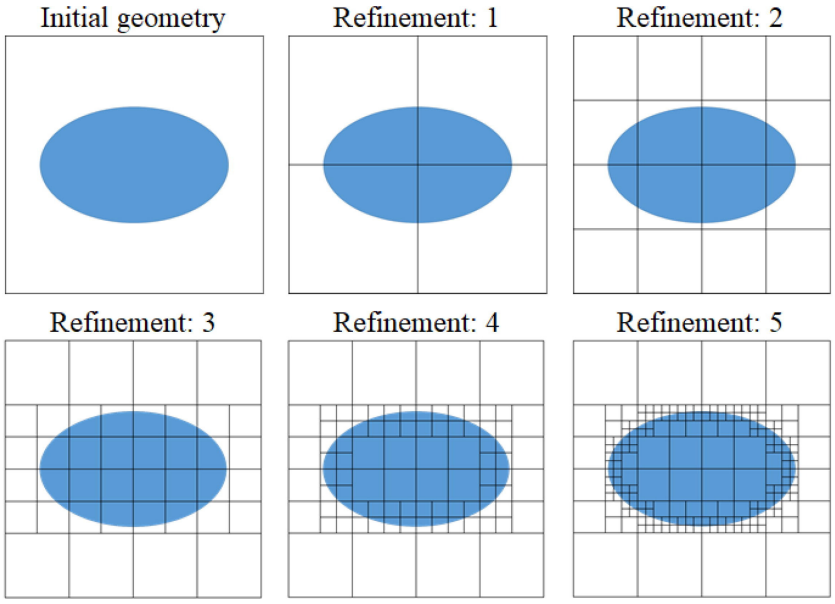

Figure 6-2 Illustration of the octree voxel meshing of a yarn cross section with subdividing of elements that contain material boundaries [20]. Each successive level of refinement refines elements along the boundary allowing the yarn surface geometry to be better resolved.

An example of an octree voxel mesh with the matrix elements suppressed is shown in Figure 6-3.

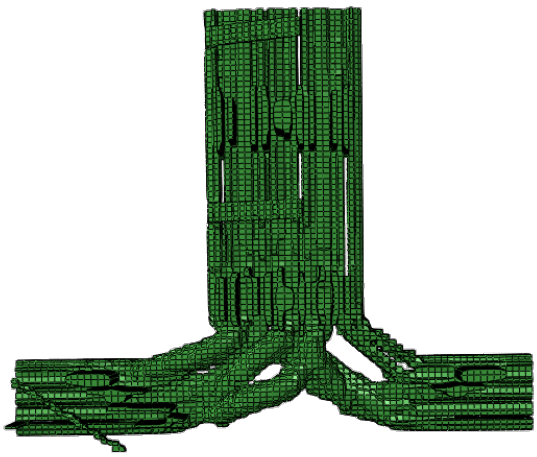

Figure 6-3 Octree voxel mesh of T-joints with matrix elements suppressed to show the mesh conforming to the yarn elements. Smoothing iterations have been applied.

The drawbacks to this method include the extra hanging nodes that are generated due to the different element sizes caused by the various levels of refinement. These require extra multi-point constraint equations to ensure the refined elements maintain continuity, which slows down the analysis.

One further advantage of using the octree voxel mesh is the ability to output element surfaces. This allows the use of cohesive surfaces as applied in Chapter 4, removing the requirement to add in cohesive surfaces by hand using third-party software such as HyperMesh [86].

6.3 Finite Element Modelling of T-Joint Weaves under Tensile Pull-off Load

The tensile pull-off test from Chapter 2 was modelled to evaluate the difference between each T-Joint weave and provide a basis for scoring each weave during the optimisation.

6.3.1 Boundary Conditions

In the tensile pull-off test, the T-Joint samples were clamped at the flanges and load applied to the web. To simulate this in the finite element model, the nodes on the outward facing surfaces of each flange were fixed in all directions using Abaqus' encastre boundary conditions, with the tensile pull-off load applied to the top surface of the web using a displacement boundary condition to a driver node connected to the top surface nodes by linear constraints (see Figure 6-4).

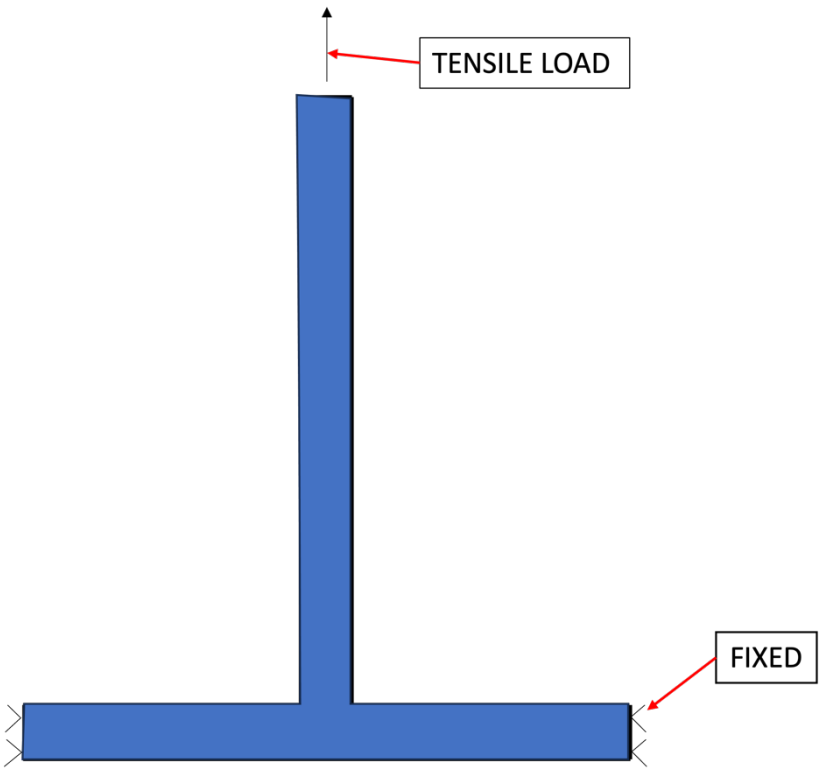

Figure 6-4 Finite element T-joint model boundary conditions for tensile pull off.

There is periodicity along the length of the 3D woven T-joint reinforcement so periodic boundaries can be applied along the length. However, single unit repeats of the weave pattern in the x-direction were used with no periodic

boundary condition along the x-axis since it had been reported by Yan [58] that this had little impact on the elastic behaviour of the T-Joints.

In the experimental set up discussed in Chapter 3, the T-joint flanges were not fixed at the ends but clamped at the top and bottom at a point further in-board from the end. This has the effect of constraining the movement of the T-joint at the clamp locations. It is proposed that for the purpose of comparing the effect of the different weave patterns on the mechanical properties of the T-joint the difference will not have much of an effect because the boundary conditions are the same for each finite element analysis in the optimisation.

6.3.2 Time Control

The quasi-static analysis was chosen to be solved using the Abaqus/Explicit solver as it was likely to reduce the analysis time. To model a quasi-static process such as the T-Joint pull-off test, a reduced time step can be used. This allows a much faster time step that is more suited to Abaqus/Explicit's usage. Trial models using the implicit solver took too long to be used within an optimisation. Abaqus documentation [80] recommends finding a lower bound on the explicit time step by examining the model's modes using the eigenvalue analysis, linear perturbation time step.

For the T-Joint models, this produced the first mode frequency of 270Hz, with a time period of 3.5ms. The general recommended lowest time period is at least 100 times this value to avoid inertial effects. This should result in a velocity graph for the machine head that increases, reaches a constant velocity and then slows down. The resulting kinetic energy and internal energy graphs ideally would then look like those presented in Figure 6-5.

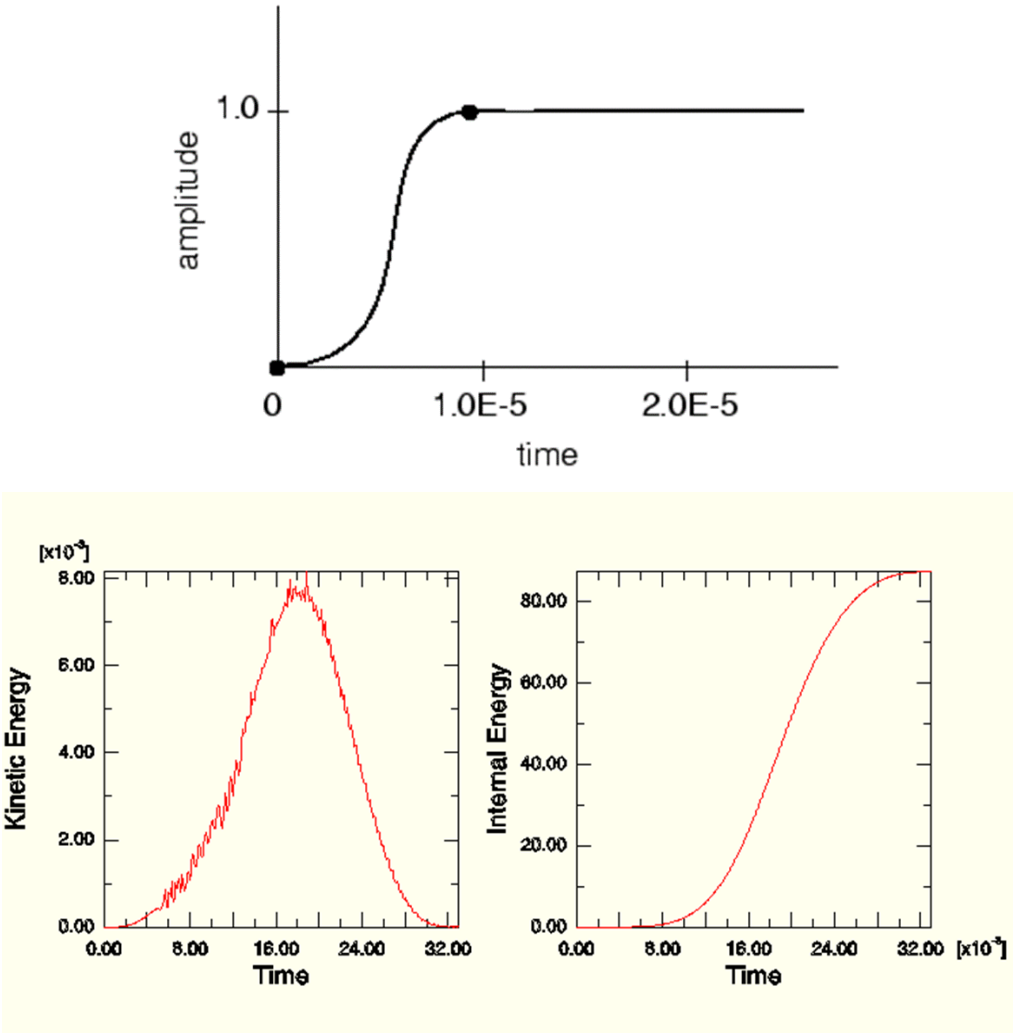

Figure 6-5 Graphs showing ideal kinetic energy and internal energy graphs for a quasi-static process. Taken from the Abaqus documentation [80].

A time period of 300s was chosen to displace the top surface of the web 5mm, resulting in a loading rate of 1mm/min. This resulted in kinetic energy and internal energy graphs as seen in Figure 6-6.

(a)

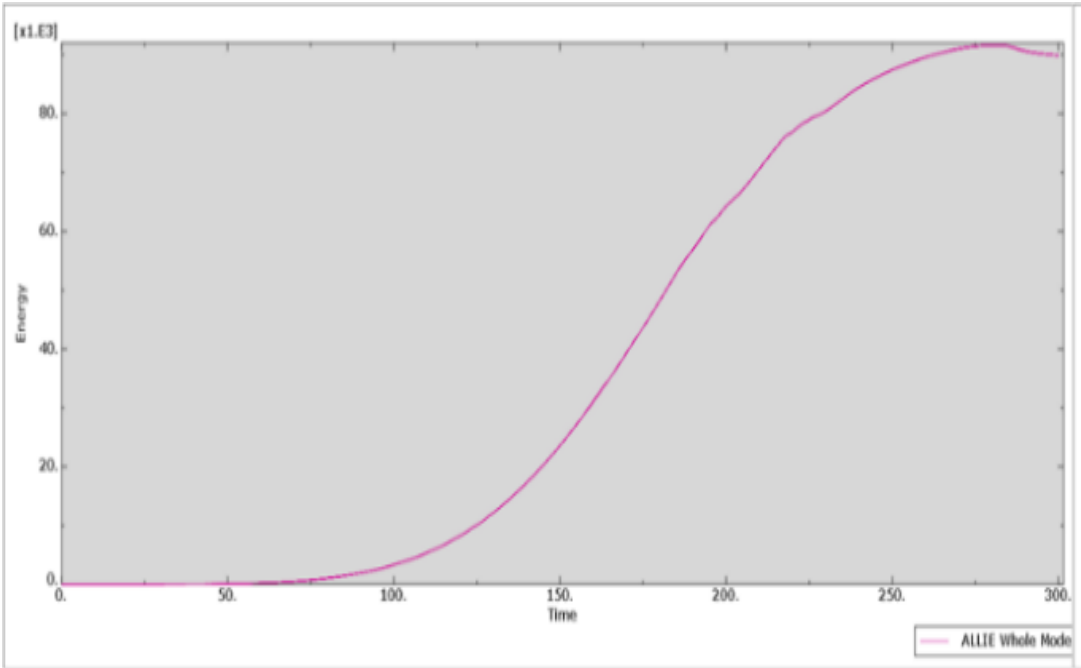

(b)

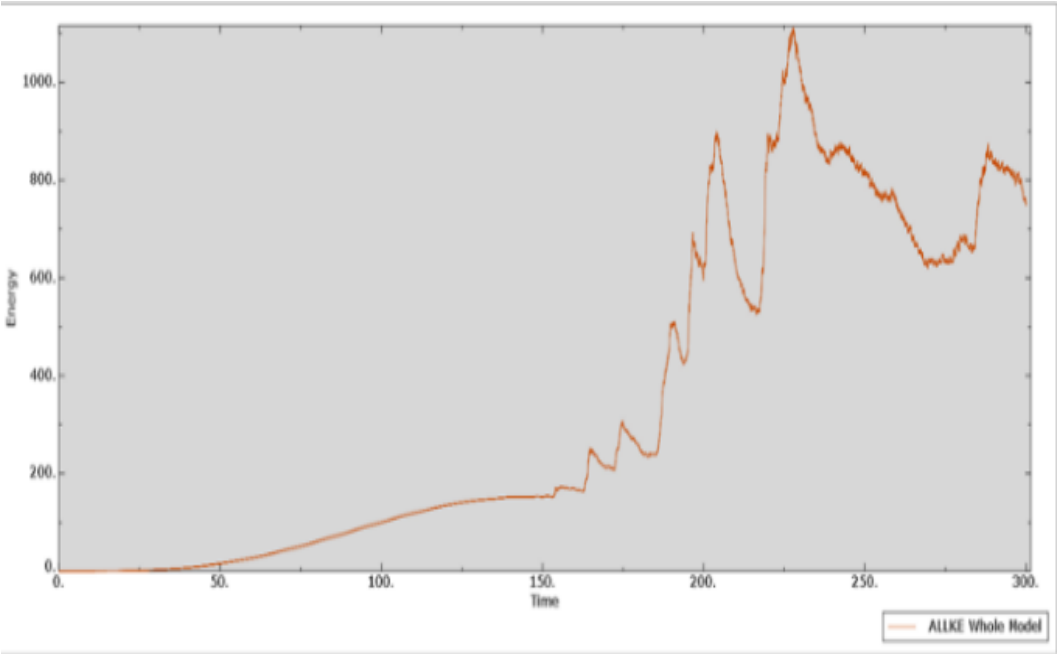

Figure 6-6 (a) Internal energy against time and (b) kinetic energy against time during the tensile pull-off process.

The process can be said to be quasi-static if the kinetic energy of the model remains small in comparison to the internal energy. From the graphs in Figure 6-6, this is the case with the maximum internal energy approximately 80 times larger than the maximum kinetic energy. The deviation after 3mm seen in the kinetic energy graph may suggest that after this point the pull-off model is no longer quasi-static. This is due to oscillations in the solution caused by the reflection of the vibrational wave. Therefore, the models were cut-off after 3mm of displacement. This provided enough displacement to cause the models to reach the failure threshold discussed in the later sections.

6.3.3 Creating Boundary Node Sets for the Octree Refinement Mesh

Boundary conditions in Abaqus can be applied to one of Abaqus' geometry references or to nodes and surfaces in the input definition. In this case, to model the T-Joint pull-off test, boundary conditions are required on the top surface of the web and the outward facing side faces of the flanges. For a voxel mesh, the consistent nature of the elements in size and shape renders it easy to find the node numbers labelling the nodes on the surface boundary. They will be consistent from one geometry to the next and can be calculated if the element size and prism domain shape are known. In the octree voxel mesh, element sizes and shapes vary across the model depending on the proximity to a yarn/matrix interface surface and the number of smoothing iterations applied. These nodes vary depending on the weave model geometry and parameters used to generate an octree voxel mesh. Therefore, there is no set method to determine these node numbers when using this meshing method.

It was possible to test whether these nodes were on the domain surface. Using this method, nodes were added to a new class *CTJointBoundaries* which is used to create boundary conditions for the T-Joint models for creating the T-Joint finite element models.

These boundary nodes are then tied by linear constraint to driver nodes to which the boundary conditions are applied. The reason for this is so that the force applied to the node is distributed equally among the nodes on a surface.

6.3.4 Material Properties

Each yarn is considered as a unidirectional composite with transverse isotropy. Material properties for such yarns can be found using Chamis' rule of mixtures [92] alongside using measured properties or those supplied by the manufacturer. As the purpose of this work is to find optimum reinforcement weave patterns, the material properties between each design produced by the optimisation algorithm will be the same. In this case, the material properties stated by the manufacturers of the materials used in Chapter 2 are used.

	E_1 (GPa)	E_2/E_3 (Gpa)	ν_{12}/ν_{13}	ν_{23}	G_{12}/G_{13} (Gpa)	G_{23} (Gpa)
Infused Hexcel Im7 Yarn	174.4	8.9	0.3	0.3	4.2	4.2
Gurit Prime 20LV Epoxy	3.5		0.5			

Table 6-1 Elastic properties of material constituents.

The strengths of the infused yarns can be found using empirical formulae [93].

	F_1^t (Mpa)	F_1^c (Mpa)	F_2^t/F_3^t (Mpa)	F_2^c/F_3^c (Mpa)	F_{12}/F_{13} (Mpa)	F_{23} (Mpa)

Infused Hexcel Im7 Yarn	3546	2754	116.7	233.4	116.7	116.7
Gurit Prime 20LV Epoxy	73	146				

Table 6-2 Strengths of material constituents.

The elastic properties of the homogenised yarns and the matrix are presented in Table 6-1. The material strengths used are presented in Table 6-2.

6.4 Mesh Sensitivity Study

Optimisation requires a compromise between finite element solution accuracy and analysis time. If the time for each weave to be analysed is too long then the overall optimisation time, which will use many individual analyses, will be too long to be useful to those wanting to perform optimisations. A mesh sensitivity study using models with no weft crossover (see Figure 6-7) was conducted to find the most accurate for optimisation. The criteria was primarily the stiffness response then the time taken for the model to run was a secondary consideration. The results from the mesh sensitivity have been balanced against the time taken for the analysis.

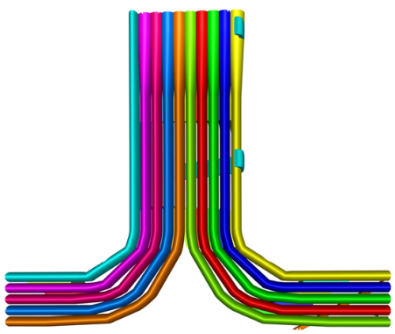

Figure 6-7 TexGen model with no crossover used for the tensile pull-off mesh sensitivity.

For the rectangular voxel mesh, all elements had the same aspect ratio so the only parameter is element size which can be reformulated as the number of voxels in the model. For the octree voxel mesh, there are three parameters: the starting number of voxels, the number of smoothing iterations to the surface element nodes and the level of refinement. The parameter study was used to find the correct balance between the three different parameters. Each mesh parameter has a different effect on the length of time it takes to generate the mesh and also the length of the analysis time, so these were both considered within the study.

For the mesh sensitivity study, each mesh was run using the boundary conditions set out earlier. Both the time taken and the force-displacement behaviour were plotted. Each weave was labelled according to the number of iterations of smoothing, the number of elements and the level of maximum refinement. The meshes are labelled in the legend by the number of smoothing iterations, if smoothed, the number of starting elements before refinement and finally the maximum refinement level.

(a)

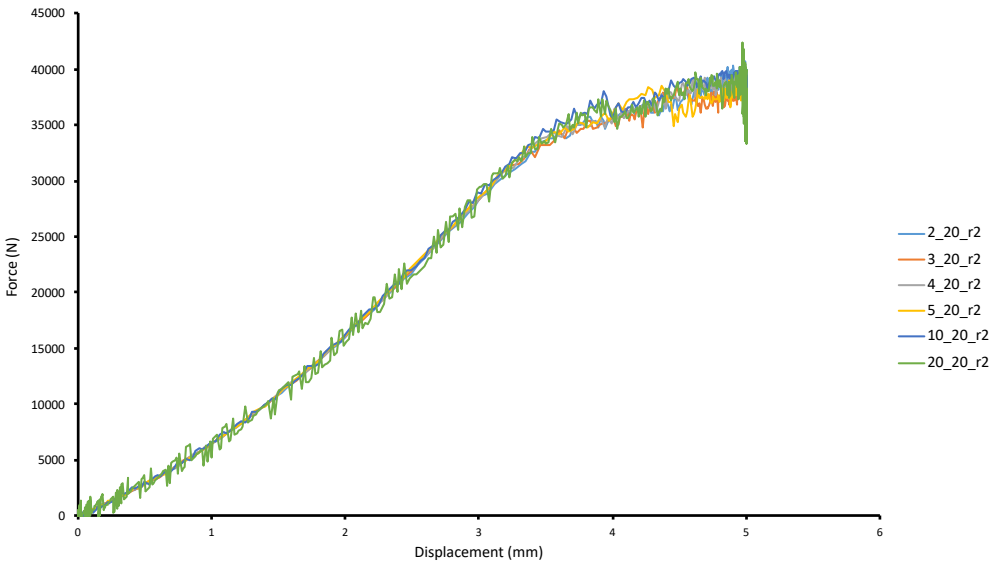

(b)

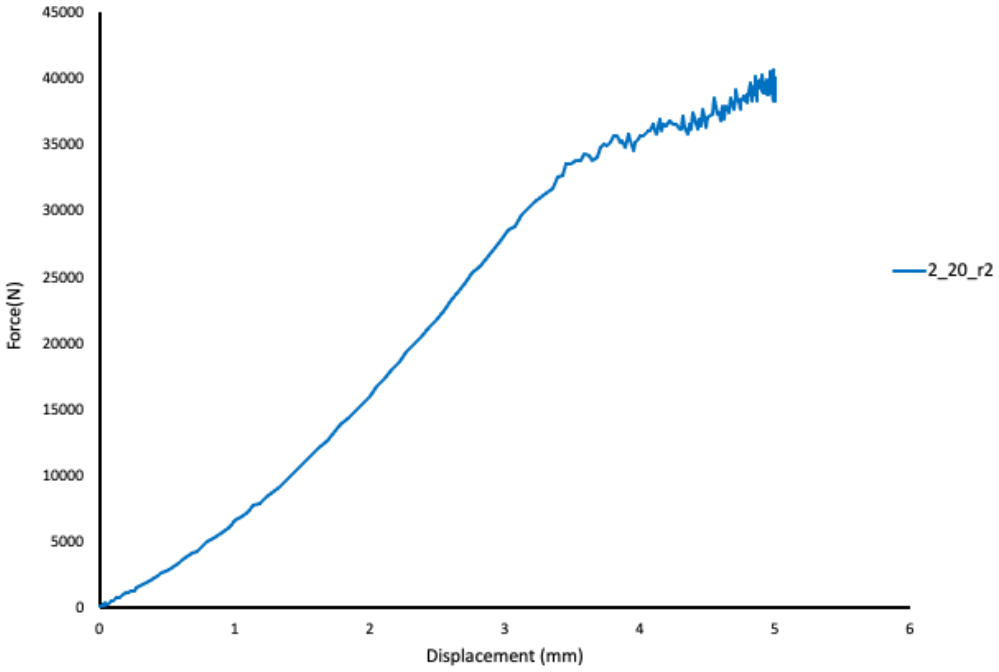

Figure 6-8 (a) Force-displacement graphs with meshes with refinement level 2 and 20 elements in each direction in plane of T-Joint profile. (b) Additional data set of the 20_2_r2 mesh, separated to improve visibility of other data sets.

The smoothed meshes all had the same number of starting elements. It can be seen in Figure 6-8 that as the number of smoothing iterations increases the oscillations in the load-displacement response increases. This is because of the effect from the increasingly poorly shaped elements produced by successive smoothing iterations. The effect can be seen starting from the models with smoothing levels over 10, so the number of smoothing iterations was set at 5.

For models with varying levels of refinement meshes with maximum refinement levels of 1, 2 and 3 were run without any smoothing iterations. Further refinements led to poor mesh construction due to the number of elements. This produced the following graphs in Figure 6-9.

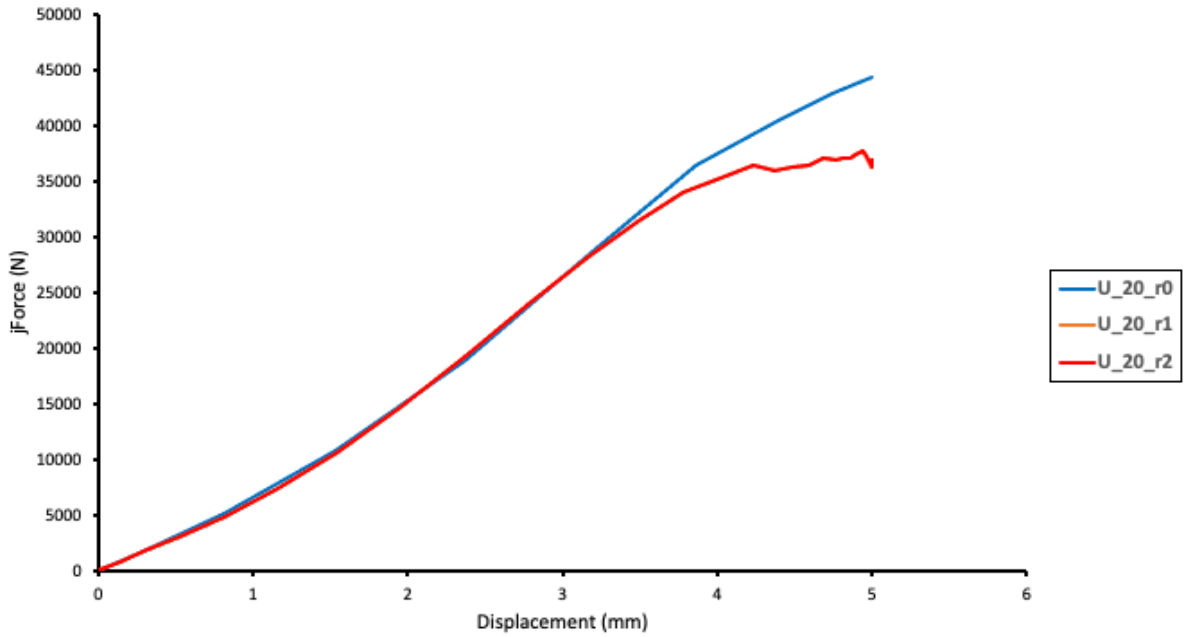

Figure 6-9 Tensile pull-off force-displacement graph for maximum refinments 1, 2 and 3. The line for U_20_r1 is obscured by the U_20_r2 line.

Refinement causes the number of elements to increase because of the subdivision of elements close to material boundaries. As can be seen the increase in refinement level between level 1 and 2 produced very similar graphs. As the refinement causes the cross-section shape to be better captured, refinement level 2 was judged to be the most appropriate.

As can be seen from Figure 6-10, increasing the starting number of elements beyond 20 did not yield any difference in the force-displacement response. However, as the number of elements increases there is an increase in the oscillation in the result. This is caused by noise from the explicit procedure. Since further increasing the number of elements only produced extra noise without altering the stiffness response, the number of elements was set to 20.

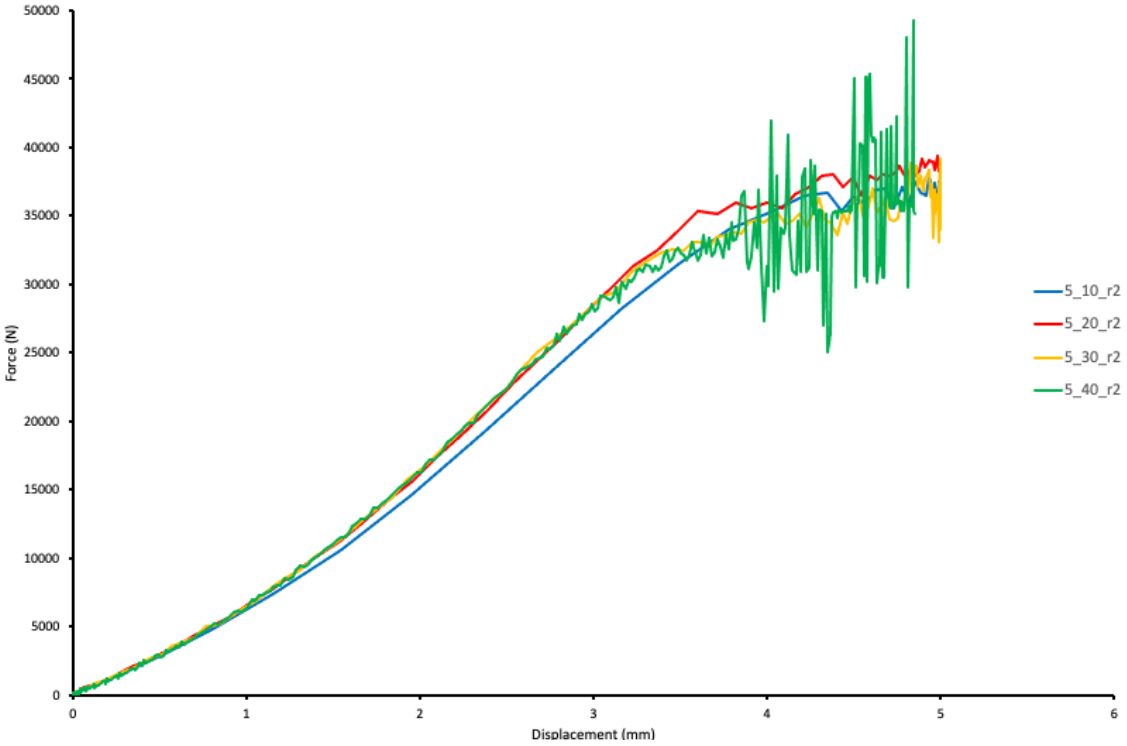

Figure 6-10 T-Joint pull-off force-displacement graphs for models with 5 smoothing iterations, refinement level 2 and varying numbers of elements in the x-y plane.

The final parameters chosen for the octree voxel mesh were 20 elements in the x-y plane, smoothed with 5 iterations of the smoothing algorithm and refined to a maximum level of 2. This mesh took 20 minutes to run on a standard desktop PC with 4 cores. This is well within a reasonable time frame for optimisation.

6.5 Selecting an Objective Function Value

One of the main purposes of this work is to use the ability to automatically generate T-Joint designs to optimise the weaving pattern. This requires the selection of an objective function to minimise. One of the main design considerations is the failure resistance of the composite joints under tensile

pull-off load. The usual finite element methods to characterise the failure behaviour of these joints is a full-scale failure analysis where the failure initiation and stiffness degradation of the joints is modelled using a user subroutine [36] and sometimes cohesive modelling of interface damage [47]. While this can reproduce high model fidelity, the use of the subroutines add significant computational cost as the subroutine is called after every increment to re-evaluate the stress state. This introduces a barrier to the use of this sort of failure modelling in an optimisation routine where hundreds of designs need to be analysed.

To compare and score the different joints, the finite element models were run using perfectly bonded elements (ie. No cohesive surfaces) and with no user supplied material models in the form of subroutines. Once the models are run, for each frame a Python script was developed that iterated through each element and evaluated its stress state which was then compared to Hashin's failure criteria [94] for the yarn elements and the pressurised Von Mises criteria for the elements in the matrix. This is to be able to determine the initial failure load which will form the basis of comparison between the different T-Joints in an optimisation. It has the advantage of being able to determine initial failure without the cumbersome cost from running user subroutines at every iteration in the finite element analysis.

6.5.1 Determining Initial Failure

To determine the point of initial failure, several methods were considered. One method involved checking the surrounding elements of those failed, to build up a chain of localised element failure that would stop once the chain reached a certain size. This was attempted but ultimately took too long for an optimisation process. This would be an interesting avenue for further research. The method decided upon determined that initial failure occurs when a failure threshold was met. This was set so that the global number of failed elements should not exceed 2% of the total elements in the mesh. This has the advantage

of not only being significantly faster to compute but also being mesh size independent.

Without stiffness degradation upon failure, each of the elements will continue to be able to support local stress to the same level, causing an increasing error in the following solution. It was chosen therefore to make an early cut-off. Therefore, elements that have failed according to the failure criteria will cause the load-displacement response to deviate immediately from the true behaviour. Experimental validation of the finite element analysis was again not possible due to the Covid pandemic and the difficulty in obtaining woven samples which is discussed in more detail in Chapter 3.

6.5.2 Failure Criteria

The yarns are treated as homogeneous unidirectional plies with transverse isotropy. This allows them to be treated like any other unidirectional composite in terms of their failure behaviour. From the numerous available failure criteria that have been postulated, none has been shown able to predict mechanical failure onset for any 3D loading condition [95], [96] with the top ranked criteria only capable of predicting failure under two dimensional stress-strain. This question of the best failure criteria to use represents an entire field to itself, where there is no clear answer. Therefore, until a more complete theory is produced and verified, it is left to the user to make their own selection. In this case, Hashin's failure criteria was chosen because it uses four criteria to predict failure: both transverse and longitudinal (in the fibre direction) failure in the yarns by compressive or tensile stress. These are given in equation below.

$I_1 \geq 0$ $$d_1 = \left(\frac{I_1}{F_1^t}\right)^2 + \frac{I_4}{F_{12}^2} = 1 \quad (6\text{-}1)$$

$I_1 \leq 0$ $$d_2 = \left(\frac{I_1}{F_1^c}\right) = 1 \quad (6\text{-}2)$$

$I_2 \geq 0$ $$d_3 = \left(\frac{I_2}{F_2^t}\right)^2 + \frac{I_3}{F_{23}^2} + \frac{I_4}{F_{12}^2} = 1 \quad (6\text{-}3)$$

$I_2 \leq 0$ $$d_4 = \left[\left(\frac{F_2^c}{2F_{23}}\right)^2 - 1\right]\left(\frac{I_2}{F_2^c}\right) + \left(\frac{I_2}{2F_{23}}\right)^2 + \left(\frac{I_3}{F_{23}^2}\right) + \left(\frac{I_4}{F_{12}^2}\right) = 1 \quad (6\text{-}4)$$

$$I_1 = \sigma_1, I_2 = \sigma_2 + \sigma_3, I_3 = \tau_{23}^2 - \sigma_2\sigma_3, I_4 = \tau_{12}^2 + \tau_{13}^2 \quad (6\text{-}5)$$

where the I_i are the four stress invariants for which $I \geq 0$ is for tensile stress and $I \leq 0$ is for compression. The F_i are the tensile and compressive strengths longitudinal and transverse to the fibre direction. The d_i are the damage parameters for longitudinal tension and compression and transverse tension and compression respectively. Generally for the infused yarns, longitudinal failure indicates fibre failure while transverse failure indicates failure of the intra-fibre matrix within the yarn.

The matrix elements are homogeneous and isotropic, the pressurised Von Mises criteria was used [97].

$$d_m = \frac{F_m^c - F_m^t}{F_m^c F_m^t} + \frac{1}{2F_m^c F_m^t}[(\sigma_1 - \sigma_2)^2 + (\sigma_2 - \sigma_3)^2 + (\sigma_1 - \sigma_3)^2] \quad (6\text{-}6)$$

where d_m is the matrix damage parameter and the F_m are the tensile and compression damage parameters.

6.6 Conclusions

A modelling schema for evaluating the fitness or the ability of the T-joint weaves under tensile pull-off load was set out to find the initial failure load for use as the objective function value in the optimisation in the next chapter. Abaqus explicit was used to achieve a faster analysis time. The time control was selected after setting a lower bound in accordance with the Abaqus user manual recommendation.

Mesh sensitivity studies for both the rectangular voxel mesh and octree voxel mesh were conducted to find a mesh that balances the accuracy required against the time taken for each analysis. This brings a subjectivity to the choice of which mesh to use as the priority between analysis time and accuracy is up to the modeller. For rectangular voxel meshes the main parameter is the number of elements as each element has the same aspect ratio. For the octree voxel mesh, there are additional parameters to be considered when conducting mesh sensitivity studies, namely the number of refinements at the material interfaces and the number of smoothing algorithm iterations. An octree voxel mesh was chosen with 5 smoothing iterations and a maximum refinement level of 2. This mesh conformed well to the yarn cross-section shape without causing over distortions to the mesh elements.

Chapter 7 - Optimisation of 3D Woven Reinforcement

7.1 Introduction

It is the aim of this section to demonstrate the possibility of optimisation for 3D profiled structures. The case study presented here is one example for orthogonal type T-joint weaves but can be extended to other profiled shapes containing bifurcations. As well as other shapes, other objective functions can be considered if obtainable from the element stresses or load-displacement graphs where the analysis time is reduced when compared to full scale failure analysis as set out in the previous chapter. The genetic algorithm introduced in Chapter 4 is used for the optimisation and is adapted for use in permutation optimisation. The methods for the automatic generation of T-joint geometries presented in Chapter 5 is used to vary the weft yarn interlacement patterns while the analysis framework presented in Chapter 6 is used to score each weave pattern design. The knowledge gained from an analysis of the experimental data in Chapter 3 is used to aid in interpreting the final optimised weave design.

Genetic algorithms work using a combination of evolutionary operators: crossover and mutation, to generate the next set of design candidates. For optimisation based on a bound set of integers, this will result in repeats of the design variables. For the T-Joint weaves, variation primarily occurs with the weft crossover at the junction. This means that the optimisation is based on permutations of the design variables. An adaptation is demonstrated to ensure the optimisation algorithm produced permutations by encoding the design variable integers as 4 bit strings in binary.

In this optimisation problem, there are 10 wefts which can be arranged in any order, giving (10! =) 3.6 million possible permutations. The development of a tool for the fast creation of T-joint geometry models means that the limitation of manual model generation has been eliminated. This can provide a step change in the optimisation of weaves of these types. The optimised textile

reinforcement is compared to the naïve first guess for a woven T-joint based on orthogonal weaves. Failure of the elements is shown to propagate within the expected junction zone where the stresses are highest.

7.2 Optimisation Problem

The optimisation problem is to maximise the initial tensile pull-off load which causes failure in the T-joint, subject to Hashin's failure criteria in the yarns and the modified pressure dependent criterion in the bulk matrix.

Maximise f(x) <0 where f is the initial failure load.

The starting point is a 10 layer orthogonal weave containing a bifurcation. The design variables are the end positions of the weft yarns after the bifurcation. Each yarn can shift to any of the final end positions and all end positions must have a yarn. No end position can be occupied by more than a single yarn. The only constraint on the design variables is that they must respect this permutation only condition.

Therefore, each design is a 10 digit string. For example, for the orthogonal weave reinforcement with no weft crossover where each weft yarn's initial and final position in the textile matches:

[0,1,2,3,4,5,6 ,7,8,9]

Each item in the string is an end position of the wefts.

Other parameters such as weft yarn cross section, binder section and filament count were omitted from the optimisation as the interlacement pattern was the focus of the study.

Each weave is scored on its tensile load at initial failure. This is calculated post finite element analysis by iterating through the elements for every time frame using the failure criteria set out in Chapter 6.

7.3 Implementation of Binary Encoding of Design Variables

Genetic algorithms generate design variables by varying the individual design variables within bounds. This is achieved using the mutation and crossover functions that seek to mimic the biological processes by which genetic characteristics are passed from one generation to the next. In most cases, this allows the individual digits that represent design variables to be present multiple times within the same design string as the algorithm selects each value independently while respecting any linear constraints. One example is

$$[1,2,3,2]$$

where the design variable “2” repeats twice in the string. In this case where the design variables represent the height positions of the wefts in the textile after the bifurcation it is not possible to have repeats.

To prevent this in the permutation-based optimisation, the design variables were encoded as 4 bit binary strings which can hold integer values from 0 to 15. Each bit becomes a design variable in the optimisation. For a design permutation with 4 variables this conversion could look like.

$$[0011\ 0001\ \ 0011\ \ 0101]$$

Which in decimal is

$$[3\ 1\ 3\ 5]$$

Each of the variables are then ranked from lowest to highest and any ties broken at random. In this case, the design variables in positions 1 and 3 have the same ranking either coming second and third or third and second from lowest. For

the example this would give the final design string permutation, containing the rankings, as:

$$[2\ 1\ 3\ 4]$$

However, if the tie is broken the other way, it could also result in the final design string of:

$$[2\ 1\ 2\ 4]$$

In this case the ties were broken at random using Python's random number generator because there is no a priori knowledge to provide a beneficial method to ranking selection for this optimisation problem. The drawback to this adaptation is that the same design string can represent more than one final design permutation. A flowchart showing where the binary encoding method sits in the optimisation flow is in Figure 7-1.

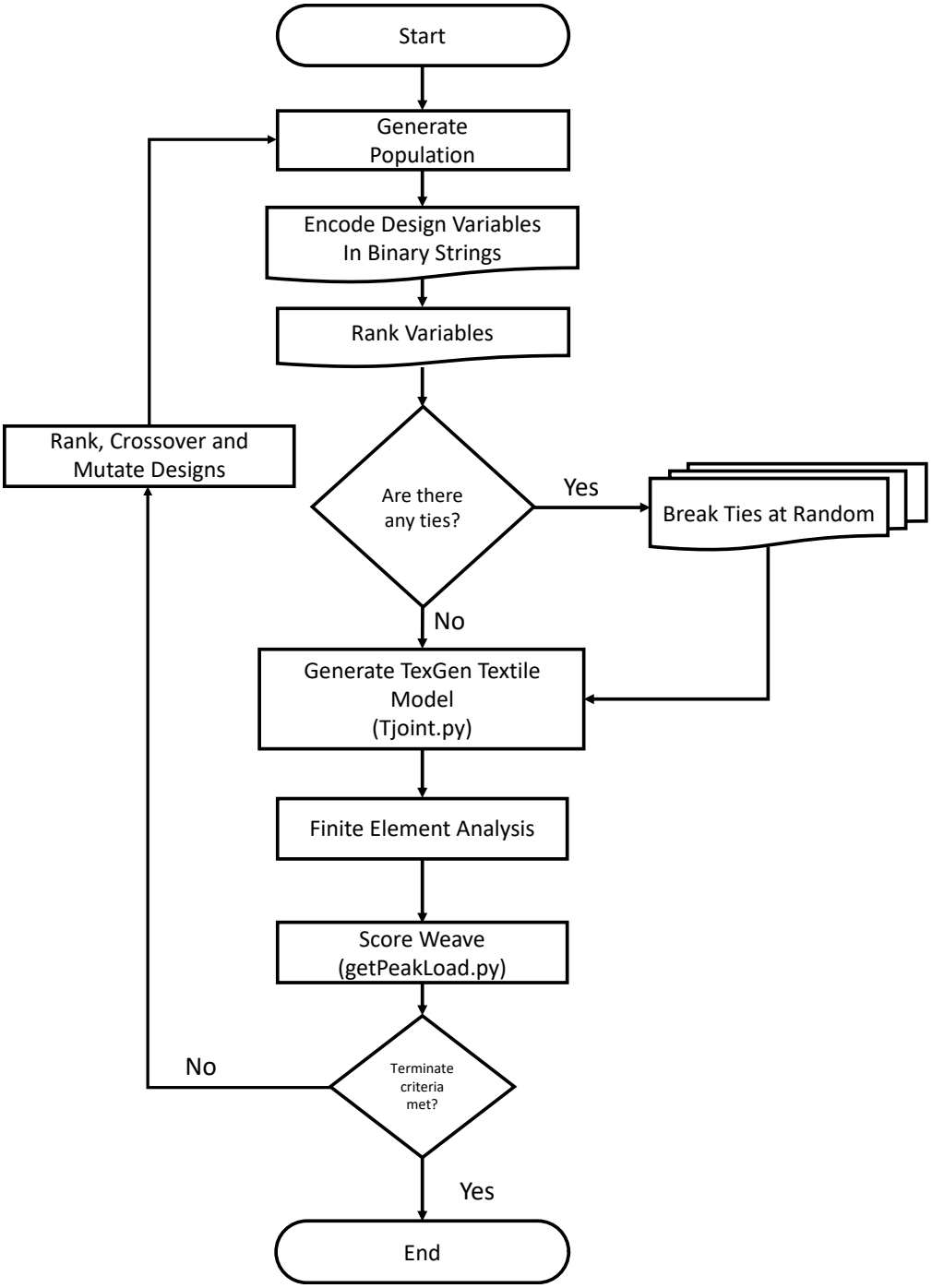

Figure 7-1 Flow chart diagram of optimisation process highlighting how the permutation operations fit within the optimisation process. Boxes in green show the binary encoding of the design variables. Trapezoids show the model generation and finite element analysis.

The design variables generated by Matlab were fed into Python functions that ranked the variables and broke any ties to generate the string of decimal

numbers making up the design permutation. These were then used to generate the geometry of the T-joint weaves for the optimisation.

The genetic algorithm was limited to crossover of its design variables to produce the next generation so that the problem is reduced to a combinatorial problem. This meant that the mutation operation parameter was set to 0. This is appropriate given that the overall design is the result of the combination of the final weft yarn positions.

7.4 Results of the Optimisation

The optimisation was run on the University of Nottingham HPC (high performing computer cluster), in parallel, using an NSGA algorithm with a population size of 30, adapted for generating permutations of the design variables as set out in section 7.3. The optimisation evaluated 519 3D woven composite T-joint weave pattern designs taking a week to complete. Further information on the algorithm performance is difficult to obtain due to limitations in the reporting output to the HPC's logging file.

Each model was run using 8 CPUs, with three separate MATLAB workers generating the input files and running the analysis. Once the stopping criteria of the optimisation was reached, the solution with the largest peak load was given by the design variable string:

[9, 5, 6, 7, 8, 4, 1, 2, 3, 7]

The geometry model generated by TexGen is shown in Figure 7-2.

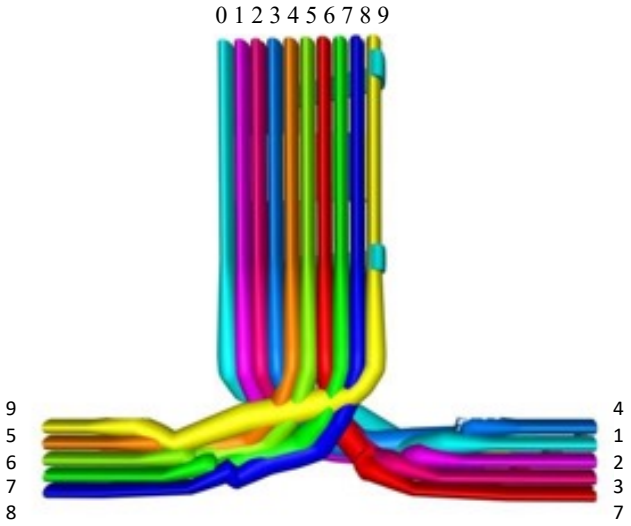

Figure 7-2 TexGen model of best performing weave reinforcement. Each half of the textile has some weft yarns that have crossed over and at least one yarn that stays in the same half of the textile.

The initial failure load was 1220.6N which when compared to the orthogonal weave's initial failure load of 1121.7N is an 8.8% increase. The worst performing textile had an initial failure load of 939.0N giving the best performing weave exhibiting a 30% higher initial failure load.

The weave shown in Figure 7-2 has some intersections between the yarns. TexGen can assign volumes within intersecting yarns to just one of the yarns. This allows the analysis to proceed despite any flaws in the model.

7.4.1 Comparison to Orthogonal Weave without Crossover

This section will be used to compare the difference between the optimised textile and the naïve guess of a bifurcated orthogonal textile and the worst performing textile. This will provide information about the weave characteristics in terms of the weft yarn crossover and junction shape that result in better performance in terms of the load at initial failure.

For the orthogonal textile, the weave model generated by TexGen after the application of the bifurcation transformation is shown in Figure 7-3.

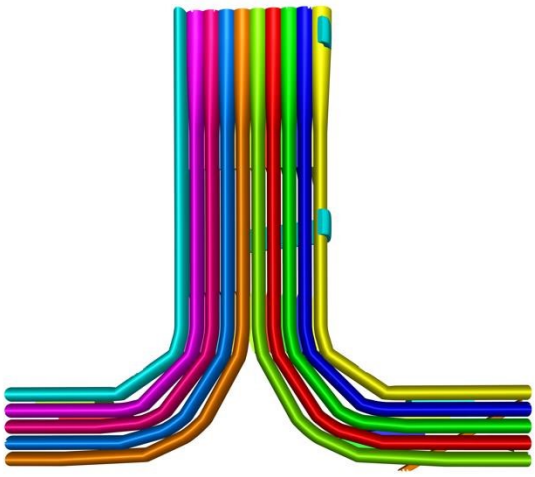

Figure 7-3 Orthogonal weave T-Joint reinforcement model generated using TexGen.

This model was meshed using the octree voxel mesh and run in Abaqus using the finite element tensile pull-off model and mesh parameters selected in the previous chapter. Shibo et al. [58] suggested that the best performing T-joint weaves with weft yarn variations had wefts that cross over and wefts that self entangle. The conclusions drawn in that case was based upon a limited number of model geometries. The numbers were limited because of the manual, time intensive nature of the model generation. Crossover is when weft yarns cross from one half of the textile to the other at the junction region. Entanglement was defined to be when wefts do not crossover into the other half of the textile at the bifurcation region but do crossover each other. The orthogonal weave model exhibits neither weft crossover nor entanglement. As a result, the junction region of the model is resin rich, containing no yarns and presenting a large triangular notch shape.

7.4.1.1 Best Performing Textile

The best performing textile reproduced in Figure 7-4 shows four of the five yarns in the top and bottom halves of the textile respectively crossing over. There is a degree of weft entanglement from both halves with the yarns switching around. This leads to a significantly reduced notch area with a higher fibre volume fraction in this region to sustain and redistribute the stress. The model is relatively symmetric with similar entanglement and crossover from both textile halves.

(a)

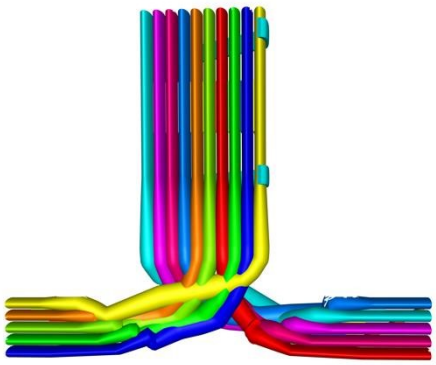

(b)

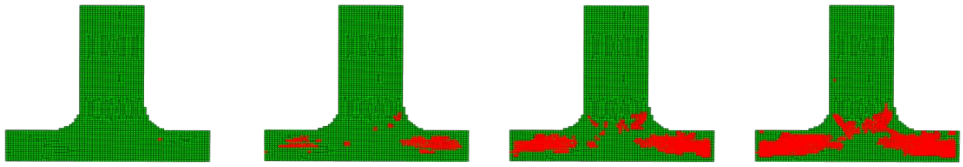

Figure 7-4 (a) TexGen model of best performing weave reinforcement and (b) the finite element mesh showing progression of element failure at displacements 0.1, 0.2, 0.3 and 0.4mm from left to right.

For this best model, the first element failure occurs on the transition zone between the junction region and the flange. As the displacement increases, failure propagates into the junction region via the yarn that has transitioned from the second from top position (in blue in Figure 7-4 (a)) to the bottom. This may be due to its relative proximity to the centre of the junction region. The number of failed yarns remains higher in the flange than in the junction region,

suggesting that the stresses have been successfully distributed by the weave configuration. One possible reason for this is the greater amount of fibre along the loading direction caused by weft crossover.

7.4.1.2 Worst Performing Textile

The worst performing textile is shown in Figure 7-5

(a)

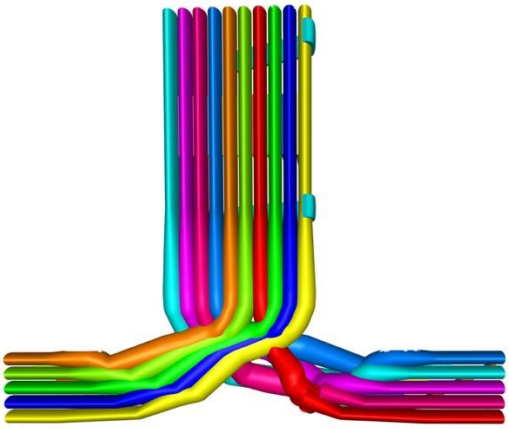

(b)

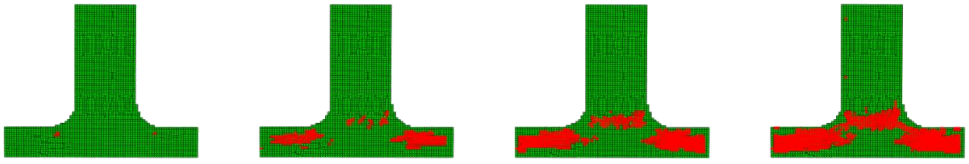

Figure 7-5 (a) TexGen model of worst performing weave reinforcement. Entanglement occurs in the right half of the textile but there is no entanglement in the left half. This leaves some resin richness in the noodle. (b) the finite element mesh showing progression of element failure at displacements 0.1, 0.2, 0.3 and 0.4mm from left to right.

The worst performing textile similarly had a high degree of weft crossover with 4 out of 5 wefts again moving to the other half of the textile. However, the textile is highly asymmetric with almost no entanglement in the yarns crossing over from the top half of the textile to the bottom half so they remain to a greater degree transverse to the loading axis. In addition, this leaves some resin

richness at the junction base. The first elements again fail in the transition zones between junction and flange. It is difficult to ascertain the proportion of elements failing in the junction for each model because this zone is not well defined, however, by the 0.2 mm displacement visually a greater proportion of the elements have failed in the junction compared to the best performing textile. In Figure 7-6 there are more failed elements in the junction region for the worst performing T-joint.

For the models in Figure 7-6, the elements failed at 0.1, 0.2, 0.3 and 0.4mm of displacement are shown, with the straight yarn model at the top followed by the worst model in the optimisation and then the best. Yarn element failure for the straight and worst models concentrates to a greater degree in the junction region of the T-Joint (see top row of Figure 7-6). A lower number of yarn elements in the junction region, created from the configuration of the weft yarns, is a probable reason for this.

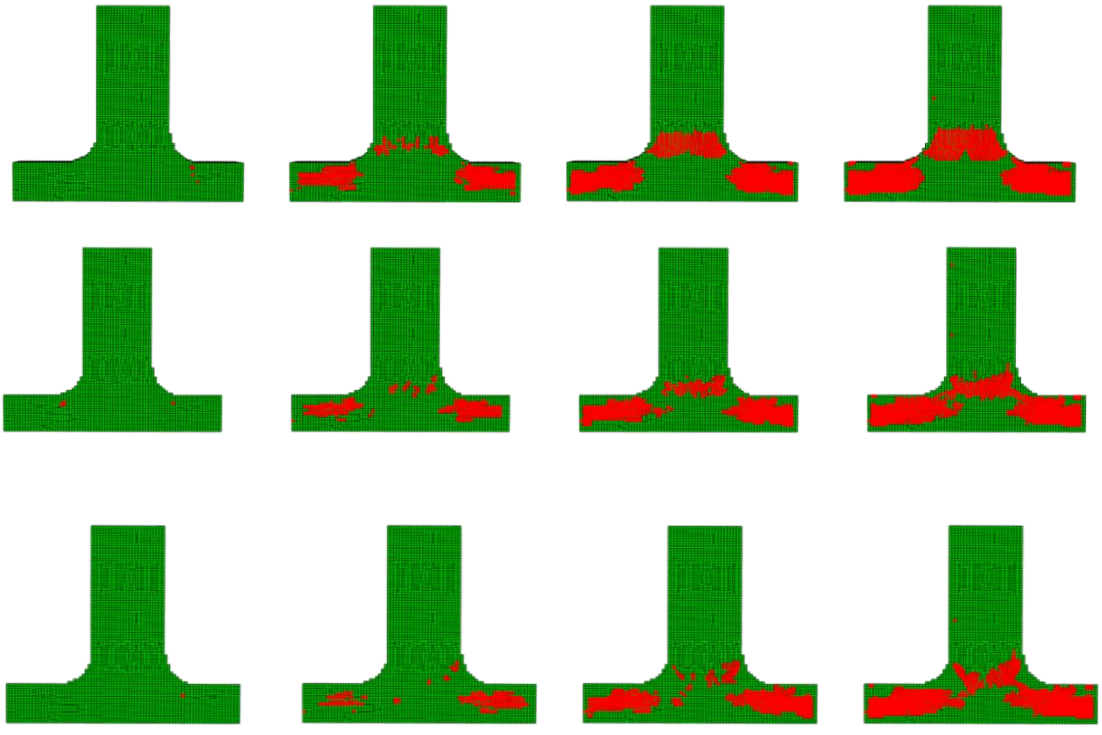

Figure 7-6 From top-to-bottom finite element models of the straight weave with no weft crossover, the worst performing textile and the best performing. Each model has the failed elements at displacements 0.1, 0.2, 0.3 and 0.4mm respectively.

Determining when initial failure can be said to have occurred was discussed in Chapter 6. The numbers of elements failed plotted against the increment time are shown in Figure 7-7. The measure of initial failure was set to 2% of the global element number. For the straight model, the models at different displacements are overlaid on the number of element graph shown in Figure 7-7. The location of failure indicated by the presence of failed elements corresponded to literature experimental data indicating that elements primarily failed along yarn/matrix interfaces within the junction region of the T-joint.

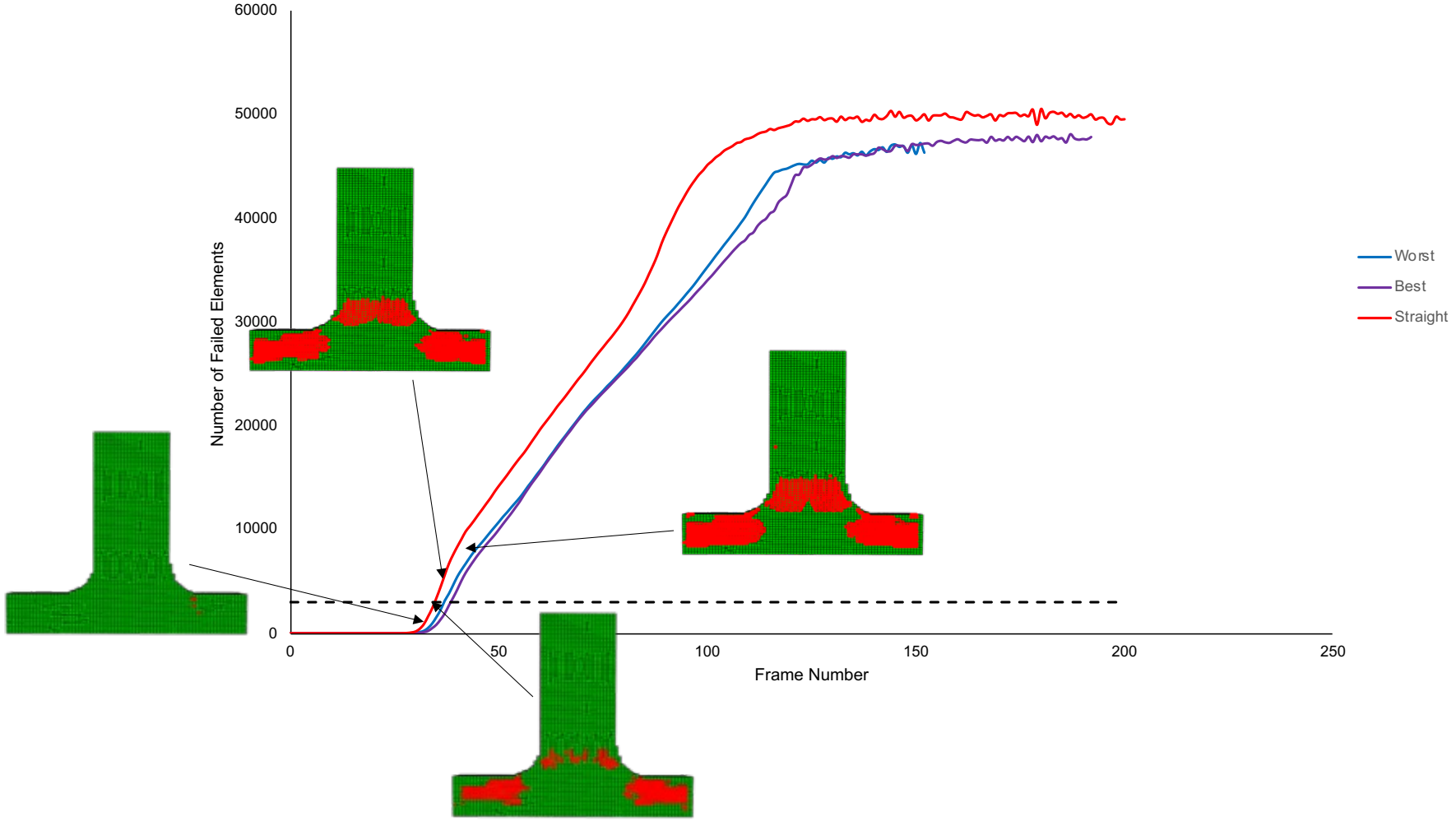

Figure 7-7 Graph of number of failed elements against increment time. The locations of element failure for the orthogonal (straight) graph are shown at 0.1, 0.2, 0.3 and 0.4mm. The horizontal dashed line shows the approximate 2% of element number line.

The number of failed elements reaches the 2% initial failure threshold for the straight T-Joint model at 0.2mm. The graphs for the best and worst models are shown in Figure 7-8. The best model has a displacement of 0.26mm at initial failure while the worst model has a displacement of 0.24mm.

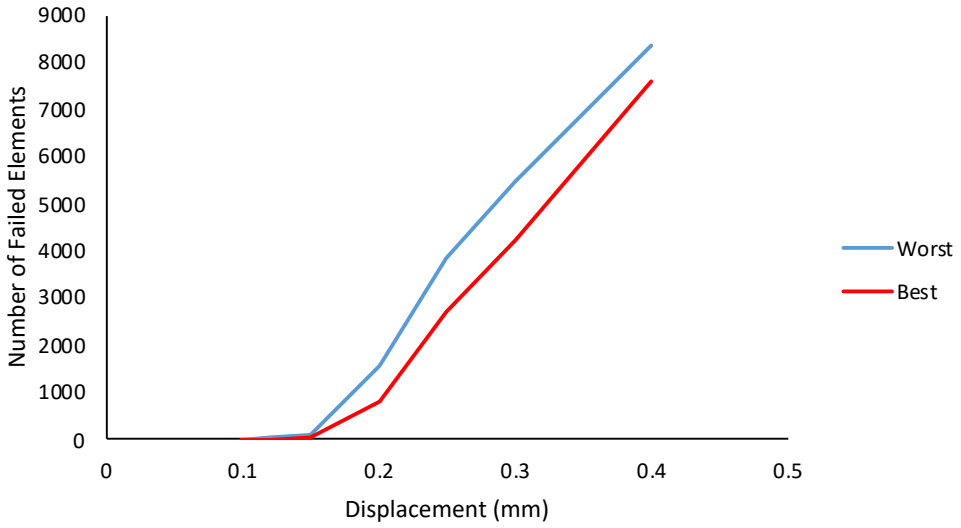

Figure 7-8 Number of Failed Elements against applied Displacement for Best and Worst performing models.

As mentioned in Chapter 3, the Covid-19 pandemic and the cost of manufacturing 3D woven T-joint reinforcements meant that an exact experimental validation of the results presented here was not possible. However, it is evident from the experimental results in Chapter 3 that the specimen 1 weave pattern design with weft yarn crossover and entanglement did better than the specimen 2 weave pattern design in both initial failure load and in its damage evolution post-initial failure. This corroborates other data in the literature, namely in [21], where an additional 3D woven specimen with weft yarn crossover was tested.

7.5 Conclusions

Optimisation of T-joint weave reinforcement under tensile pull-off load has been carried out using binary encoding of design variables to allow optimisation based on the permutations of weft yarn variations using a genetic algorithm on an HPC.

The optimum textile showed an 8.8% increase in the load at initial failure when compared to the orthogonal weave with no crossover of the weft yarn and a 30% increase over the worst performing weave.

The optimum textile found had a reduced junction region, achieved by a combination of weft yarn crossover and entanglement. Four yarns of the five in each half crossover while one remains in the same half. This arrangement allows the volume at the junction to be flattened out and stresses redistributed so that the failure occurs further away from the junction region. The crossover and entanglement allows there to be more fibre placed along the direction of the loading within the junction region. This can be contrasted with the worst performing weave reinforcement and the orthogonal (straight) weave which both had reduced levels of weave entanglement resulting in a greater proportion of the yarns aligned transverse to the loading direction.

Chapter 8 - Discussion

8.1 Introduction

The purpose of this work was to develop and demonstrate an optimisation design process for the weaving patterns of 3D woven carbon fibre reinforced T-joints. This was to aid in solving the problems associated with designing weave patterns for 3D woven reinforced structures, namely the large design space and difficulty in knowing the effect of weave changes on the mechanical properties of T-joints. The challenges included picking the correct optimisation algorithm, developing a method to predict and implement the interlacement pattern, automatic generation of meshes, overcoming the length of time it takes to run each candidate design through the objective function evaluation and running a permutation optimisation of the initial failure load of the composite T-Joints.

This chapter will discuss the results from the previous chapters and evaluate them against the aims and objectives set out in the Chapter 1. It will be noted for each whether these fill research gaps identified in the literature review. The methodology used will be discussed including an overview of the software developments associated with the work completed. This will be followed by a summary of the work completed and a suggestion for next steps.

8.2 Comparison of Research Work to Aims and Objectives

In the introduction, the main research question on whether it is possible to use optimisation algorithms to improve the design of 3D woven composite T-joints, was broken down into five aims and objectives. This section will evaluate each of the five core aims and objectives against the work included in the subsequent chapters. The purpose is to identify where they were met and whether the overall research question posed at the start of the work has been answered, noting where gaps in the literature have been filled. Each of the aims are listed followed by an assessment of the work completed against whether those aims were achieved.

8.2.1 Experimentally investigating T-Joint Behaviour

The literature review identified that there had only been one example [58] of published data regarding 3D woven carbon fibre reinforced composite T-joints. This is in addition to a limited amount of μCT data [55] of the junction region of 3D weaves with weft yarn crossover. More data was needed before being able to conclude that the nesting of the weft yarns was a phenomenon not restricted to the textile in the paper.

A set of μCT data was collected for the T-joint with crossover; the same nesting effect of the weft yarns can be seen. However, due to the size of the carbon fibre sample used, the resolution of the images was low. Even so, the images were enough to provide some extra validation for the nesting effect.

In Chapter 2, the manufacturing process for two different 3D woven composite T-joint reinforcements was set out. This included preparing the reinforcement samples, mixing the epoxy and the RTM process. The two weave patterns had several key differences, one had axial weft and warp yarns (±45°) with no crossover of the weft yarns at the junction, the other had straight (0°) yarns with weft yarn crossover. It was found that the straight yarned T-joints were both stiffer and able to reach a higher peak load than the T-joints made from the axial reinforcement. One hypothesis in [21] is that weft crossover in T-joints has a crack arresting effect due to the misalignment of the yarns in the junction region shortening the average crack length. The results in this chapter provide further evidence to support this.

An ideal way to achieve the main aim of the research to optimise 3D woven T-joints would have been to perform the tensile pull-off test on a T-joint made using a reinforcement in the final optimised weaving pattern. This would have validated the modelling work done in Chapter 6 and provided confidence in the overall optimisation process. However, as mentioned in Chapter 2, the Covid-19 pandemic alongside the cost of setting up a loom to produce the fabric meant that it was not possible.

8.2.2 Composite Optimisation

Previous work completed at the University of Nottingham [14], [23] had demonstrated optimisation of the unit cell of flat 3D woven textiles using genetic algorithms. These unit cell optimisations relied upon periodic boundary conditions finite element analyses to obtain an objective function value made up of the elastic constants and so were only applicable to periodic textiles. This raised the question of whether it would be possible to use numerical optimisation algorithms for a significantly more complex structure like T-joints. Furthermore, the T-joint design criteria includes the failure behaviour to a greater extent than for flat unit cells because it is a structural component. This meant that some failure-based modelling approaches such as modelling the yarn/matrix interface, would be of interest. However, as the flat 3D weaves are smaller models than the full T-joint models in terms of mesh size and problem complexity, they provided a good opportunity to test cohesive surfaces in the context of an optimisation.

In Chapter 4, three optimisation algorithms were compared to find the most appropriate for flat 3D woven unit cells, the genetic algorithm alongside the particle swarm and pattern search algorithms. The objective function value was the through-thickness stiffness, E3. As part of that work, a new test for feasibility was developed to rule weave designs that would not be able to be woven out of the optimisation, thereby reducing the overall time to reach a solution. The genetic algorithm was chosen out of the three because it reached a solution in significantly fewer function evaluations.

In the next part, an optimisation was run again for unit cell 3D woven textiles, optimising for peak load in the through-thickness direction. Cohesive surfaces were used to model the yarn/matrix interface. One of the barriers to the use of cohesive surfaces in previous optimisation attempts was the length of time it took to generate the surfaces. To speed up the surface generation in TexGen, OpenMP was used to parallelise the key parts of the code. This significantly cut down the length of time to automatically generate the mesh with the cohesive surfaces. However, when applied to T-joint models the length of time remained too long to include cohesive surfaces as part of an optimisation run. An extension of this is also that using UMATs to model material failure was

evidently not going to be possible for T-joints as they take longer to run than cohesive models.

This work on composite optimisation of flat 3D woven textiles may not have been directly linked to T-joint optimisation but contributed overall by guiding the process. An example is by ruling out the possibility of using cohesive surfaces, and consequently UMATs, within optimisation runs.

8.2.3 Automatic Generation of T-joint Models

One of the main barriers to the optimisation of 3D woven T-joints at the start of this work was the ability to automatically generate the weft interlacement pattern from any starting weave pattern. This was difficult because of the need to be able to predict the order in which the wefts wrap around each other and the difficulty in then Python scripting a parameterised model that would be able to take the inputs from the predicted interlacement ordering and generate a high quality geometry model to accurately model the as-woven textile. This represented a gap in the literature that previous work by Yan and Brown had tried to fill.

The models generated in this work are idealised representations of the actual textile architecture. To get a parameterised model that is more representative would be difficult and require a large amount of μCT data to validate against. One of the key differences between the idealised models and the actual textile is yarn path waviness and cross-section variability. TexGen already has the capability to model these types of woven features so this is an area for future research.

This work was the most pivotal in paving the way towards running an optimisation and answering the research question posed by the work. An additional outcome is the Python scripts can be used as a tool to automatically generate T-joint textile designs. This is useful for weave pattern designers of 3D woven T-joint reinforcements.

8.2.4 Automatic Generation of Meshes

One of the key aspects of numerical optimisation algorithms is the lack of user interaction once the optimisation process has begun. This means once the textile geometry models have been generated, they need to be meshed. Previously, automatic generation methods for T-joints relied on using voxel meshes, this allowed fast generation of a good quality mesh with elements of a consistent aspect ratio. However, they produce a stepped interface between the yarn and the matrix which can act as stress concentrators and require many elements to get a sufficiently accurate mesh of the yarn volumes. The effect of the stress concentration effect can be seen in Chapter 4 when choosing a mesh for the peak load optimisation where the denser meshes with the smaller elements have lower peak shear stresses.

Subsequent to the commencement of this work, a new version of TexGen was released that used an octree voxel mesh refinement [20] to subdivide elements close to the yarn/matrix interfaces. This had the advantages of the voxel mesh while also being able to mesh yarn volumes more closely with fewer elements. In addition to this the octree voxel mesh came with a smoothing algorithm which was able to reduce the stepped effect along the material interfaces, the disadvantage of this is a less consistent mesh quality as there is no longer a constant aspect ratio. This work tested out the octree voxel mesh on the T-joint models and compared it to the voxel mesh while also varying the degree of refinement and the number of smoothing iterations.

For the optimisation, the accuracy of the finite element mesh, which usually increases with the number of elements, must balance with the length of time it takes to run the model. As a result, choosing the best mesh relies on judgement. Increasing the number of smoothing iterations above 5 led to oscillations in the force-displacement response, probably due to the generation of poor-quality elements by the smoothing algorithm. Increasing the number of refinements above 2 did not yield a change in the force-displacement curve and the number of elements was chosen to be 20 as increasing the number of elements again saw oscillations in the force-displacement response.

Overall, the ability to use an octree voxel mesh with the optimisation facilitated the optimisation of the T-joint weave pattern by providing a robust method of

automatically meshing the geometry in a similar way to the voxel mesh but with the advantage of the refinement and smoothing.

8.2.5 Method to Score Each Weave Pattern

The final aim and objective from the literature review was to find a method of scoring each 3D woven T-joint weave pattern design. The literature review revealed that one of the key aspects of T-joint design is its resistance to failure. Previous runs of optimisations for 3D woven composites have used elastic properties calculated from periodic boundary conditions analyses as the basis of the objective functions. These are not so applicable to T-joints so a different method of scoring the weaves was needed that would satisfy the design requirements.

In Chapter 4, the optimisation of the peak load for the flat 3D woven models using cohesive surfaces to model the interface damage, while successful, took too long. The T-joint models were larger so would have taken much longer meaning that using cohesive surfaces to model yarn delamination in the T-joints was a less favourable option. Following on from that, modelling the failure behaviour of the T-joints using Abaqus user subroutines, which are also time intensive, was also not a realistic option for the optimisation.

In Chapter 6, a new idea was developed to score the weaves. A post-finite element analysis script was used to iterate through each point in the time step and evaluate the stress levels against Hashin's failure criteria. Once 2% of the elements were deemed to have failed, the load at that point in the analysis was determined and used as the initial failure load. It would have been better if this was able to be validated against experimental data but shows a new approach that was able to provide a consistent measure across all the T-joint designs generated in the optimisation.

8.3 Methodology

The strategy for this work was a combination of developing the software capability to carry out the geometry modelling and analysis needed for the optimisation alongside a program of experimental work. This section will focus on the software development as the experimental work has been touched upon and discussed in previous sections. A link to a GitHub repository holding a copy of the code used throughout this thesis is found in appendix B.

8.3.1 Software Development to Facilitate Research Work

To facilitate the optimisation processes, the further development of several aspects of TexGen was required alongside Python scripts to automatically generate the woven reinforcement geometries of both the flat woven and the T-joint textiles and mesh the full composite domain.

In Chapter 4, the *CheckBinderPaths* Python code is used to evaluate whether the binder yarn path of different weave designs represent feasible textiles. This meant that an unfeasible textile design generated by the algorithms would have been removed from the process without being run through the finite element analysis. A large penalty value is used in its place as the objective function value. In addition to this, the OpenMP library was introduced to the *COctreeVoxelMesh* TexGen class to split up the processing of surface elements across multiple CPUs. This allowed surfaces for the cohesive contact analysis optimisation to be output quicker, which was important for reducing overall function evaluation time.

In Chapter 5, the *CTextileOrthogonal* class was modified to allow placement of binder yarns at any height in the weft stack. This was so that the separated woven flanges could be completely bound by binders looping above and below the new reduced weave pattern formed after the junction. A set of Python scripts were used to generate the woven T-joint geometry. The *GenerateTextile* script was used to set up the *CTextileOrthogonal* class and call the

WeavePattern module which reads the weave pattern and calculates the information required to determine the weft yarn interlacement order.

Further work, detailed in Chapter 6, required the new *CPrismDomain,* developed prior to the start of the T-joint modelling work detailed in Chapter 5, to work with the *COctreeVoxelMesh* class. This allowed the T-shape profile of the composite T-joint to be meshed with the octree voxel mesh.

In addition to the Python and TexGen software, code was developed to run the optimisation of the T-joints using a parallel architecture on the HPC as detailed in Chapter 7.

8.4 Future Work

The following section describes suggested future research work that would continue to develop the work set out in this thesis.

It would be useful to manufacture the optimised textile and use the results to validate the results of the finite element analysis. This would provide further confidence in the optimisation process.

A further extension of the finite element modelling work would be to explore the T-joint designs more closely by creating full failure models with cohesive surfaces to do a back to back comparison to the optimised textile model presented here. Additionally, with the aid of more μCT data, additional real life weave features such as yarn waviness and crimp could be included in the geometry models.

It would be instructive to conduct optimisations with other objective function values. For example, the same models could be used to optimise 3D woven T-joints for initial load in the T-bend test. Additionally, the methodology to model the weft yarn interlacement ordering could be applied to 3D woven I-beam reinforcements and could then be used to optimise the I-beam architecture in a similar way to the approach set out in this thesis.

It would be beneficial to users interested in designing T-joint architecture to integrate the T-joint code deeper into TexGen. This could use C++ to rewrite some of the Python code. A further benefit could be gained by the creation of

a user interface for the T-joint design tool, this would make it easier to expand the range of T-joints able to be designed.

8.5 Conclusions

The purpose of the work set out in this thesis was to address the issue of optimising T-joint performance by bridging the gap in the existing literature between optimisation of flat woven models using genetic algorithms and the modelling of 3D profiled structures such as 3D woven T-joint reinforcements.

The literature review revealed some barriers to the optimisation of 3D profiled structures at the start of the work. The first is that while periodic boundary conditions allow elastic properties to be optimised in flat 3D woven models, 3D woven T-Joint textiles only have periodicity along one axis so these methods are not applicable. The second is that elastic properties are not particularly relevant to T-Joint design where the important mechanical properties relate to the failure behaviour. Finally, 3D woven T-joint reinforcements have been successfully modelled in the past, but these models required extensive manual modification to accurately model the interlacement of the weft yarns in the junction region. These were produced in limited number so any conclusions drawn about the weft yarn configuration's effect on the mechanical properties were from a limited set of designs.

The behaviour of two types of 3D woven T-Joints were characterised under tensile pull off loading. One textile had a layer-to-layer weave pattern with weft crossover in the junction region while the other was an axial textile with no weft yarn crossover. The T-joints with no crossover performed poorly reaching a peak load of approximately 3.1kN, unable to sustain the same load as the layer-to-layer T-joints which were able to reach 5.2kN. Images from μCT scanning were used to measure the yarn widths and heights to set these values in the geometry of the T-joint models in the later chapters. They were also used to set the circular cross sections of the weft yarns in the junction regions.

By starting with optimising flat 3D woven structures, barriers to the use of applying optimisation to T-joints were identified: slow manual modelling of

geometries, automatic meshing and limited periodicity of weave reinforcement as well as the large computational cost of such methods. A novel method was developed to reduce the number of spurious function evaluations during optimisation of flat woven structures. The effect of this was the ruling out of weave pattern designs that are unable to hold their own integrity from the optimisations. The method consisted of using a set of simple checks applied using Python scripting. This was able to significantly reduce the computational cost by 94% compared to literature values. This was achieved by reducing the number of function evaluations that needed to run the finite element analysis. Furthermore, alternative optimisation algorithms were used and compared to find the most suitable for use.

Reducing delamination in composite materials is one of the reasons to use 3D woven reinforcement where the binding yarns can apply closure pressure on cracks. This work also explored the use of cohesive surfaces in optimisation algorithm runs by applying them to the flat woven models. While its use is a possibility for flat woven models with limited size and number of design variables in the optimisation, the duration to both generate the mesh and analyse the model would altogether exceed reasonable timescales for optimisation, using the current HPC facilities, of more complex reinforcement models such as those of T-Joints. However, methods to speed up the generation of surfaces in TexGen using the OpenMP C++ library to parallelise the code were implemented as part of this work.

The 3D woven T-Joint reinforcements were modelled using TexGen. Parameterised models were developed to enable them to be automatically generated with varying weft yarn configurations. Determining the ordering of the weft yarns as they wrap around each other from the pattern draft was automated with a new Python tool, allowing the generation of T-Joints for input into the optimisation. The methodology for producing the geometry models by determining the ordering of the weft interlacement was described with the process of adding nodes, changing yarn cross-sections and moving them into the correct positions.

Voxel meshing was compared against smoothed octree voxel meshing to establish which is the most efficacious for the automatic meshing needed for optimisations of T-Joint weave patterns. Voxel meshing has historically been the standard meshing method for 3D woven textiles due to its robustness and quick method of generating good aspect ratio, consistent quality elements. Octree voxel meshing builds on this by subdividing the elements at the material interfaces allowing a closer approximation of the true interface surfaces. Further smoothing iterations remove the stepped interface but can lead to distorted elements so care should be taken to limit the number of iterations ensure the element quality does not deteriorate. In either case, it was found these do not contribute to the overall stiffness response but can reduce interface stresses caused by shear locking. The T-joint models were created within a TexGen prism domain which allowed the outline of the T-shape to be specified before being meshed with a voxel mesh. As part of the work to generate finite element models of 3D woven T-joints, the octree voxel mesh was extended to be used with this form of domain.

After this a modelling scheme for determining the failure initiation load under tensile pull off testing was described using Hashin's failure criteria and the modified Von Mises criteria for the yarns and matrix respectively. This relied on evaluating the stresses, post-completion of the finite element analysis, in the elements at each frame and accumulating the number of failed elements until a threshold was reached. The advantage to this approach is the speed of determining an initial failure load without having to run user subroutines which are called at every iteration.

Building on the work in the earlier chapters, the ability to automatically generate weave patterns from the pattern draft, mesh them and model the tensile pull-off test determining a point of initial failure enabled an optimisation to be run to find 3D woven composite T-joints with the highest initial failure load under tensile pull-off testing. To perform the optimisation, which relies on generating permutations of design strings, the design variables were encoded as 4 bit binary strings. The best weave pattern was compared against both an orthogonal weave pattern with no weft yarn crossover and the worst performing weave pattern evaluated during the optimisation. The feature that

caused the weave pattern chosen to be the best performing was determined to be the flattened junction region which was formed by a combination of some crossover and self-entanglement of the weft yarns as they entered the bifurcation region.

Automatic generation of the T-joint geometry is not only useful for performing optimisations. Full scale models with higher mesh densities and more expensive modelling techniques can be accurately produced for finite element analysis using the methodology set out in Chapter 5. Furthermore, the use of the OpenMP library to speed up the generation of surfaces is another advantageous outcome of this work for those seeking to employ cohesive surfaces on textile models. Finally, the application of the octree voxel meshing technique to the prism domains is an important step in the process of generating these meshes for textiles that do not fit the regular cuboidal flat woven profile.

By providing an advancement in the methodology with which to automatically generate 3D woven T-joint models, automatically mesh them with good quality elements and evaluate an objective function, this work paves the way for optimisation of other forms of complex structures.

References

[1] Y. Liu, B. Zwingmann, and M. Schlaich, "Carbon Fiber Reinforced Polymer for Cable Structures—A Review," *Polym. 2015, Vol. 7, Pages 2078-2099*, vol. 7, no. 10, pp. 2078–2099, Oct. 2015, doi: 10.3390/POLYM7101501.

[2] A. R. Bunsell, S. Joannes, and ThionnetA., *Fundamentals of Fibre Reinforced Composites*, 2nd ed. CRC Press, 2021.

[3] S. Gholizadeh, "A review of non-destructive testing methods of composite materials," *Procedia Struct. Integr.*, vol. 1, pp. 50–57, 2016, doi: 10.1016/J.PROSTR.2016.02.008.

[4] J. Galos, "Thin-ply composite laminates: a review," *Compos. Struct.*, vol. 236, p. 111920, Mar. 2020, doi: 10.1016/J.COMPSTRUCT.2020.111920.

[5] A. Tabiei and W. Zhang, "Composite laminate delamination simulation and experiment: A review of recent development," *Appl. Mech. Rev.*, vol. 70, no. 3, May 2018, doi: 10.1115/1.4040448/367470.

[6] L. Lee, S. Rudov-Clark, A. P. Mouritz, M. K. Bannister, and I. Herszberg, "Effect of weaving damage on the tensile properties of three-dimensional woven composites," *Compos. Struct.*, vol. 57, no. 1–4, pp. 405–413, Jul. 2002, doi: 10.1016/S0263-8223(02)00108-3.

[7] A. P. Mouritz, M. K. Bannister, P. J. Falzon, and K. H. Leong, "Review of applications for advanced three-dimensional fibre textile composites," *Compos. Part A Appl. Sci. Manuf.*, vol. 30, no. 12, pp. 1445–1461, Dec. 1999, doi: 10.1016/S1359-835X(99)00034-2.

[8] C. Mullen and P. Roy, "Fabrication and properties description of

AVCO 3D carboncarbon cylindrical composites," in *National SAMPE Symposium*, 1972, pp. 11–13.

[9] G. Marsh, "Aero engines lose weight thanks to composites," *Reinf. Plast.*, vol. 56, no. 6, pp. 32–35, Nov. 2012, doi: 10.1016/S0034-3617(12)70146-7.

[10] K. Sharp, A. Bogdanovich, R. Boyle, J. Brown, and D. Mungalov, "Wind blade joints based on non-crimp 3D orthogonal woven Pi shaped preforms," *Compos. Part A Appl. Sci. Manuf.*, vol. 49, pp. 9–17, Jun. 2013, doi: 10.1016/j.compositesa.2013.01.012.

[11] F. Bianchi, T. M. Koh, X. Zhang, I. K. Partridge, and A. P. Mouritz, "Finite element modelling of z-pinned composite T-joints," *Compos. Sci. Technol.*, vol. 73, no. 1, pp. 48–56, Nov. 2012, doi: 10.1016/j.compscitech.2012.09.008.

[12] S. Yan, X. Zeng, and A. Long, "Experimental assessment of the mechanical behaviour of 3D woven composite T-joints," *Compos. Part B Eng.*, vol. 154, pp. 108–113, Dec. 2018, doi: 10.1016/J.COMPOSITESB.2018.08.007.

[13] S. Rudov-Clark, A. P. Mouritz, L. Lee, and M. K. Bannister, "Fibre damage in the manufacture of advanced three-dimensional woven composites," *Compos. Part A Appl. Sci. Manuf.*, vol. 34, no. 10, pp. 963–970, Oct. 2003, doi: 10.1016/S1359-835X(03)00213-6.

[14] M. Matveev, V. Koncherry, S. S. Roy, P. Potluri, and A. Long, "Novel textile preforming for optimised fibre architectures," *IOP Conf. Ser. Mater. Sci. Eng.*, vol. 406, 2018, doi: 10.1088/1757-899X/406/1/012050.

[15] P. Potluri, D. Jetavat, and S. Sharma, "METHOD AND APPARATUS FOR WEAVING ," 2012

[16] A. R. Labanieh, Y. Liu, D. Vasiukov, D. Soulat, and S. Panier, "Influence of off-axis in-plane yarns on the mechanical properties of 3D composites," *Compos. Part A Appl. Sci. Manuf.*, vol. 98, pp. 45–57,

Jul. 2017, doi: 10.1016/j.compositesa.2017.03.009.

[17] A. R. Labanieh, X. Legrand, V. Koncar, and D. Soulat, “Development in the multiaxis 3D weaving technology,” *Text. Res. J.*, vol. 86, no. 17, pp. 1869–1884, Oct. 2016, doi: 10.1177/0040517515612365.

[18] L. Brown, M. Matveev, and G. Spackman, “louisepb/TexGen: TexGen v3.12.0 (Version v3.12.0).”

[19] E. Potter, S. T. Pinho, P. Robinson, L. Iannucci, and A. J. McMillan, “Mesh generation and geometrical modelling of 3D woven composites with variable tow cross-sections,” *Comput. Mater. Sci.*, vol. 51, no. 1, pp. 103–111, Jan. 2012, doi: 10.1016/J.COMMATSCI.2011.06.034.

[20] M. Y. Matveev, L. P. Brown, and A. C. Long, “Efficient meshing technique for textile composites unit cells of arbitrary complexity,” *Compos. Struct.*, p. 112757, Jul. 2020, doi: 10.1016/j.compstruct.2020.112757.

[21] S. Yan, “Design optimisation of 3D woven reinforcements with geometric features. PhD thesis, University of Nottingham.,” University of Nottingham, 2017.

[22] L. P. Brown, F. Gommer, X. Zeng, and A. C. Long, “Modelling framework for optimum multiaxial 3D woven textile composites,” Sep. 2016, Accessed: Jan. 16, 2018. [Online]. Available: http://eprints.nottingham.ac.uk/37018/

[23] X. Zeng, A. C. A. Long, I. Ashcroft, and P. Potluri, “Fibre architecture design of 3D woven composite with genetic algorithms: a unit cell based optimisation framework and performance assessment,” Jul. 2015, Accessed: Nov. 28, 2017. [Online]. Available: http://eprints.nottingham.ac.uk/28920/

[24] A. P. Mouritz, K. H. Leong, and I. Herszberg, “A review of the effect of stitching on the in-plane mechanical properties of fibre-reinforced polymer composites,” *Compos. Part A Appl. Sci. Manuf.*, vol. 28, no. 12, pp. 979–991, Jan. 1997, doi: 10.1016/S1359-835X(97)00057-2.

[25] Q. Yang, K. Rugg, B. Cox, and M. Shaw, “Failure in the junction region of T-stiffeners: 3D-braided vs. 2D tape laminate stiffeners,” *Int. J. Solids Struct.*, vol. 40, no. 7, pp. 1653–1668, Apr. 2003, doi: 10.1016/S0020-7683(03)00026-X.

[26] P. Stickler, M. Ramulu, and P. Johnson, “Experimental and numerical analysis of transverse stitched T-joints in bending,” *Compos. Struct.*, vol. 50, no. 1, pp. 17–27, Sep. 2000, doi: 10.1016/S0263-8223(00)00006-4.

[27] J. A. Soden, G. Weissenbach, and B. J. Hill, “The design and fabrication of 3D multi-layer woven T-section reinforcements,” *Compos. Part A Appl. Sci. Manuf.*, vol. 30, no. 3, pp. 213–220, Mar. 1999, doi: 10.1016/S1359-835X(98)00167-5.

[28] F. Hélénon, M. R. Wisnom, S. R. Hallett, and R. S. Trask, “Numerical investigation into failure of laminated composite T-piece specimens under tensile loading,” *Compos. Part A Appl. Sci. Manuf.*, vol. 43, no. 7, pp. 1017–1027, Jul. 2012, doi: 10.1016/J.COMPOSITESA.2012.02.010.

[29] L. Burns, A. P. Mouritz, D. Pook, and S. Feih, “Strengthening of composite T-joints using novel ply design approaches,” *Compos. Part B Eng.*, vol. 88, pp. 73–84, Mar. 2016, doi: 10.1016/J.COMPOSITESB.2015.10.032.

[30] P. Stickler and M. Ramulu, “Investigation of mechanical behavior of transverse stitched T-joints with PR520 resin in flexure and tension,” *Compos. Struct.*, vol. 52, no. 3–4, pp. 307–314, May 2001, doi: 10.1016/S0263-8223(01)00023-X.

[31] C. Li, Y. Sun, C. Duan, and R. Li, “Study on Properties of Z-pin-reinforced and Rivet-reinforced Composite T-joint: Experiment and Simulation,” *Appl. Compos. Mater.*, vol. 28, no. 2, pp. 395–408, Feb. 2021, doi: 10.1007/s10443-021-09866-2.

[32] C. Sun, P. Jia, C. Chen, A. Moradi, J. Zhou, M. Al Teneiji, W.J. Cantwell, Z.W. Guan, “The effect of carbon fibre

stitching on the tensile behaviour of secondary bonded single- and double-lap composite joints," *Compos. Struct.*, vol. 265, Jun. 2021, doi: 10.1016/j.compstruct.2021.113774.

[33] L. Francesconi and F. Aymerich, "Numerical simulation of the effect of stitching on the delamination resistance of laminated composites subjected to low-velocity impact," *Compos. Struct.*, vol. 159, pp. 110–120, Jan. 2017, doi: 10.1016/j.compstruct.2016.09.050.

[34] K. Dransfield, C. Baillie, and Y. W. Mai, "Improving the delamination resistance of CFRP by stitching-a review," *Compos. Sci. Technol.*, vol. 50, no. 3, pp. 305–317, 1994, doi: 10.1016/0266-3538(94)90019-1.

[35] A. E. Lovejoy and F. A. Leone, "Tension and Bending Testing of an Integral T-Cap for Stitched Composite Airframe Joints", Accessed: Jun. 07, 2018. [Online]. Available: https://ntrs.nasa.gov/archive/nasa/casi.ntrs.nasa.gov/20160007731.pdf

[36] J. Bigaud, Z. Aboura, A. T. Martins, and S. Verger, "Analysis of the mechanical behavior of composite T-joints reinforced by one side stitching," 2017, doi: 10.1016/j.compstruct.2017.06.041.

[37] K. K. Verma, G. Padmakara, K. M. Gaddikeri, S. Ramesh, S. Kumar, and S. Bose, "The key role of thread and needle selection towards 'through-thickness reinforcement' in tufted carbon fiber-epoxy laminates," *Compos. Part B Eng.*, vol. 174, p. 106970, Oct. 2019, doi: 10.1016/j.compositesb.2019.106970.

[38] G. Dell'Anno, D. D. Cartié, I. K. Partridge, and A. Rezai, "Exploring mechanical property balance in tufted carbon fabric/epoxy composites," *Compos. Part A Appl. Sci. Manuf.*, vol. 38, no. 11, pp. 2366–2373, Nov. 2007, doi: 10.1016/J.COMPOSITESA.2007.06.004.

[39] H. M. Clegg, G. Dell'Anno, and I. K. Partridge, "Creating damage tolerant intersections in composite structures using tufting and 3D woven connectors," *Adv. Aircr. Spacecr. Sci.*, vol. 6, no. 2, pp. 145–156, 2019, doi: 10.12989/aas.2019.6.2.145.

[40] G. Dell'Anno, J. W. G. Treiber, and I. K. Partridge, "Manufacturing of composite parts reinforced through-thickness by tufting," *Robot. Comput. Integr. Manuf.*, vol. 37, pp. 262–272, Feb. 2016, doi: 10.1016/J.RCIM.2015.04.004.

[41] Y. Wang and C. Soutis, "Fatigue Behaviour of Composite T-Joints in Wind Turbine Blade Applications," *Appl. Compos. Mater.*, vol. 24, no. 2, pp. 461–475, Apr. 2017, doi: 10.1007/s10443-016-9537-9.

[42] D. D. R. Cartié, G. Dell'Anno, E. Poulin, and I. K. Partridge, "3D reinforcement of stiffener-to-skin T-joints by Z-pinning and tufting," *Eng. Fract. Mech.*, vol. 73, no. 16, pp. 2532–2540, Nov. 2006, doi: 10.1016/j.engfracmech.2006.06.012.

[43] A. P. Mouritz, "Review of z-pinned composite laminates," *Composites Part A: Applied Science and Manufacturing*, vol. 38, no. 12. Elsevier, pp. 2383–2397, Dec. 01, 2007. doi: 10.1016/j.compositesa.2007.08.016.

[44] T. M. Koh, S. Feih, and A. P. Mouritz, "Experimental determination of the structural properties and strengthening mechanisms of z-pinned composite T-joints," *Compos. Struct.*, vol. 93, no. 9, pp. 2222–2230, Aug. 2011, doi: 10.1016/j.compstruct.2011.03.009.

[45] G. Allegri and X. Zhang, "On the delamination and debond suppression in structural joints by Z-fibre pinning," *Compos. Part A Appl. Sci. Manuf.*, vol. 38, no. 4, pp. 1107–1115, Apr. 2007, doi: 10.1016/j.compositesa.2006.06.013.

[46] R.B.Ladani, A.R. Ravindran, S. Wu, K. Pingkarawat, A.J. Kinloch, A. P. Mouritz, R.O. Ritchie, and C.H. Wang, "Multi-scale toughening of fibre composites using carbon nanofibres and z-pins," *Compos. Sci. Technol.*, vol. 131, pp. 98–109, Aug. 2016, doi: 10.1016/j.compscitech.2016.06.005.

[47] F. Bianchi and X. Zhang, "A cohesive zone model for predicting delamination suppression in z-pinned laminates," *Compos. Sci. Technol.*, vol. 71, no. 16, pp. 1898–1907, Nov. 2011, doi:

10.1016/j.compscitech.2011.09.004.

[48] S. Heimbs, A. C. Nogueira, E. Hombergsmeier, M. May, and J. Wolfrum, “Failure behaviour of composite T-joints with novel metallic arrow-pin reinforcement,” *Compos. Struct.*, vol. 110, no. 1, pp. 16–28, Apr. 2014, doi: 10.1016/j.compstruct.2013.11.022.

[49] X. Chen, L. W. Taylor, and L.J. Tsai, “An overview on fabrication of three-dimensional woven textile preforms for composites,” *Text. Res. J.*, vol. 81, no. 9, pp. 932–944, Jun. 2011, doi: 10.1177/0040517510392471.

[50] K. C. Warren, R. A. Lopez-Anido, and J. Goering, “Experimental investigation of three-dimensional woven composites,” *Compos. Part A Appl. Sci. Manuf.*, vol. 73, pp. 242–259, Jun. 2015, doi: 10.1016/J.COMPOSITESA.2015.03.011.

[51] S. Dai, P. R. Cunningham, S. Marshall, and C. Silva, “Influence of fibre architecture on the tensile, compressive and flexural behaviour of 3D woven composites,” *Compos. Part A Appl. Sci. Manuf.*, vol. 69, pp. 195–207, Feb. 2015, doi: 10.1016/J.COMPOSITESA.2014.11.012.

[52] A. R. Labanieh, X. Legrand, V. Koncar, and D. Soulat, “Development in the multiaxis 3D weaving technology,” *Text. Res. J.*, vol. 86, no. 17, pp. 1869–1884, Oct. 2016, doi: 10.1177/0040517515612365.

[53] M. Kashif, S. Talha Ali Hamdani, Y. Nawab, M. A. Asghar, M. Umair and K. Shaker, “Optimization of 3D woven preform for improved mechanical performance,” vol. 48, no. 7, pp. 1206–1227, 2019, doi: 10.1177/1528083718760802.

[54] F. Stig and S. Hallström, “Influence of crimp on 3D-woven fibre reinforced composites,” *Compos. Struct.*, vol. 95, pp. 114–122, Jan. 2013, doi: 10.1016/j.compstruct.2012.07.022.

[55] S. Yan, X. Zeng, L. Brown, and A. Long, “Geometric modeling of 3D woven preforms in composite T-joints,” *Text. Res. J.*, p. 004051751771209, Jun. 2017, doi: 10.1177/0040517517712098.

[56] S. Li and A. Wongsto, “Unit cells for micromechanical analyses of particle-reinforced composites,” *Mech. Mater.*, vol. 36, no. 7, pp. 543–572, Jul. 2004, doi: 10.1016/S0167-6636(03)00062-0.

[57] B. Sugun and D. Sandeep, “Integral weaving of orthogonal 3D ‘T’ stiffeners based on pleat weaving concept,” vol. 47, no. 7, pp. 1626–1644, 2018, doi: 10.1177/1528083717702009.

[58] S. Yan, A. Long, and X. Zeng, “EXPERIMENTAL ASSESSMENT AND NUMERICAL ANALYSIS OF 3D WOVEN COMPOSITE T-JOINTS UNDER TENSILE LOADING,” 2015, Accessed: Feb. 22, 2018. [Online]. Available: http://www.iccm-central.org/Proceedings/ICCM20proceedings/papers/paper-3110-1.pdf

[59] Z. Michalewicz, D. Dasgupta, R. G. Le Riche, and M. Schoenauer, “Evolutionary algorithms for constrained engineering problems,” *Comput. Ind. Eng.*, vol. 30, no. 4, pp. 851–870, Sep. 1996, doi: 10.1016/0360-8352(96)00037-X.

[60] M. Autio, “Determining the real lay-up of a laminate corresponding to optimal lamination parameters by genetic search,” *Struct Multidisc Optim*, vol. 20, pp. 301–310, 2000, Accessed: Nov. 06, 2017. [Online]. Available: https://link.springer.com/content/pdf/10.1007%2Fs001580050160.pdf

[61] R. LE RICHE and R. T. HAFTKA, “Optimization of laminate stacking sequence for buckling load maximization by genetic algorithm,” *AIAA J.*, vol. 31, no. 5, pp. 951–956, May 1993, doi: 10.2514/3.11710.

[62] G. Soremekun, Z. Gürdal, R. T. Haftka, and L. T. Watson, “Composite laminate design optimization by genetic algorithm with generalized elitist selection,” *Comput. Struct.*, vol. 79, no. 2, pp. 131–143, Jan. 2001, doi: 10.1016/S0045-7949(00)00125-5.

[63] S. D. Cardozo, H. M. Gomes, A. M. Awruch, and L. American, “Optimization of laminated composite plates and shells using genetic algorithms, neural networks and finite elements,” *J. Solids Struct.*, vol. 8, no. 8, pp. 413–427, 2011, Accessed: Jun. 03, 2018. [Online].

Available: http://www.scielo.br/pdf/lajss/v8n4/a03v8n4.pdf

[64] A. Todoroki and R. T. Haftka, “Stacking sequence optimization by a genetic algorithm with a new recessive gene like repair strategy,” *Compos. Part B Eng.*, vol. 29, no. 3, pp. 277–285, Jan. 1998, doi: 10.1016/S1359-8368(97)00030-9.

[65] L. Aydin and H. Secil Artem, “Multiobjective Genetic Algorithm optimization of the composite laminates as a satellite structure material for coefficient of thermal expansion and elastic modulus,” in *2009 4th International Conference on Recent Advances in Space Technologies*, Jun. 2009, pp. 114–119. doi: 10.1109/RAST.2009.5158179.

[66] K. J. Callahan and G. E. Weeks, “Optimum design of composite laminates using genetic algorithms,” *Compos. Eng.*, vol. 2, no. 3, pp. 149–160, Apr. 1992, doi: 10.1016/0961-9526(92)90001-M.

[67] The Mathworks Inc., “Matlab and Statistics Toolbox Release 2017b.” Natick, Massachusetts, United States.

[68] J. Blank and K. Deb, “Pymoo: Multi-Objective Optimization in Python,” *IEEE Access*, vol. 8, pp. 89497–89509, 2020, doi: 10.1109/ACCESS.2020.2990567.

[69] A. Fawzy Gad, “PyGAD: An Intuitive Genetic Algorithm Python Library.” 2021. [Online]. Available: https://github.com/ahmedfgad/GeneticAlgorithmPython

[70] C. Audet and J. E. Dennis, “Analysis of Generalized Pattern Searches,” *SIAM J. Optim.*, vol. 13, no. 3, pp. 889–903, Jan. 2002, doi: 10.1137/S1052623400378742.

[71] J. Kennedy and R. Eberhart, “Particle swarm optimization,” *Proc. ICNN’95 - Int. Conf. Neural Networks, Perth, WA, Aust.*, vol. 4, pp. 1942–1948, 1995.

[72] F. Gommer, L. P. Brown, X. Zeng, and A. C. Long, “Discovery of Optimum Textile Composites,” 2016.

[73] L. P. Brown and A. C. Long, “Modeling the geometry of textile

reinforcements for composites: TexGen," *Compos. Reinf. Optim. Perform.*, pp. 237–265, Jan. 2021, doi: 10.1016/B978-0-12-819005-0.00008-3.

[74] M. Sherburn, "Geometric and Mechanical Modelling of Textiles," 2007, Accessed: Jun. 24, 2018. [Online]. Available: http://eprints.nottingham.ac.uk/10303/

[75] H. Lin, L. P. Brown, and A. C. Long, "Modelling and Simulating Textile Structures Using TexGen," *Adv. Mater. Res.*, vol. 331, pp. 44–47, Sep. 2011, doi: 10.4028/www.scientific.net/AMR.331.44.

[76] SiHang, "TetGen, a Delaunay-Based Quality Tetrahedral Mesh Generator," *ACM Trans. Math. Softw.*, vol. 41, no. 2, Feb. 2015, doi: 10.1145/2629697.

[77] I. Verpoest and S. V. Lomov, "Virtual textile composites software WiseTex: Integration with micro-mechanical, permeability and structural analysis," *Compos. Sci. Technol.*, vol. 65, no. 15–16, pp. 2563–2574, Dec. 2005, doi: 10.1016/J.COMPSCITECH.2005.05.031.

[78] S. V. Lomov, "Modeling the geometry of textile composite reinforcements: WiseTex," *Compos. Reinf. Optim. Perform.*, pp. 199–236, Jan. 2021, doi: 10.1016/B978-0-12-819005-0.00007-1.

[79] Ansys Inc., "Ansys® Academic Research Mechanical, Release 18.1, Help System, Coupled Field Analysis Guide".

[80] "Abaqus 2016 User Manual." Dassault Systemes, Providence, RI, USA.

[81] N. N. Nemeth, S. Mital, and J. Lang, "Evaluation of Solid Modeling Software for Finite Element Analysis of Woven Ceramic Matrix Composites." 2010. Accessed: Jul. 19, 2021. [Online]. Available: http://www.sti.nasa.gov

[82] E. V. Iarve, D. H. Mollenhauer, E. G. Zhou, T. Breitzman, and T. J. Whitney, "Independent mesh method-based prediction of local and volume average fields in textile composites," *Compos. Part A Appl.*

Sci. Manuf., vol. 40, no. 12, pp. 1880–1890, Dec. 2009, doi: 10.1016/J.COMPOSITESA.2009.04.034.

[83] R. Wentorf, R. Collar, M. S. Shephard, and J. Fish, "Automated modeling for complex woven mesostructures," *Comput. Methods Appl. Mech. Eng.*, vol. 172, no. 1–4, pp. 273–291, Apr. 1999, doi: 10.1016/S0045-7825(98)00232-1.

[84] H. J. Kim and C. C. Swan, "Voxel-based meshing and unit-cell analysis of textile composites," *Int. J. Numer. METHODS Eng. Int. J. Numer. Meth. Engng*, vol. 56, pp. 977–1006, 2003, doi: 10.1002/nme.594.

[85] A. Doitrand, C. Fagiano, F.-X. Irisarri, and M. Hirsekorn, "Comparison between voxel and consistent meso-scale models of woven composites," *Compos. Part A Appl. Sci. Manuf.*, vol. 73, pp. 143–154, Jun. 2015, doi: 10.1016/J.COMPOSITESA.2015.02.022.

[86] "HyperMesh." Altair Engineering, Inc., Troy MI, United States.

[87] C. A. Schneider, W. S. Rasband, and K. W. Eliceiri, "NIH Image to ImageJ: 25 years of image analysis," *Nat. Methods 2012 97*, vol. 9, no. 7, pp. 671–675, Jun. 2012, doi: 10.1038/nmeth.2089.

[88] N. Castaneda, B. Wisner, J. Cuadra, S. Amini, and A. Kontsos, "Investigation of the Z-binder role in progressive damage of 3D woven composites," *Compos. Part A Appl. Sci. Manuf.*, vol. 98, pp. 76–89, Jul. 2017, doi: 10.1016/J.COMPOSITESA.2016.11.022.

[89] B. El Said, D. Ivanov, A. C. Long, and S. R. Hallett, "Multi-scale modelling of strongly heterogeneous 3D composite structures using spatial Voronoi tessellation," *J. Mech. Phys. Solids*, vol. 88, pp. 50–71, Mar. 2016, doi: 10.1016/J.JMPS.2015.12.024.

[90] L. P. Brown, S. Yan, X. Zeng, and A. C. Long, "Mesoscale geometric modelling of bifurcation in 3D woven T-beam preforms," May 2015.

[91] F. Stig and S. Hallström, "A modelling framework for composites containing 3D reinforcement," *Compos. Struct.*, vol. 94, no. 9, pp.

2895–2901, Sep. 2012, doi: 10.1016/j.compstruct.2012.03.009.

[92] C. C. Chamis, “Mechanics of composite materials: Past, present, and future,” *J. Compos. Technol. Res.*, vol. 11, no. 1, pp. 3–14, 1989, doi: 10.1520/CTR10143J.

[93] S.V. Lomov, D.S. Ivanov, I. Verpoest, M.Zako, T. Kurashiki, H. Nakai, and S. Hirosawa, “Meso-FE modelling of textile composites: Road map, data flow and algorithms,” *Compos. Sci. Technol.*, vol. 67, no. 9, pp. 1870–1891, Jul. 2007, doi: 0.1016/J.COMPSCITECH.2006.10.017.

[94] J. B. Bai, C.H. Dong, J. J. Xiong, C.Y. Luo, and D. Chen, “Progressive damage behaviour of RTM-made composite T-joint under tensile loading,” *Compos. Part B Eng.*, vol. 160, pp. 488–497, Mar. 2019, doi: 10.1016/J.COMPOSITESB.2018.12.069.

[95] M. J. Hinton and A. S. Kaddour, “The background to the Second World-Wide Failure Exercise:,” *http://dx.doi.org/10.1177/0021998312449885*, vol. 46, no. 19–20, pp. 2283–2294, Jun. 2012, doi: 10.1177/0021998312449885.

[96] M. J. Hinton, A. S. Kaddour, and P. D. Soden, “The world-wide failure exercise: Its origin, concept and content,” *Fail. Criteria Fibre-Reinforced-Polymer Compos.*, pp. 2–28, Jan. 2004, doi: 10.1016/B978-008044475-8/50002-0.

[97] R. M. Caddell, R. S. Raghava, and A. G. Atkins, “Pressure dependent yield criteria for polymers,” *Mater. Sci. Eng.*, vol. 13, no. 2, pp. 113–120, Feb. 1974, doi: 10.1016/0025-5416(74)90179-7.

Appendix A

Containing drawings for T-Joint mould tool. In order: Base plate, L plate 1, L plate 2, base spacer 1, base spacer 2, spacer 1, spacer 2 and cap.

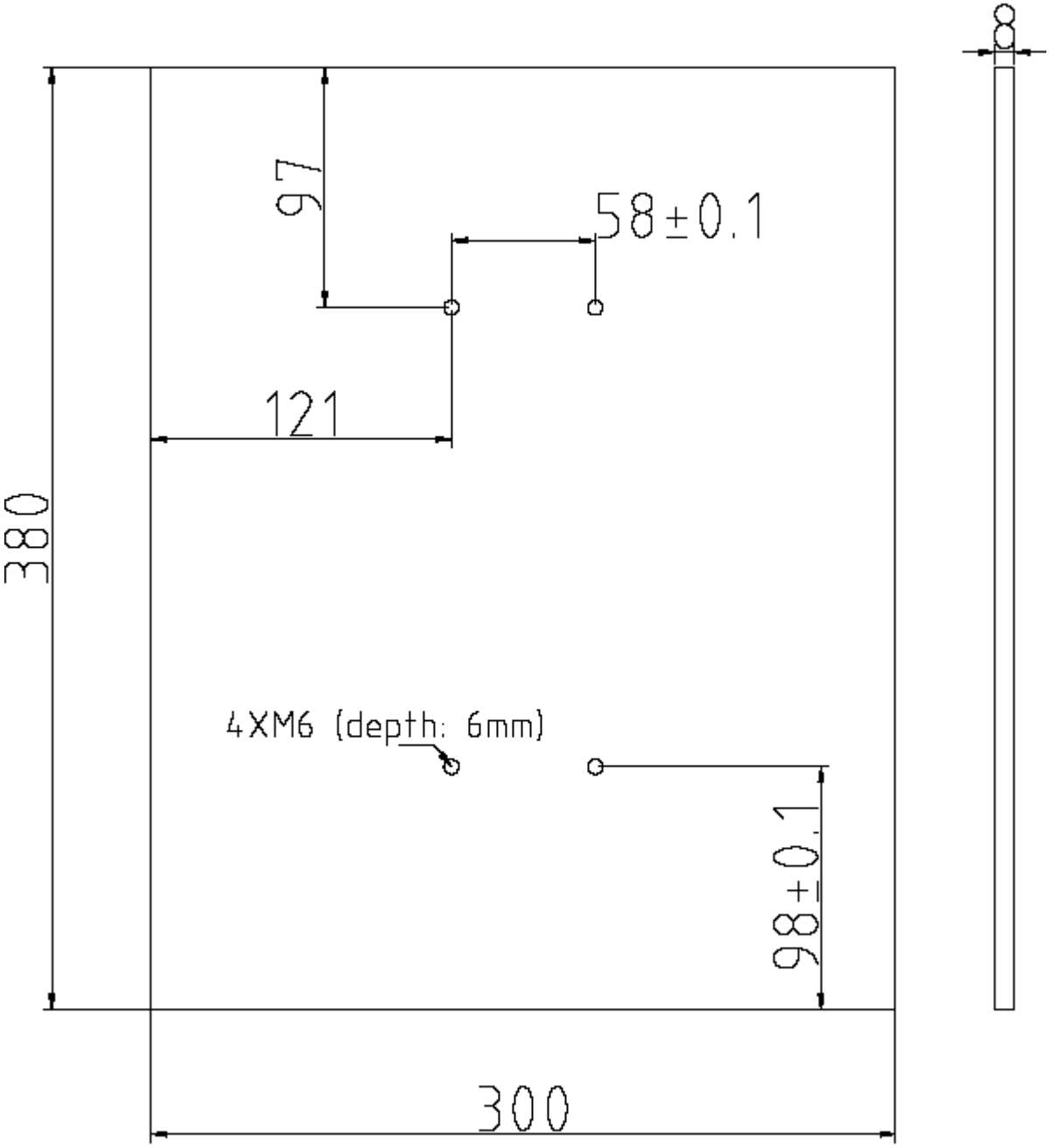

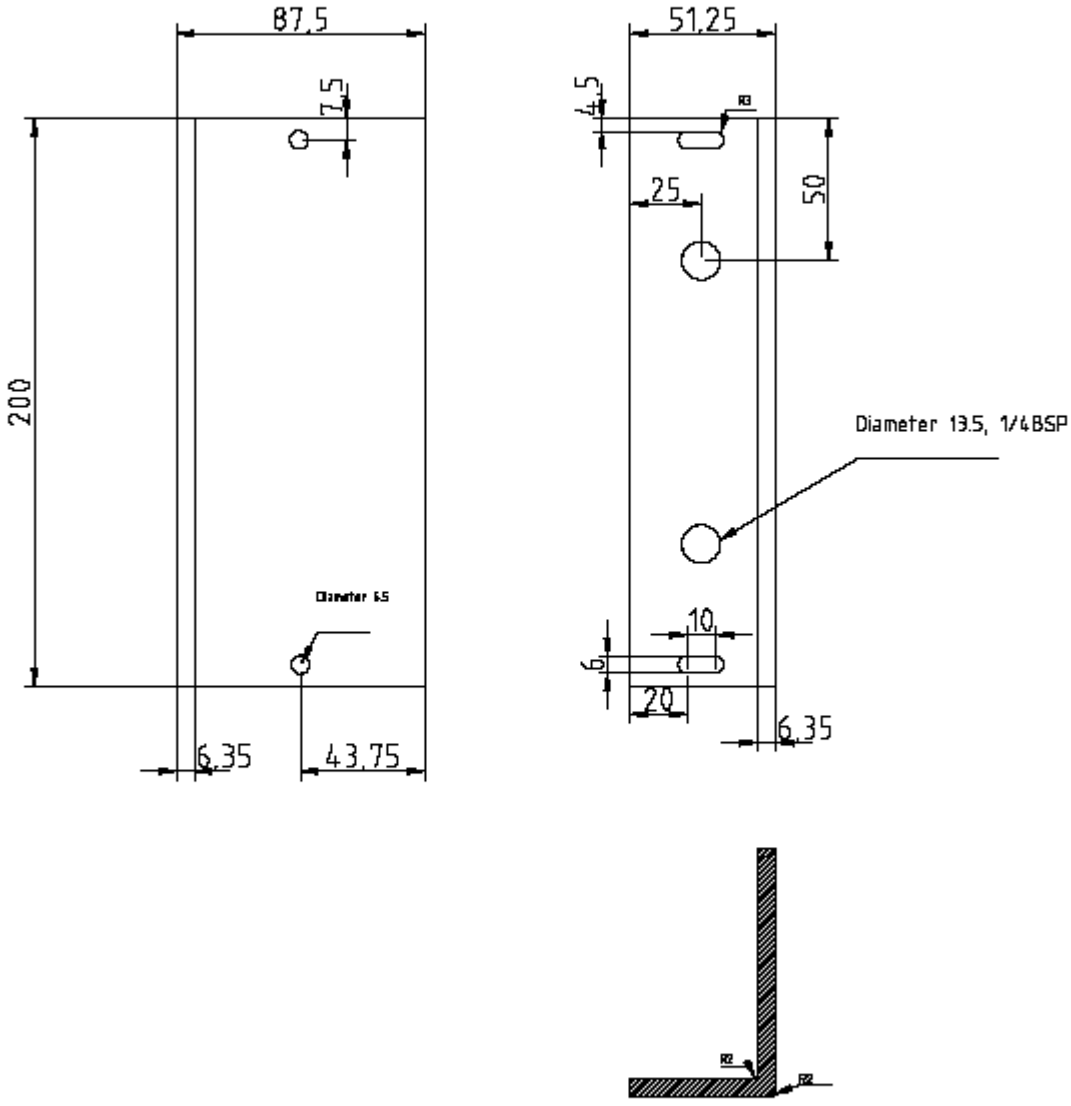
87.5
7.5
200
Diameter 6.5
6.35
43.75
51.25
4.5
R3
25
50
Diameter 13.5, 1/4BSP
10
6
20
6.35
R2
R2

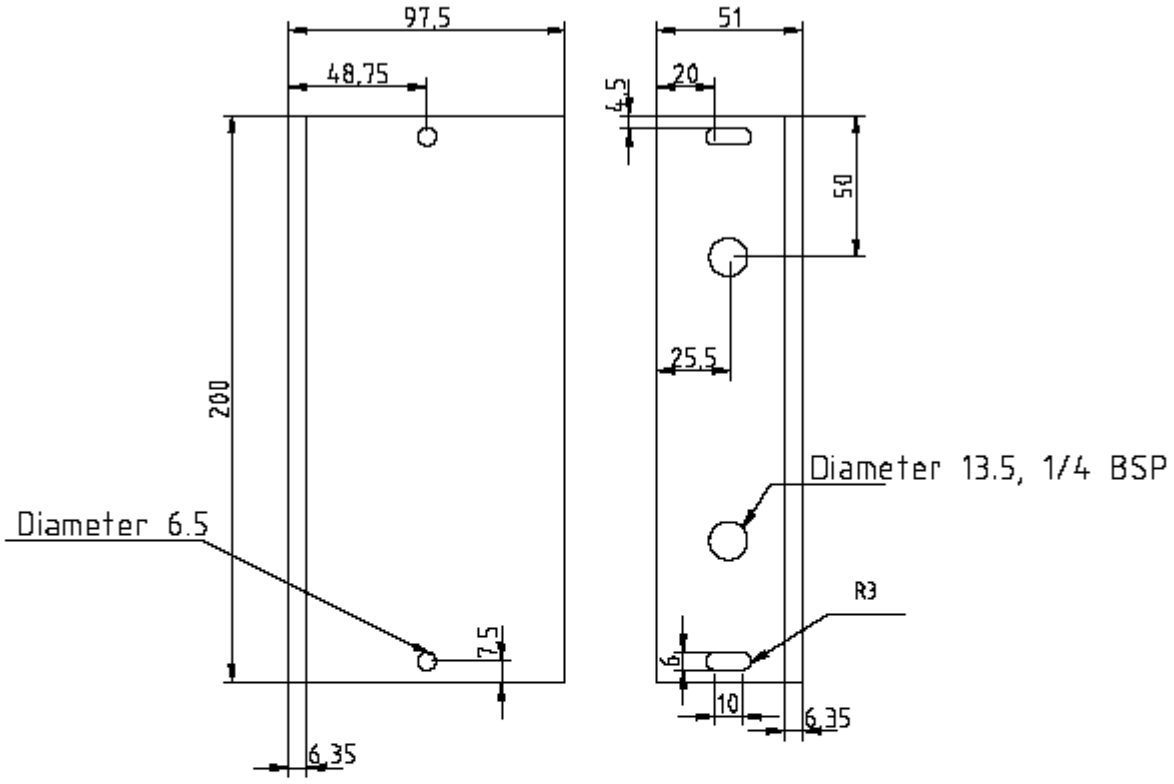
97.5
48.75
200
Diameter 6.5
7.5
6.35
51
20
4.5
50
25.5
Diameter 13.5, 1/4 BSP
R3
6
10
6.35

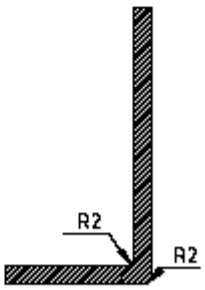
R2
R2

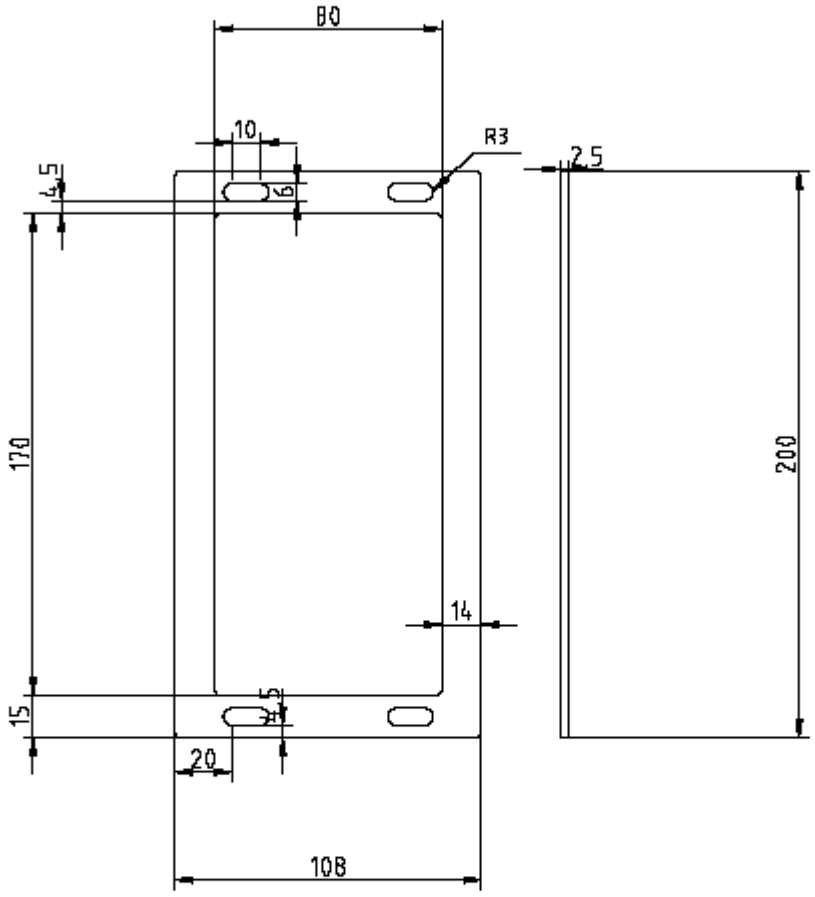
80
10
R3
2.5
4.5
6
170
200
14
15
3.5
20
108

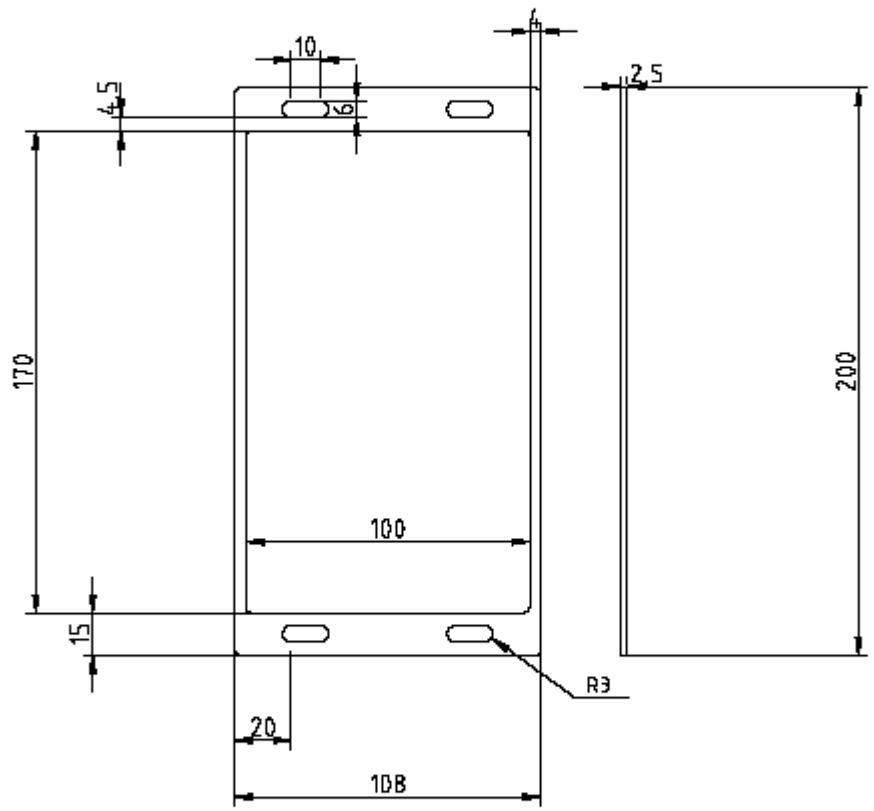
10
4
4,5
6
2,5
170
200
100
15
R3
20
108

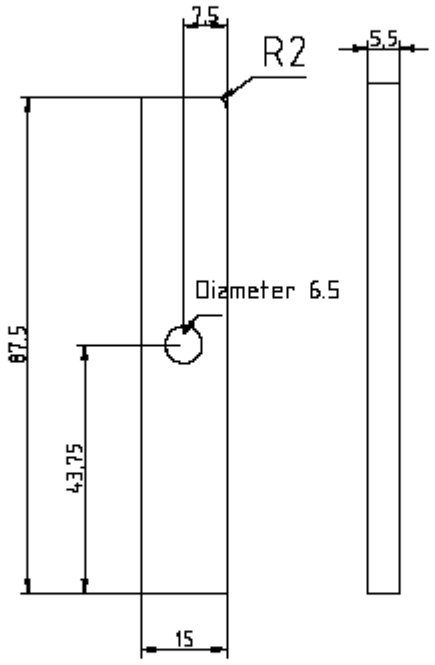
2.5
R2
5.5
Diameter 6.5
87.5
43.75
15

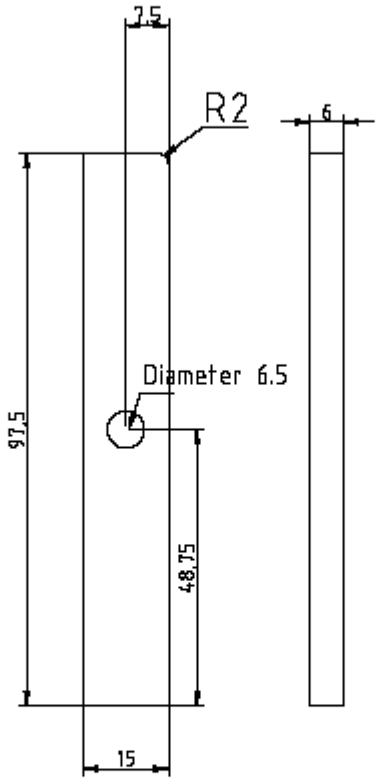
7.5
R2
6
Diameter 6.5
97.5
48.75
15

Appendix B

The code used in the work contained in this thesis is stored in the GitHub repository found at the following link.

https://github.com/georgespackman/PhDThesis

The version of TexGen used is present along with the Python code presented in chapters 4, 5 and 6.